

ABSTRACT

Title: ESTIMATING LAND SURFACE ALBEDO FROM SATELLITE DATA

Tao He, Doctor of Philosophy, 2012

Directed by: Dr. Shunlin Liang, Professor

Department of Geographical Sciences

Land surface albedo, defined as the ratio of the surface reflected incoming and outgoing solar radiation, is one of the key geophysical variables controlling the surface radiation budget. Surface shortwave albedo is widely used to drive climate and hydrological models. During the last several decades, remotely sensed surface albedo products have been generated through satellite-acquired data. However, some problems exist in those products due to instrument measurement inaccuracies and the failure of current retrieving procedures, which have limited their applications. More significantly, it has been reported that some albedo products from different satellite sensors do not agree with each other and some even show the opposite long term trend regionally and globally. The emergence of some advanced sensors newly launched or planned in the near future will provide better capabilities for estimating land surface albedo with fine resolution spatially and/or temporally.

Traditional methods for estimating the surface shortwave albedo from satellite data include three steps: first, the satellite observations are converted to surface directional reflectance using the atmospheric correction algorithms; second, the surface bidirectional

reflectance distribution function (BRDF) models are inverted through the fitting of the surface reflectance composites; finally, the shortwave albedo is calculated from the BRDF through the angular and spectral integration. However, some problems exist in these algorithms, including: 1) “dark-object” based atmospheric correction methods which make it difficult to estimate albedo accurately over non-vegetated or sparsely vegetated area; 2) the long-time composite albedo products cannot satisfy the needs of weather forecasting or land surface modeling when rapid changes such as snow fall/melt, forest fire/clear-cut and crop harvesting occur; 3) the diurnal albedo signature cannot be estimated in the current algorithms due to the Lambertian approximation in some of the atmospheric correction algorithms; 4) prior knowledge has not been effectively incorporated in the current algorithms; and 5) current observation accumulation methods make it difficult to obtain sufficient observations when persistent clouds exist within the accumulation window.

To address those issues and to improve the satellite surface albedo estimations, a method using an atmospheric radiative transfer procedure with surface bidirectional reflectance modeling will be applied to simultaneously retrieve land surface albedo and instantaneous aerosol optical depth (AOD). This study consists of three major components. The first focuses on the atmospheric radiative transfer procedure with surface reflectance modeling. Instead of executing atmospheric correction first and then fitting surface reflectance in the previous satellite albedo retrieving procedure, the atmospheric properties (e.g., AOD) and surface properties (e.g., BRDF) are estimated simultaneously to reduce the uncertainties produced in separating the entire radiative transfer process. Data from the Moderate Resolution Imaging Spectroradiometer

(MODIS) onboard Terra and Aqua are used to evaluate the performance of this albedo estimation algorithm. Good agreement is reached between the albedo estimates from the proposed algorithm and other validation datasets. The second part is to assess the effectiveness of the proposed algorithm, analyze the error sources, and further apply the algorithm on geostationary satellite – the Spinning Enhanced Visible and InfraRed Imager (SEVIRI) onboard Meteosat Second Generation (MSG). Extensive validations on surface albedo estimations from MSG/SEVIRI observations are conducted based on the comparison with ground measurements and other satellite products. Diurnal changes and day-to-day changes in surface albedo are accurately captured by the proposed algorithm. The third part of this study is to develop a spatially and temporally complete, continuous, and consistent albedo maps through a data fusion method. Since the prior information (or climatology) of albedo/BRDF plays a vital role in controlling the retrieving accuracy in the optimization method, currently available multiple land surface albedo products will be integrated using the Multi-resolution Tree (MRT) models to mitigate problems such as data gaps, systematic bias or low information-noise ratio due to instrument failure, persistent clouds from the viewing direction and algorithm limitations.

The major original contributions of this study are as follows: 1) this is the first algorithm for the simultaneous estimations of surface albedo/reflectance and instantaneous AOD by using the atmospheric radiative transfer with surface BRDF modeling for both polar-orbiting and geostationary satellite data; 2) a radiative transfer with surface BRDF models is used to derive surface albedo and directional reflectance from MODIS and SEVIRI observations respectively; 3) extensive validations are made on the comparison between the albedo and AOD retrievals, and the satellite products from other sensors; 4)

the slightly modified algorithm has been adopted to be the operational algorithm of Advanced Baseline Imager (ABI) in the future Geostationary Operational Environmental Satellite-R Series (GOES-R) program for estimating land surface albedo; 5) a framework of using MRT is designed to integrate multiple satellite albedo products at different spatial scales to build the spatially and temporally complete, continuous, and consistent albedo maps as the prior knowledge in the retrieving procedure.

ESTIMATING LAND SURFACE ALBEDO FROM
SATELLITE DATA

By
Tao He

Dissertation submitted to the Faculty of the Graduate School of the
University of Maryland, College Park, in partial fulfillment
of the requirements for the degree of
Doctor of Philosophy
2012

Advisory Committee:

Dr. Shunlin Liang, Chair

Dr. Ralph Dubayah

Dr. Eric Vermote

Dr. Yunyue Yu

Dr. Rachel Pinker

©Copyright by

Tao He

2012

DEDICATION

To my parents.

ACKNOWLEDGEMENTS

I would like to thank my primary advisor Professor Shunlin Liang, for his excellent guidance, caring, patience, and advising me how to become a real researcher with scientific insights. He has always been available to help me solve any crisis. Without his continuous academic and financial support, this research would have been simply impossible. Special thanks to Professor Xiaowen Li and Professor Jindi Wang in Beijing Normal University for advising me through the very beginning and leading me into the world of quantitative remote sensing.

I also wish to express my thanks to my group. This group is always like a big family. I would like to thank Dr. Kaicun Wang and Dr. Dongdong Wang for providing a lot of good and specific guidance and suggestions on my research. I learned a lot in our routine group meeting from the other group members. I really appreciate the help from Xiufang Zhu, Dr. Xiaotong Zhang, and Dr. Sheng Gui on the accommodations when I first came to the U.S. Also thanks to Dr. Hongyi Wu for helping me collect and process a lot of data. I would also like to express my thanks to the other colleagues in my group, including Bo Jiang, Xin Tao, Xiangge Liu, Qinqing Shi, Dr. Wonkook Kim, Dr. Tongren Xu, Dr. Bo Li. It would have been a lonely lab without them.

I would also thank Dr. Yunyue Yu for providing continuous financial support to my research work. Special thanks to the faculty and staff in Beijing Normal University and the Chinese Scholarship Council for the financial support.

Also thanks to Ms. Sharon von Bergener, Pui-Yu Ling, and Dr. Wonkook Kim for the proofreading of this dissertation.

Thanks to my parents. They have always been my supporters, encouraging me with their best wishes.

Finally, I would like to thank my fiancé Danxia Song. She was always there with me through the good time and bad. Without her continuous support, sacrifice, and love, it would have been totally impossible for me to finish my dissertation research in the U.S.

TABLE OF CONTENTS

ACKNOWLEDGEMENTS	iii
TABLE OF CONTENTS.....	v
LIST OF TABLES	viii
LIST OF FIGURES	ix
CHAPTER 1 INTRODUCTION	1
1.1 Literature review	2
1.2 Objectives.....	5
1.3 Structure of this dissertation.....	9
CHAPTER 2 ESTIMATION OF SURFACE ALBEDO FROM MODIS OBSERVATIONS	11
2.1 Methodology	11
2.1.1 Overall framework.....	11
2.1.2 Atmosphere radiative transfer formulation with surface BRF models.....	14
2.1.3 BRF/Albedo modeling.....	18
2.1.4 Integration of BRF and spectral albedo	20
2.1.5 Albedo climatology	23
2.2 Data	25
2.2.1 MODIS TOA reflectance and atmospheric products	25
2.2.2 Atmospheric parameters	26
2.2.3 Ground measurements	27
2.2.4 MODASRVN data set	29
2.2.5 Algorithm implementation	30
2.3 Results and discussions	31
2.3.1 SURFRAD sites.....	31
2.3.2 GC-Net sites	37
2.3.3 Comparisons with MODASRVN data set	42

2.3.4 Summary and conclusions	53
CHAPTER 3 ESTIMATION OF SURFACE ALBEDO FROM SEVIRI OBSERVATIONS	55
3.1 Methodology	55
3.1.1 Optimal estimation	55
3.1.2 Broadband shortwave albedo calculation	55
3.2 Data and retrieving procedure	58
3.2.1 MSG/SEVIRI data	58
3.2.2 Albedo climatology	59
3.2.3 Atmospheric look-up table (LUT)	61
3.2.4 Algorithm implementation	61
3.3 Results and discussion	62
3.3.1 Albedo comparison at IMECC sites	62
3.3.2 AOD comparison with MISR products	73
3.3.3 Albedo map	75
3.4 Summary and conclusions	77
CHAPTER 4 GENERATING CONSISTENT SURFACE ALBEDO PRODUCTS ACROSS SCALES FROM DIFFERENT SATELLITE SENSORS USING A MULTI-RESOLUTION TREE (MRT) METHOD	79
4.1 Introduction	79
4.2 Methodology	79
4.3 Characterization of the data uncertainties of different satellite products	83
4.3.1 Ground measurements	83
4.3.2 Landsat data	83
4.3.3 MODIS albedo products	84
4.3.4 MISR albedo products	85
4.3.5 Inter-comparison at AmeriFlux sites	85
4.4 Results and discussion	91

4.4.1 Data selection and preprocess.....	91
4.4.2 Comparison on data before and after MRT	92
4.4.3 Summary and conclusions	96
CHAPTER 5 CONCLUSIONS	98
5.1 Major findings.....	98
5.2 Major contributions.....	100
5.3 Suggestions for future study.....	103
REFERENCES	105

LIST OF TABLES

Table 2-1 Coefficients used to calculate albedo from BRDF parameters	21
Table 2-2 SURFRAD site information	28
Table 2-3 GC-Net site information	28
Table 2-4 MODASRVN – AERONET site information	30
Table 2-5 Statistics of the retrieved values from this study with comparison to ground measurements over SURFRAD sites	32
Table 2-6 Statistics of the retrieved values from this study with comparison to ground measurements over GC-Net sites.....	40
Table 2-7 Statistics of the retrieved reflectance values from this study with comparison to MODASRVN reflectance products ground measurements over sixteen AERONET sites	50
Table 2-8 Impacts of solar zenith angle and estimation accuracies of AOD on surface reflectance estimations.....	50
Table 3-1 Albedo spectrum samples from USGS library	57
Table 3-2 Information of the chosen IMECC sites.....	63
Table 3-3 Statistics of daily-aggregated albedo estimation accuracies with comparison to ground measurements	67
Table 3-4 Statistics of instantaneous albedo estimation accuracies with comparison to ground measurements	72
Table 3-5 Accuracy assessment of net radiation estimations	73
Table 4-1 AmeriFlux sites	83
Table 4-2 Statistical comparison of different datasets before and after MRT	96

LIST OF FIGURES

Figure 1-1 Overall methodology used in this study.....	7
Figure 2-1 Flowchart of estimating surface albedo and reflectance.....	14
Figure 2-2 Comparison of current polynomial and MODIS equation for angular integration based on Maignan’s BRF kernel model	22
Figure 2-3 Ten-year average white-sky shortwave albedo (a) and its multi-year standard deviation (b) for Julian Day 121 from MODIS albedo product 2000–2009 over North America and Greenland (white color means water/ocean or lack of data).....	24
Figure 2-4 Verification of time series shortwave albedo from MODIS observations in 2005 over seven SURFRAD sites (red diamond: ground measured shortwave albedo; blue diamond: estimated albedo from MODIS observations; green diamond: MODIS 16-day snow-free albedo; black cross: MODIS 16-day snow albedo).....	33
Figure 2-5 Verification of time series total shortwave albedo from MODIS observations in 2003 over six GC-Net sites (red diamond: ground measured visible albedo; blue diamond: estimated albedo from MODIS observations; green diamond: MODIS 16-day albedo).....	38
Figure 2-6 Scattering plots of the 16-day averaged albedo values over nine GC-Net sites	41
Figure 2-7 Verification of time series instantaneous reflectance from MODIS observations in 2005 over six AERONET sites (dark blue circle: estimated red band reflectance; green cross: MODASRVN red band reflectance; red square: estimated near-Infrared band reflectance; light blue triangle: MODASRVN near-Infrared band reflectance) and time series of differences between the retrieved values and MODASRVN data (red square: difference for red band; blue cross: difference for near-Infrared band).....	43
Figure 2-8 Scatter plot of estimated and MODASRVN instantaneous bidirectional reflectance for each of the seven MODIS bands over all the selected AERONET sites during 2005	46
Figure 2-9 AOD estimation accuracies from (a) the proposed algorithm and (b) the MODIS algorithm at MODASRVN sites during 2005.....	52
Figure 3-1 Narrowband-to-broadband conversion accuracy from all the samples.....	57
Figure 3-2 Albedo climatology for day of year (DOY) 065 in SEVIRI projection from ten years’ MODIS shortwave albedo: (a) mean value of MODIS white-sky albedo; (b) standard deviation of MODIS white-sky albedo in ten years	60
Figure 3-3 Comparison of daily-aggregated albedo from estimates in this study and ground measurements with MODIS 5 km products as reference at the IMECC sites.....	63

Figure 3-4 Comparison of instantaneous albedo from estimates in this study and ground measurements with MODIS 5 km products as reference at the IMECC sites	69
Figure 3-5 Histogram of the AOD estimation error.....	74
Figure 3-6 Comparison of shortwave albedo in MSG2/SEVIRI projection on DOY 121, 2005: (a) black-sky albedo estimations from SEVIRI proxy data; (b) reprojected MODIS black-sky albedo products (white color means no data or water).....	76
Figure 3-7 Statistics of the comparisons over the scene	77
Figure 4-1 MRT data structure	80
Figure 4-2 Framework of MRT albedo data fusion from multiple satellite products.....	82
Figure 4-3 Time-series comparisons of different albedo datasets at the AmeriFlux sites	87
Figure 4-4 Evaluation of Landsat data using ground measurements: (a) paired comparison and (b) histogram	90
Figure 4-5 Error comparisons between albedo maps before and after MRT for the three products on DOY 184.....	94
Figure 4-6 Time-series comparison of albedo maps before and after MRT (left-right order: original MISR albedo, MISR albedo after MRT, original MODIS albedo, MODIS albedo after MRT, original Landsat albedo, and Landsat albedo after MRT)	95

CHAPTER 1 INTRODUCTION

Land surface albedo is defined as the ratio of the surface reflected radiation to the incident radiation that reaches the surface, a key geophysical parameter controlling the energy budget in the land-atmosphere interactions (Dickinson 1983). Land surface albedo varies spatially and evolves seasonally, based on solar illumination changes, vegetation cover and growth and human activities such as cutting/planting forests, and slash-and-burn agricultural practices. Sensitivity analysis, for estimating the impacts of albedo uncertainties in climate modeling, shows that the absolute albedo accuracy of ± 0.02 - ± 0.03 equivalent to $\pm 10 \text{ W m}^{-2}$ will result in significant change (e.g., surface temperature, precipitation change) in regional climate simulations (Nobre et al. 1991; Sellers et al. 1995).

Satellite remote sensing is an essential technique in estimating land surface albedo at various spectral, spatial, temporal and angular resolutions. During the last decade, with the emergence of onboard remote sensors, many satellite-generated albedo products have been derived. However, in terms of albedo changes over the globe across a relatively long time period (several years to decades), different trends have been found based on the analyses of different global albedo products. A recent study on the 10-year (2000–2009) Moderate Resolution Imaging Spectroradiometer (MODIS) albedo product showed significant differences among albedo products generated by different satellite data (Zhang et al. 2010). Extensive validations of current shortwave albedo products have been made on the comparison with ground measurements or through the inter-comparison between different satellite products from which the albedo accuracy is reported to be 10% to 28%

(e.g., Liu et al. 2009; Roman et al. 2009; Rutan et al. 2009; Stroeve et al. 2005). This accuracy can be translated into absolute values that are around 0.03 to 0.09. It has also been reported that the absolute bias and Root Mean Square Error (RMSE) of surface albedo increase with the solar zenith and the bias can be larger than 0.06 when solar zenith is beyond 55° (Grant et al. 2000; Liu et al. 2009). Moreover, there is a common problem that many data gaps exist in current albedo products due to either cloud contamination or rapid surface changes. For a typical 16-day compositing period, the global mean annual probability of obtaining enough clear sky observations is 80% combining MODIS onboard Terra and Aqua, and when the temporal window reduces to 10 days, the percentage of data gaps increases to 40% (Roy et al. 2006). Therefore, in order to help understand the science questions, the albedo/reflectance estimation has to be improved.

1.1 Literature review

In order to derive albedo directly from satellite observations, a lot of researchers have been working on various sensors. The Advanced Very High Resolution Radiometer (AVHRR) onboard the National Oceanic and Atmospheric Administration (NOAA) satellite series provided global coverage of albedo product (Strugnell and Lucht 2001). The POLarization and Directionality of the Earth's Reflectances (POLDER) onboard the ADvanced Earth Observing System (ADEOS) and the Multiangle Imaging SpectroRadiometer (MISR) on Terra allowed researchers to use the wide-range of angular information to obtain better understanding of surface reflectance anisotropy (Diner et al. 1999; Leroy et al. 1997). The MODIS albedo product (Schaaf et al. 2002)

provided global coverage of both the black-sky (directional) and white-sky (diffuse) albedo at 1 km spatial resolution, which utilizes multiple spectral bands to derive more accurate broadband albedo estimations. With the development of geostationary satellite sensors, many recent research interests have been focusing on deriving the diurnal changes of surface albedo based on a much wider range of solar illumination direction for the Meteosat Visible and Infrared Imager (MIVIRI)/Meteosat (Ba et al. 2001) and the Spinning Enhanced Visible and Infra-Red Imager (SEVIRI) on board Meteosat Second Generation (MSG) satellites (Geiger et al. 2008; Pinty et al. 2000). Many of the above algorithms are based on searching the optimal estimation of surface albedo and/or Bidirectional Reflectance Distribution Function (BRDF) parameters.

Based on the “dark object” atmospheric correction algorithm in products from satellite sensors such as MODIS and SEVIRI, the retrievals of aerosol distribution and properties over land have shown valuable results. However, the use of this algorithm is restricted to land surface with low reflectance (e.g., water and dense vegetation), while over bright surfaces (snow, desert and urban areas), it often fails to estimate the aerosol information accurately. In other words, this algorithm based on densely vegetated areas is incapable of atmospheric correction to retrieve the surface reflectance and albedo over highly reflective surfaces.

The other problem of separating atmospheric correction and surface BRDF fitting lies in the Lambertian approximation in the radiative transfer procedure. Both atmospheric path and surface directional reflectance will change with the solar and viewing angles (as the scattering path changes). However, a Lambertian surface is usually assumed in

atmospheric correction when surface albedo is not known. Therefore, biases will emerge with “atmospheric corrected surface reflectances” and will further deteriorate the BRDF fitting process. Systematic biases have been found when MODIS reflectance is underestimated/overestimated at high/low zenith angles and bias increases as the wavelength decreases where there is more scattering in the atmosphere (Wang et al. 2010).

An approach was proposed by retrieving the surface reflectance and aerosol optical depth jointly using the optimization method based on SEVIRI data (Govaerts et al. 2010; Wagner et al. 2010). However, in their algorithm, aerosol’s information is retrieved as the average of its daily distribution, and climatology information is not fully utilized to constrain the estimation. Given the finer resolution both on temporal and spatial observations that can be obtained by future satellite sensors, the full use of the broad range of solar angular distribution during a day can be made by adding the aerosol variables to its retrieving procedure.

Many researchers have been focusing on reducing the data gaps and producing spatially and temporally continuous albedo maps based on currently available satellite products. There are two major methodologies to generate this kind of albedo dataset to satisfy the needs in land surface modeling studies. The first one is the physical method which relies on the surface BRDF information. Research has been done using BRDF information from dataset with better angular sampling to convert surface reflectance with reduced angular sampling to albedo (e.g., Jin et al. 2002; Ju et al. 2010; Roy et al. 2008; Shuai et al. 2011). However, these methods assume that there are some homogeneous

pixels with coarser spatial resolution that are corresponding to the finer resolution data for each of the land cover types. Therefore, it is difficult to translate information across scales if no pure pixels can be found at the coarser resolution. The second methodology is using the data-driven models that are directly based on the albedo products by utilizing the spatial and/or temporal information to fill the gaps (e.g., Fang et al. 2007; He et al. 2008; Moody et al. 2005). Most of the existing algorithms that follow the second methodology use only one dataset that will introduce the systematic bias in the final albedo maps. Another issue with the data-driven method is the uncertainty evaluation for the original satellite products which has to be done before the implementation of the data-driven models.

1.2 Objectives

Considering that there are many problems of current available albedo algorithms and datasets in this dissertation, several general scientific questions need to be addressed to improve the understanding of the impacts of albedo change in climate studies that follows the NASA scientific goals: 1) Is it possible to characterize the temporal and spatial changes in surface albedo? 2) Is it possible to produce spatially and temporally consistent albedo products from different satellite sensors? If so, how can it be done? 3) How can we monitor the rapid changes (e.g., snowfall/melt, forest fire and crop harvesting) by the proposed algorithm? Is it possible to improve the estimation of diurnal albedo changes using current satellite data?

The overall objectives of this study include two parts. The first one is to develop a unified framework for estimating surface albedo from different satellite observations.

Based on this framework, we should be able to apply the unified algorithm to both polar-orbiting satellite data and geostationary satellite data. The proposed surface albedo algorithm should generate consistent albedo estimations from different satellite data and be able to provide accurate estimations over all kinds of surface types including vegetated surfaces and non-vegetated surfaces. Another requirement of this algorithm is that it should be capable of capturing rapid changes in surface albedo caused by events such as ephemeral snow, crop harvesting, and forest fires. The understanding of diurnal changes in surface albedo mainly caused by solar illumination and surface anisotropy should also be considered in this algorithm framework.

The other overall objective is to improve albedo product by integrating multiple satellite datasets. In one aspect, differences have been found among different satellite datasets and some are beyond the accuracy requirements for climate change and land surface modeling studies. A set of temporally and spatially complete and continuous albedo products across different scales should be generated through the data fusion method that can improve the accuracy estimations. Also, the methodology should be applicable to generate global albedo products. In the other aspect, this dataset can also serve as the prior information in the instantaneous estimation of surface albedo and aerosol. In particular, the surface albedo estimating procedure in the first part of this dissertation will need this background information to produce reliable and stable results.

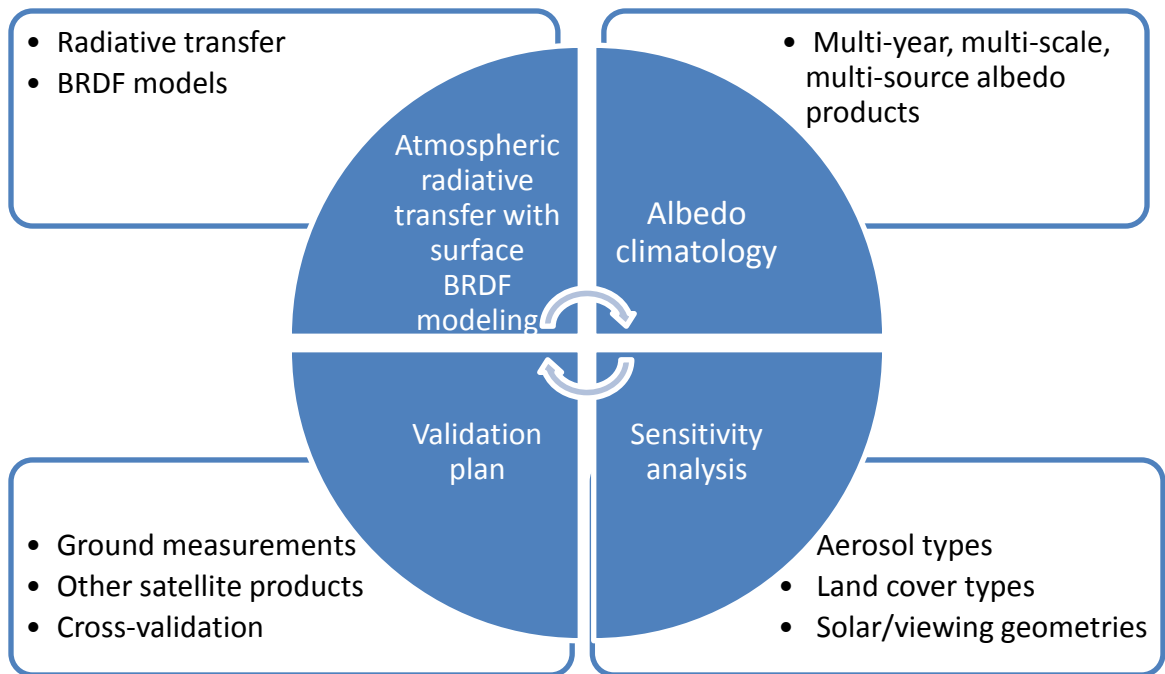


Figure 1-1 Overall methodology used in this study

To achieve the goal, several major tasks are proposed in this study (Figure 1-1):

First, based on similar principles mentioned above, this study proposes an improved algorithm using polar-orbiting and geostationary observations to account for surface anisotropy considering temporal variations of aerosol optical depth for better estimating the surface albedo. The atmospheric radiative transfer procedure with surface BRDF modeling is the major framework of retrieving surface albedo from MODIS and SEVIRI observations. This part of study consists of forming the main framework by introducing the atmospheric radiative transfer equation with the surface BRDF modeling, and then integrating broadband albedo from spectral BRDF.

Second, a specific validation plan is made assessing the performance of the final operational estimating algorithm. Various data sets used for validation will be collected

and compared with the retrievals from the proposed algorithm. The validation data sets include ground measurements and satellite albedo products with improved atmospheric correction. Inter-comparison between different datasets is carried out as well. Different validation data sets have their own characteristics in terms of spatial representation and temporal continuity, and therefore will help improve the retrieving procedure under various circumstances.

Third, sensitivity analysis will be carried out to assess the performance of the overall estimating procedure. Both the atmospheric radiative transfer and the surface BRDF modeling will be examined under different scenarios, including the aerosol, land cover type, solar/viewing geometries.

Finally, in order to produce spatially and temporally complete and continuous albedo/reflectance products, the albedo climatology needs to be built beforehand. Data across various spatial scales and temporal resolutions will be used and analyzed to generate the albedo climatology maps based on different land cover types and latitudes. Researchers have been focusing on generating albedo climatology through multiyear satellite data (e.g., Fang et al. 2007; Moody et al. 2007; Moody et al. 2008); however, their products are based on only one source of satellite data so the bias from this satellite estimation algorithm will remain in their products. Moreover, data with an old version and limited temporal range of their study also constrain the application for long-term global studies. In this part, with its ability to make use of multiple datasets, the multi-resolution tree (MRT) method will be employed to build the albedo maps together with the uncertainty based on MODIS, MISR, Landsat Thematic Mapper (TM), and Enhanced

Thematic Mapper Plus (ETM+) data. The albedo maps will help understand the albedo spatial distribution and temporal evolution on both global and regional scales, which therefore can be used as constraints in the albedo retrieving procedure.

1.3 Structure of this dissertation

Chapter 2 introduces the improved methodology of simultaneously estimating surface albedo and instantaneous aerosol optical depth (AOD) from MODIS observations. Theoretical basis and formulations are given in this chapter before the introduction of various ancillary datasets including the atmospheric variables and the albedo climatology maps. Extensive validations are given as well as the error analysis to evaluate the performance and the generate accuracy of both albedo and AOD estimations.

Chapter 3 presents the procedure of applying the proposed algorithm over SEVIRI observations. Following the ancillary data preparation, the algorithm implementation is illustrated on how generate albedo and AOD estimations. Site validations are given over some European ground stations. Inter-comparison is made between the retrievals from this study and other satellite products.

Chapter 4 proposes a new method of albedo data fusion using MRT to generate continuous and consistent albedo maps at different spatial scales. The uncertainties of the original satellite products are evaluated through comparison with ground measurements and inter-comparison among different satellite products. After that, the implementation of MRT will be introduced and the improved results are shown in time-series comparisons.

Chapter 5 summarizes the major findings and contributions of this dissertation. Conclusions are made on the general performance of the two proposed methodologies on improving surface albedo products. Future work is planned based on the merits and shortcomings of current preliminary results.

CHAPTER 2 ESTIMATION OF SURFACE ALBEDO FROM MODIS OBSERVATIONS

2.1 Methodology

2.1.1 Overall framework

Currently, to obtain the broadband shortwave albedo estimations most albedo retrieving algorithms require three major procedures: atmospheric correction, surface Bidirectional Reflectance Factor (BRF) fitting, and narrowband-to-broadband conversion. With each procedure implemented separately, errors propagate from the atmospheric correction to the final broadband albedo estimates irrespective of the algorithms used. To avoid these increasing errors, it is advantageous to combine those procedures. In the framework of this proposed MODIS surface albedo estimation algorithm, several components are included: atmospheric radiative transfer process with anisotropic reflectance of land surface, surface albedo/BRF modeling, and albedo climatology.

Based on the available prior information on albedo and the satellite observations, the unknown variables (e.g., the surface BRF kernel parameters, AOD) are determined in the context of the least-square approach through the minimization of the cost function:

$$J(X) = \left(A(X) - A^{Clim} \right) B^{-1} \left(A(X) - A^{Clim} \right) + \left(R^{Est}(X) - R^{Obs} \right) O^{-1} \left(R^{Est}(X) - R^{Obs} \right) + J_c \quad (2-1)$$

Here, X denotes the unknown variables to be estimated in one sliding window and it includes the surface BRF model parameters and AOD. Two general assumptions are made here to reduce the complexity of the retrieving procedure and to generate the stable

estimates as well: 1) the surface BRF shape is stable within the sliding window; 2) the aerosol type and its properties (e.g., Angström exponent) do not change within the sliding window, but AOD varies from time to time. Since the predefined aerosol types are used in this study, the intrinsic properties for each of the aerosol types are not part of the unknown variables to be estimated. Then, X can be written in the following form:

$$X = [P_1, P_2, \dots, P_{NB}, AOD_1, AOD_2, \dots, AOD_{NO}]^T, \quad (2-2)$$

NB is the number of spectral bands from a certain satellite sensor, NO is the number of cloud-free observations involved in the inversion, P_i $i \in [1, NB]$ is a set of BRF model parameters (e.g., for kernel models, one set of P_i refers to three parameters: f_{iso} , f_{vol} , and f_{geo}), AOD_j $j \in [1, NO]$ is the AOD value for the corresponding observation j , and $R_{i,j}^{Obs}$ and $R_{i,j}^{Est}$ refer to the observed and modeled TOA reflectance for a band and a given set of geometries (e.g., solar angle and viewing angle), respectively.

$R_{i,j}^{Obs}$ are obtained from satellite observations. However, $R_{i,j}^{Est}$ values need to be derived by a forward simulation based on the radiative transfer procedures from both surface and atmosphere components. For this purpose, the use of the atmospheric radiative transfer formulation with surface BRF is recommended. In this manner, $R_{i,j}^{Est}$ can be expressed using both the surface properties (e.g., albedo and BRF) and the atmospheric properties (e.g., AOD, water vapor, and ozone).

$A(X)$ is the calculated broadband surface albedo, and A^{Clm} is the prior information of broadband albedo from albedo climatology. Albedo climatology is used to constrain the retrieving procedure of surface albedo and reflectance. It describes the major seasonal and inter-annual changes in the surface signature. At this stage, multiyear satellite albedo products are collected to form the spatially and temporally continuous and complete albedo climatology. B and O are the error matrices for the climatology and the fitting of satellite remotely sensed data, respectively. As the uncertainties for both the climatology and the data fitting involve a large number of components, most of which are difficult to estimate, two simplifications need to be made here: 1) the albedo climatology used here is unbiased, and B is calculated from the uncertainty of the albedo climatology using multi-year satellite albedo products; 2) reflectances are band-independent and the diagonal components of O are determined by the magnitude of spectral reflectance multiplied by the contribution to the shortwave albedo for each band. J_c is the penalty function accounting for the validity of BRF values calculated from the estimated BRF parameters, etc. For any particular geometry, when the reflectance or albedo calculated from the BRF model is negative or greater than one, J_c is set to a large value (e.g., 100). In addition, all the BRF model parameters are constrained to be non-negative, in particular for the kernel model used in this study. To minimize the cost function $J(X)$, the optimal values of X having physical meaning need to be found. However, owing to the non-linearity of the atmospheric radiative transfer equations and the dimensions of the unknown variables, it is always difficult to find the optimal values that can minimize the cost function globally. The algorithm of the shuffled complex evolution (SCE) (Duan et al. 1993; Duan et al. 1994) is used here to obtain physically reasonable global optimal

estimations based on albedo climatology and surface BRDF model priors. The overall framework is shown in Figure 2-1.

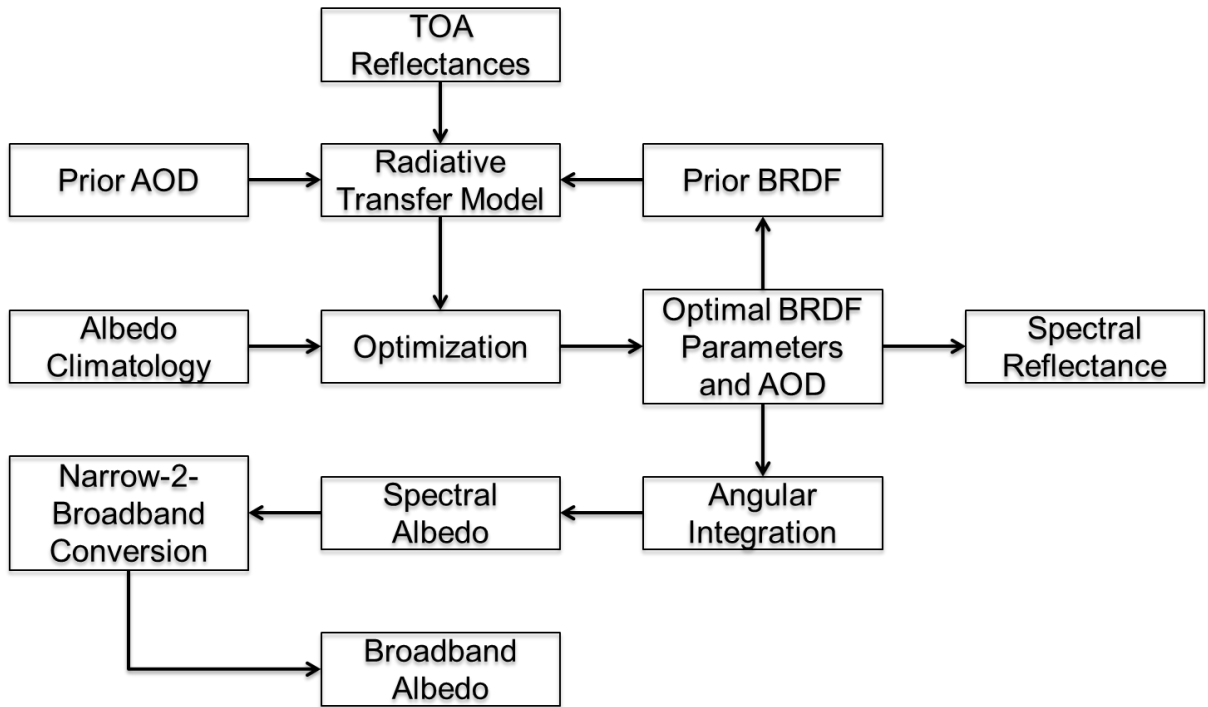


Figure 2-1 Flowchart of estimating surface albedo and reflectance

2.1.2 Atmosphere radiative transfer formulation with surface BRDF models

The satellite-observed radiance contains information from both the atmospheric components (aerosol, water vapor, ozone, etc.) and the land surface reflectivity. Aerosol properties, such as optical depth, size distribution, and refractive index have a great impact on the representation of land surface information in the satellite observations. Instead of using a “dark object” algorithm, it is advantageous to combine the retrieval of both the AOD and the surface BRDF parameters from the TOA reflectance in the radiative

transfer process. In order to do so, the relationship between TOA reflectance, AOD, and surface BRF needs to be established.

Theoretically, the overall procedure proposed here is similar to the proposed algorithm based on the MSG/SEVIRI data (Govaerts et al. 2010; Wagner et al. 2010), which retrieves the daily aerosol and surface reflectance simultaneously. Since the overall retrieving procedure is underdetermined, which means there are fewer observations than unknown variables, an assumption needs to be made, as follows: as the surface properties change slowly, the surface BRF shape is assumed to be invariant within a sliding window (7 days or less). A smaller the window size results in better capability over a rapidly changing surface. Cloud-free observations are collected within the sliding window. However, the number of collected observations should be limited in order to reflect the rapid change in the surface. Only those observations that are closest to the center of the sliding window are used in one procedure to retrieve surface BRF and AOD simultaneously. Details on how the minimum number of cloud-free MODIS observations can be determined are discussed in Section 2.2.1. Given the surface BRF and AOD retrievals, the instantaneous “blue-sky” albedo can be calculated based on the black-sky and white-sky albedo using diffuse skylight ratio:

$$\alpha_{blue} = f_{dif} \cdot \alpha_{ws} + (1 - f_{dif}) \cdot \alpha_{bs} \quad (2-3)$$

Here, α_{blue} , α_{bs} , and α_{ws} are the blue-sky, black-sky, and white-sky albedo, respectively, and f_{dif} is the diffuse skylight ratio.

Based on the comparison with the SEVIRI estimating procedure, the proposed algorithm for MODIS has several improvements in terms of coupling the land-atmosphere radiation interaction, as follows:

1) The AOD is treated as non-identical throughout the retrieving temporal window. Since satellite observations within the sliding window can sometimes have a broad range of solar/viewing zenith/azimuth angles, assuming only that the aerosol does not change within the retrieving temporal window does not fully utilize the abundant angular information that can capture the directional variation in the surface reflectivity. Moreover, this assumption is not valid over such a long time period (one day or more, etc.) and can bias the atmospheric correction at large angles.

2) Many forward models have been proposed recently to approximate different components of radiation fluxes at the media boundary. These models include various two-stream methods (Meador and Weaver 1980) and four-stream methods (Liang and Strahler 1994, 1995). However, although two-stream models are time-efficient, their accuracy is low. Instead of using the radiative transfer model with a two-stream approximation, this study adopted a simple and fast 3D formulation of radiative transfer by incorporating the surface BRDF models (Qin et al. 2001). The authors state that this approach does not introduce any approximation into the formulation, and their numerical experiments demonstrate that this formulation is very accurate (Qin et al. 2001). The TOA reflectance ρ_a is expressed as

$$\rho_a(\Omega_s, \Omega_v) = \rho_0(\Omega_s, \Omega_v) + \frac{T(\Omega_s)R(\Omega_s, \Omega_v)T(\Omega_v) - t_{dd}(\Omega_s)t_{dd}(\Omega_v)|R(\Omega_s, \Omega_v)|\rho}{1 - r_{hh}\rho} \quad (2-4)$$

In the equation, $\Omega_s \in (\theta_s, \phi_s)$ is the solar incoming direction and $\Omega_v \in (\theta_v, \phi_v)$ is the viewing direction. There are two groups of coefficients in the above equation that are independent of each other: atmosphere-dependent and surface-dependent coefficients. The coefficients in each group represent the inherent properties of either the atmosphere or the surface and can be regarded as separate groups.

For the atmosphere, $\rho_0(\Omega_s, \Omega_v)$ is the atmospheric reflectance associated with path radiance, ρ is the atmospheric spherical albedo, and $T(\Omega_s)$ and $T(\Omega_v)$ are defined as combinations of direct transmittance (t_{dd}) and directional-hemispheric (or hemispheric-directional) transmittance (t_{dh} and t_{hd}), respectively. For the algorithm implementation, it is usually very time-consuming to calculate each element in the transmittance matrices together with the atmospheric reflectance. To expedite the computation for the forward modeling, those atmospheric variables are pre-calculated by simulation using the radiative transfer software 6S (Kotchenova et al. 2006) and stored in the look-up table (LUT). Details on the design of the LUT are given in Section 2.2.2.

For the surface, the reflectance matrix is defined as

$$R(\Omega_s, \Omega_v) = \begin{bmatrix} r_{dd}(\Omega_s, \Omega_v) & r_{dh}(\Omega_s) \\ r_{hd}(\Omega_v) & r_{hh} \end{bmatrix}, \quad (2-5)$$

where $r_{dd}(\Omega_s, \Omega_v)$ is the bi-directional reflectance, $r_{dh}(\Omega_s)$ is the directional-hemispherical reflectance (also called black-sky albedo), $r_{hd}(\Omega_v)$ is the hemispherical-directional reflectance (which is equal to $r_{dh}(\Omega_v)$ under the reciprocity law), and r_{hh} is bi-hemispherical reflectance (also called white-sky albedo).

The determinant $|R|$ is easily calculated as

$$|R(\Omega_s, \Omega_v)| = r_{dd}(\Omega_s, \Omega_v)r_{hh} - r_{dh}(\Omega_s)r_{hd}(\Omega_v), \quad (2-6)$$

It is evident that as long as the surface BRF is known, the surface reflectance matrix can be determined.

2.1.3 BRF/Albedo modeling

BRF models quantify the angular distribution of radiance reflected by an illuminated surface. Various models have been proposed to simulate or capture the anisotropic characteristics of the land surface (Liang 2007; Widlowski et al. 2007), including computer simulation models (Gastellu-Etchegorry et al. 2004), physical models using the canopy radiative transfer process (Kuusk 1995a, b; Pinty et al. 2006), and (semi)empirical models based on various approximations of the radiative transfer process (Li and Strahler 1992; Rahman et al. 1993; Roujean et al. 1992). The quality of these models can be evaluated either through a comparison with simulations by other models of higher complexity, or through a comparison with measurements. In order to expedite the inversion procedure, complex computer simulation and physical models are not considered to be the optimal BRF model herein. Pokrovsky and Roujean (2003) made

comparisons based on different kernel-based BRDF models and found that the Li-Sparse and Roujean models perform best when fitting the bidirectional reflectances. Maignan et al. (2004) evaluated a set of analytical models based on POLDER measurements and proposed an improved Ross-Li kernel model by adding an angular factor based on Breon's finding (2002) to better account for the "hot spot" effect, which occurs when the viewing and illumination directions coincide. By introducing the multiple scattering between the canopy and the soil, and the relationship between the soil moisture and the soil reflectance into the Ross-Li kernel models, a recent method was proposed to build an angular and spectral kernel model (Liu et al. 2010). However, this method requires prior knowledge of soil moisture, which is difficult to obtain and therefore limits its operational application. Therefore, in this study, the improved Ross-Li kernel model proposed by Maignan et al. (2004) and Breon et al. (2002) is used to account for the surface anisotropic reflectance. It is given by

$$R(\theta_s, \theta_v, \varphi) = f_{iso} + f_{vol} K_{vol}(\theta_s, \theta_v, \varphi) + f_{geo} K_{geo}(\theta_s, \theta_v, \varphi), \quad (2-7)$$

where θ_s , θ_v , and φ are the solar zenith, view zenith, and relative azimuth angles, respectively. $K_{vol}(\theta_s, \theta_v, \varphi)$ and $K_{geo}(\theta_s, \theta_v, \varphi)$ are simplified kernels based on physical or empirical approximations over the specific illumination and viewing geometries. K_{vol} is based on the approximation of the radiative transfer within the canopy, whereas K_{geo} is based on the distribution of the size and the orientation of surface canopies within a certain area. f_{iso} , f_{vol} and f_{geo} are the coefficients for those kernels. Further details can be found in the referenced studies.

For the bias of the MODIS reflectance products, it has been reported (Wang et al. 2010) that the derived reflectance is underestimated at high solar or view zenith angles but is overestimated at low solar or view zenith angles. When the solar zenith angle increases beyond 70° , increases in the negative bias and the RMSE compared to the ground measurements have also been identified (Liu et al. 2009). The problem of the separation of atmospheric correction and surface BRF modeling could be one possible reason for this bias, which can be solved using the method proposed in this study. A recent study (Liu et al. 2012) suggests that the possible underestimation of MODIS albedos may come from the insufficient angular sampling of the surface anisotropy. In order to resolve this second problem, one method is introduced here to correct the change in albedo caused by the illumination geometry and the diffuse skylight impacts, especially for a solar zenith angle larger than 70° . The method is based on the dependence of surface albedo on the solar zenith angle over snow-free land surfaces and uses the intensive observations of surface shortwave fluxes made by the U. S. Department of Energy Atmospheric Radiation Measurement (ARM) Program and SURFRAD Network (Yang et al. 2008).

2.1.4 Integration of BRF and spectral albedo

An angular integration of BRF over all the viewing angles is required to calculate the albedo because only the directional reflectance can be calculated directly from the BRF models. Instead of directly calculating the integral, the same method proposed in the MODIS albedo estimating procedure (Schaaf et al. 2002) is used, based on the improved

kernel models above, fitting the black-sky albedo with a polynomial function. In this study, a higher order of the polynomial function was used to achieve better accuracy:

$$\alpha_{bs}(\theta_s) = f_{iso}(a_0 + a_1\theta_s + a_2\theta_s^2 + a_3\theta_s^3) + f_{vol}(b_0 + b_1\theta_s + b_2\theta_s^2 + b_3\theta_s^3) + f_{geo}(c_0 + c_1\theta_s + c_2\theta_s^2 + c_3\theta_s^3), \quad (2-8)$$

where θ_s is the solar zenith angle, and a , b , and c are the regression coefficients.

Similarly, the white-sky albedo can be computed by using the equation

$$\alpha_{ws} = f_{iso}a_w + f_{vol}b_w + f_{geo}c_w \quad (2-9)$$

The regression coefficients are listed in Table 2-1. Figure 2-2 shows the fitting capability of the black-sky albedo using the polynomial function (Eq. (2-8)). The calculated black-sky albedo from the regression coefficients matches the BRF-integrated albedo very well. Contrastingly, simply using the MODIS equations and coefficients will result in a 0.02 albedo difference in this case when the solar zenith angle is greater than 80°. Experiments on extending the polynomial function to a higher order show no significant improvement in the BRF/albedo fitting accuracy.

Table 2-1 Coefficients used to calculate albedo from BRF parameters

Variable	a_0	a_1	a_2	a_3	b_0	b_1	b_2	b_3
Value	1.0	0	0	0	-0.0374	0.5699	-1.1252	0.8432
Variable	c_0	c_1	c_2	c_3	a_w	b_w	c_w	
Value	-1.2665	-0.1662	0.1829	-0.1489	1.0	0.2260	-1.3763	

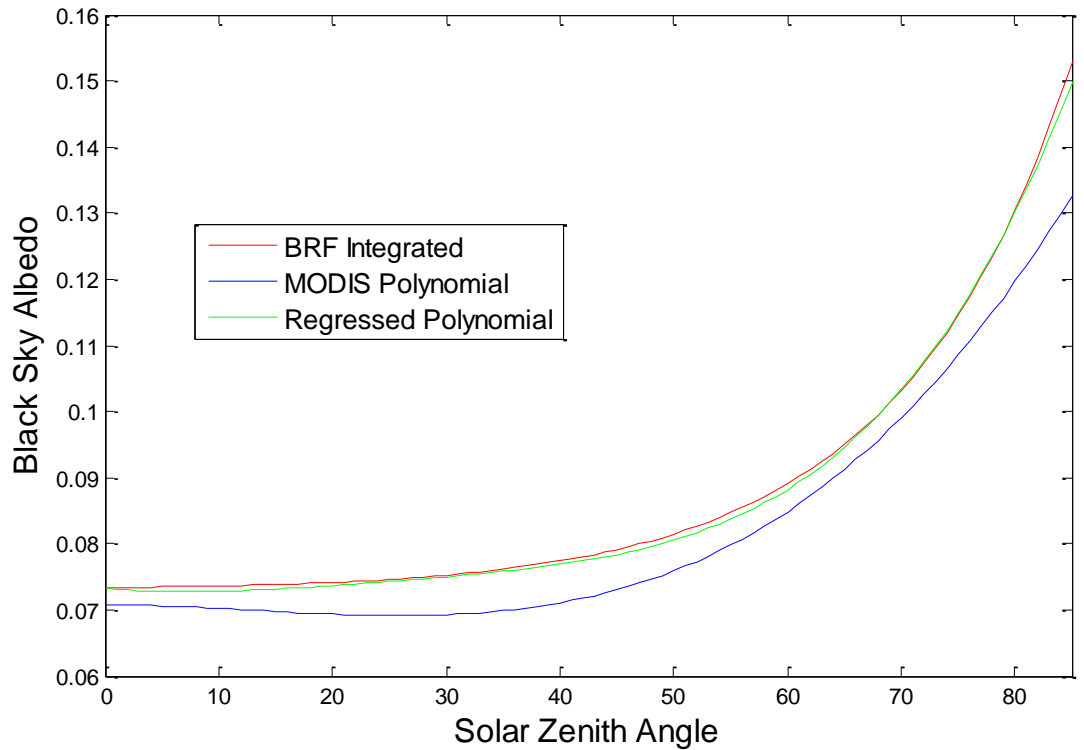


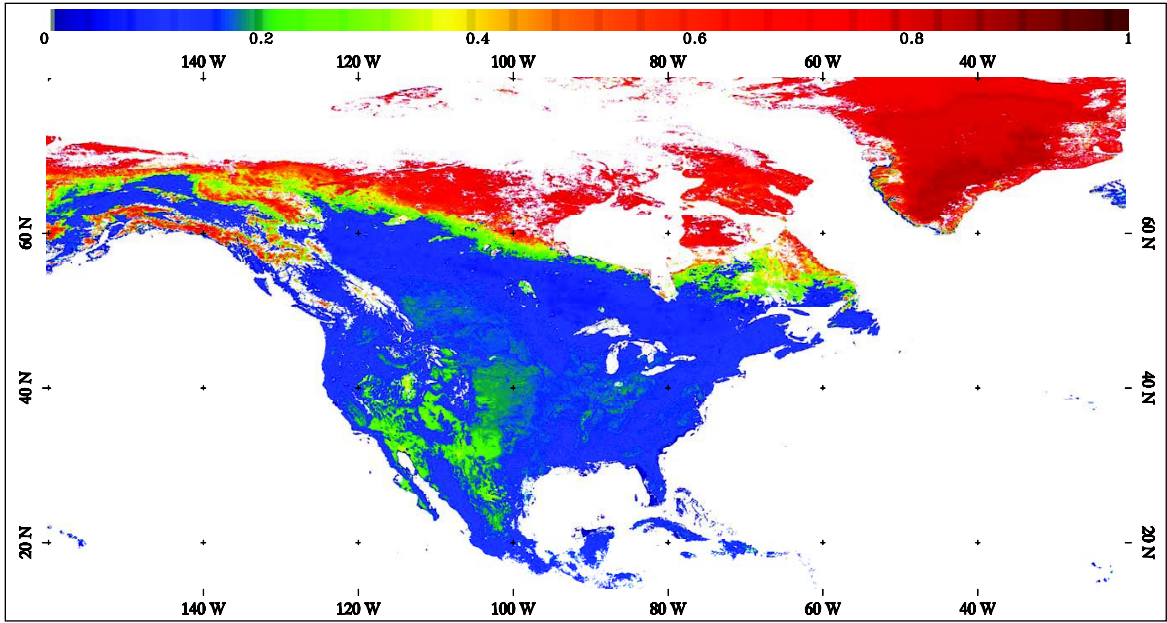
Figure 2-2 Comparison of current polynomial and MODIS equation for angular integration based on Maignan’s BRF kernel model

Most of the current land surface models and weather forecast applications use an albedo that can account for a wide range of wavelengths (e.g., total shortwave, total visible, and total near-infrared band). However, the BRF models are designed to carry out the calculation of all the components defined in the reflectance matrix (Eq. (2-5)) individually for each spectral band. Moreover, the distribution of the downward solar radiation varies significantly with the change in aerosol density, precipitable water vapor content, ozone, and other profiles of atmospheric variables. As a result, the reflected solar radiation of the surface changes when the definition of the albedo changes. The spectral albedo needs to be converted into broadband albedo based on the spectral albedo characteristics over different surfaces and different atmospheric conditions. An approach for establishing the linear relationship between broadband albedo and the spectral value

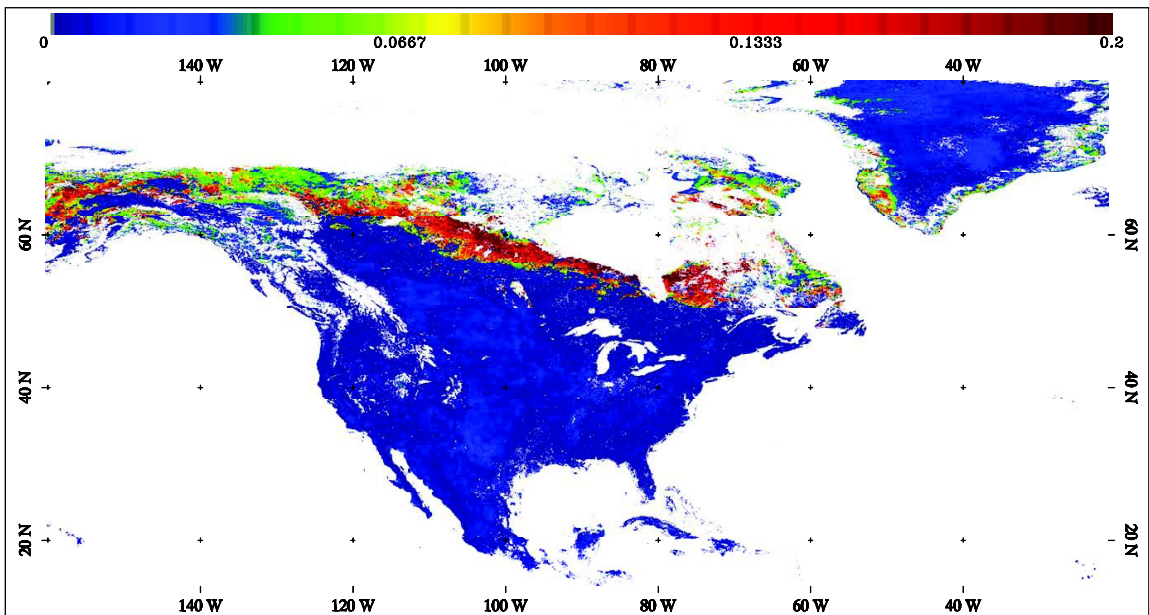
from each band has been proposed by Liang (2001). In the present study, the conversion equations are adopted from Liang (2001) and Stroeve et al. (2005), the latter providing an improved equation to derive the shortwave broadband albedo for snow-covered surfaces.

2.1.5 Albedo climatology

The climatology of the surface broadband albedo reflects both the seasonal and the inter-annual changes in the surface status. It is very important because it places constraints on the BRF retrieving procedure. The TOA radiance/reflectance observed by the satellite sensor can be biased by the calibration error or an inaccurate estimation of atmospheric components (e.g., ozone and water vapor). “Prior” information is much more reliable when its associated (co)variance is small whereas the calibrated TOA observations contain a large amount of noise. The “prior” can help the optimization procedure to achieve reasonable global optimal estimations. However, owing to persistent and transient cloud contamination as well as ephemeral and seasonal snow cover, most satellite albedo products contain a large number of gaps for a snow-free land surface. In this study, 10 years (2000–2009) of MODIS broadband albedo products and the corresponding quality control data (for detailed information please refer to the MODIS website) were collected. In the quality control data set, the broadband albedo values are identified as “good quality” and “other quality”. To avoid the effects (e.g., cloud contamination and low BRF fitting accuracy), only “good-quality” data were used to calculate the 10-year mean of the broadband albedo over North America and Greenland. The standard deviation for multiyear broadband albedo data was calculated for the same time of year to reflect the inter-annual variation in albedo over the same location.



(a)



(b)

Figure 2-3 Ten-year average white-sky shortwave albedo (a) and its multi-year standard deviation (b) for Julian Day 121 from MODIS albedo product 2000–2009 over North America and Greenland (white color means water/ocean or lack of data)

White-sky albedo products were used in this study with no solar zenith dependence (an example for Julian day 121 is shown in Figure 2-3). Many gaps can be found over west and north Canada. When the latitude is greater than 50° , both the mean and variation of the shortwave albedo values become very large. This indicates that the snow situation over these areas changes annually at this time of year, whereas over central North America and Greenland, the surface is quite stable. The multiyear mean of shortwave albedo is used as the climatology data in Eq. (2-1) and the one-year standard deviation is used as an approximation to the uncertainty of the climatology. In this study, a simple method was used to build the albedo climatology. Generating complete and continuous spatial-temporal albedo climatology is beyond the scope of this study.

2.2 Data

2.2.1 MODIS TOA reflectance and atmospheric products

The sensor of MODIS has seven spectral bands within the shortwave range that can be used for land applications. The MODIS Level 1B (Collection 5) calibrated radiance data, together with their corresponding geo-location data, were collected and converted into the TOA bidirectional reflectances. According to Eq. (2-4), the total unknown variables to be estimated include three BRDF kernel parameters for each spectral band and AOD for each observation time given that the aerosol type is known from MODIS product. For example, for n clear observations cumulated within a sliding temporal window (the surface is assumed to be stable in the temporal window), the total number of unknown variables is $3 \times 7 + n$. Here, to make the whole procedure invertible, the number of variables should be no more than the number of observations: $3 \times 7 + n \leq n \times$

7. Therefore, n should be at least four, which implies that four sets of MODIS clear sky TOA reflectances (one set = seven bands) need to be collected within the temporal window to make it possible to retrieve the unknown variables. Since it is not always easy to obtain the angular sampling suitably within such a short temporal window, the BRDF parameter retrievals from the preceding day were used as “first guess” constraints to limit the retrievals for the current procedure. MODIS level 2 cloud mask products (MOD35_L2/MYD35_L2) were used to screen cloudy observations. As a supplement to Terra MODIS, the one onboard Aqua (launched 2002) provides TOA observations as well. Commonly, over a mid-latitude location, there are two or three overpasses a day, combining data from Terra and Aqua. Considering that around two-thirds of the observations are under cloudy conditions over most of North America, the length of the temporal sliding window is usually less than seven days in order that a sufficient number of clear sky observations can be obtained for the retrieving procedure. During the winter season, the window size can be slightly smaller when the sky tends to be clearer than in other seasons. This is a great advantage for monitoring the rapid surface changes, especially for snow conditions.

2.2.2 Atmospheric parameters

To implement a forward simulation of TOA bidirectional reflectances using Eq. (2-4), parameters such as path reflectance, both upward and downward direct/diffuse transmittance and spherical albedo need to be calculated. In addition to simulating the TOA signal, the diffuse light ratio needs to be generated to produce the actual surface albedo considering the redistribution of solar illumination caused by aerosol scattering.

Instead of an online calculation of these atmospheric functions on a point basis for every observation time, which will be computationally expensive, they were prepared as a function of the viewing geometries and AOD. The 6S software (Kotchenova et al. 2006) was used for the calculation of the LUT. It enables accurate simulations of satellite observation while accounting for elevated targets, the use of anisotropic and Lambertian surfaces, and the calculation of gaseous absorption based on the method of successive orders of scatterings approximations (Kotchenova et al. 2006). In this study, the following values were used as the entries in the 6S simulations: solar zenith angle (0° – 75° ; at 5° intervals), viewing zenith angle (0° – 75° ; at 5° intervals), relative azimuth angle (0° – 180° ; at 10° intervals), AOD at 550 nm (0.01, 0.05, 0.1, 0.15, 0.2, 0.3, 0.4, 0.6, 0.8, and 1.0) for five predefined aerosol types in 6S software (urban, biomass, continental, desert, and maritime). Through the forward simulation, for each particular solar/viewing geometry and aerosol loading (AOD at 550 nm), 6S generates path reflectance, upward and downward transmittances, spherical albedo, diffuse skylight ratio, and AOD for each of the seven MODIS bands respectively.

2.2.3 Ground measurements

The ground observational data used for this study were obtained from the SURFRAD website and the GC-Net web site. Details about instruments, data processing, and quality controls can be found on their websites.

For vegetated areas, the SURFRAD instruments measure surface downward and upward radiation. Based on the availability and quality of both satellite data and ground observations, this study used the SURFRAD observations at several sites (names and

locations are listed in Table 2-2) for the year 2005. The SURFRAD sites provide the shortwave upward flux together with the downward global flux every three minutes. The “ground truth” blue-sky albedo was calculated by averaging the ratio between the upward and downward radiation within a 15-min range before and after the satellite observing time to reduce the ground measurement errors and temporal/partial cloud effects. In addition to radiation flux data, AOD measurements are also available at these sites. Aerosol information is measured for five channels (415, 500, 614, 670, 868, and 940 nm) at a 2-min temporal resolution. In order to make comparisons with AOD retrievals in this study, the ground measurements were converted to AOD at 550 nm with the Angström exponent data provided and then averaged within ± 10 -min range of the MODIS overpass time.

Table 2-2 SURFRAD site information

Site Name	Location	Land Cover Type
Bondville, IL	40.05N, 88.37W	Crop
Boulder, CO	40.13N, 105.24W	Grass
Desert Rock, NV	36.63N, 116.02W	Open Shrub
Fort Peck, MT	48.31N, 105.10W	Grass
Goodwin Creek, MS	34.25N, 89.87W	Grass & Forest
Penn State, PA	40.72N, 77.93W	Crop
Sioux Falls, SD	43.73N, 96.62W	Grass

Table 2-3 GC-Net site information

Site Name	Location	Site Name	Location
Swiss Camp	69.57N, 49.30W	NASA-SE	66.48N, 42.50W
JAR1	69.50N, 49.68W	NASA-E	75.00N, 30.00W
JAR3	69.40N, 50.31W	GITS	77.14N, 61.10W
Summit	72.58N, 38.50W	DYE-2	66.48N, 46.28W
Saddle	66.00N, 44.50W		

Ground radiation measurements over Greenland are regularly collected at GC-Net. This dataset provides unique and extensive observations, which can help verify the validity of this proposed algorithm over snow-covered surfaces. Shortwave upward and downward radiation at the surface is observed on an hourly basis. To account for the reduced sensitivity of the GC-Net instruments, ground data were preprocessed using the method proposed by Stroeve et al. (2005). The “ground truth” blue-sky albedo is calculated based on that. Thirteen sites were chosen in this study according to data availability and data quality during the year 2003 (information listed in Table 2-3).

2.2.4 MODASRVN data set

Due to the limited spatial representation of ground measurements, it is always difficult to validate satellite pixel-based surface albedo estimations solely through comparison with ground measured data, especially when the pixel is not quite homogeneous. Using other satellite-derived data sources can help verify the algorithm estimations. Based on the ancillary information on aerosol and water vapor from the Aerosol Robotic Network (AERONET) sites, a set of surface albedo and reflectance data is retrieved through an independent atmospheric correction with the Ross-Li BRDF kernel models using TOA data from MODIS observations (Wang et al. 2009). The MODASRVN data products from the year 2000 onwards are stored with the AERONET site in the center of the image covering $50 \times 50 \text{ km}^2$ at 1-km resolution.

According to the location, land cover type, and MODASRVN data availability from the AERONET sites, sixteen sites were chosen in this study for the validation of the estimated surface reflectance (see detailed information in Table 2-4). Similar to the

ground measurement section, data for the year 2005 for MODASRVN and MODIS L1B TOA observations were collected and processed.

Cloud-screened AOD data from AERONET are available all year round at minimum intervals of 3-min for almost all the MODASRVN sites. Around 16 channels of AOD measurements are provided from 340 nm to 1640 nm. Data were converted into AOD at 550 nm for comparison. Similar to the data processing for SURFRAD AOD, ± 10 -min average AOD values were calculated.

Table 2-4 MODASRVN – AERONET site information

Site Name	Location	Land Cover	Site Name	Location	Land Cover
Bondville	40.05N, 88.37W	Crop	Mexico City	19.33N, 99.18W	Urban
GSFC	38.99N, 76.84W	Forest & Urban	Rimrock	46.49N, 116.99W	Grass
Missoula	46.92N, 114.08W	Grass & Urban	MD Science Center	39.28N, 76.62W	Urban
SERC	38.88N, 76.50W	Forest & Wetland	KONZAEDC	39.10N, 96.61W	Grass
CARTEL	45.38N, 71.93W	Grass & Urban	BSRNBAO Boulder	40.05N, 105.01W	Grass
Bratts Lake	50.28N, 104.70W	Crop	Railroad Valley	38.50N, 115.96W	Grass
Sioux Falls	43.76N, 96.63W	Grass	Frenso	36.78N, 119.77W	Urban
Egbert	44.23N, 79.75W	Crop	Halifax	44.64N, 63.59W	Urban

2.2.5 Algorithm implementation

As mentioned in the previous section, MODIS TOA reflectances were calculated from the 1km MODIS L1B dataset and collected within the sliding temporal window. Cloud pixels were excluded based on the MODIS cloud mask product. Following the

flowchart in Figure 2-1, all the clear sky observations were used in the retrieving procedure as long as they satisfied the minimum number required. The aerosol type was adopted from the MODIS aerosol product (MOD04/MYD04). Monthly statistics of AOD were calculated from the ground aerosol observations (Augustine et al. 2008; Holben et al. 2001) and used as a “first guess” in the retrieving process to constrain the AOD retrievals. BRF kernel parameters from the preceding day supported the radiative transfer and optimization process by providing the “first guess” BRF shape. This prior information can also help reduce the uncertainty that may be introduced by the insufficient angular sampling of the TOA signal during a short period of time. The SCE algorithm then searched for the optimal kernel parameters and instantaneous AODs, which best fit the satellite observations and the albedo climatology considering the error distributions for both parts of Eq. (2-1). The retrieved BRF models can generate bidirectional reflectances for all the seven spectral bands as well as spectral black-sky/white-sky albedos through angular integration based on Eq. (2-8) and Eq. (2-9). With the retrieved AOD as an inference, the “blue-sky” albedo was calculated using Eq. (2-3) following the narrowband-to-broadband conversion based on spectral albedos.

2.3 Results and discussions

2.3.1 SURFRAD sites

Ground measurements from SURFRAD sites have been extensively used for validating the MODIS albedo product (Jin et al. 2003; Liu et al. 2009; Salomon et al. 2006). The direct comparisons of the retrieved albedo values with ground measurements and MODIS data over the seven SURFRAD sites are shown in the time series in Figure

2-4, and the statistics listed in Table 2-5(a). MODIS 1-km albedo products (MCD43B3) and the corresponding quality products (MCD43B2) were used in this study. Only the best quality MODIS albedo values are shown for snow-free conditions in the comparison. While the MODIS albedo algorithm intends to produce snow-free albedo values, the total shortwave albedo products for snowy conditions are always flagged as having lower quality. Those snow data are included in the comparison, in black color.

Table 2-5 Statistics of the retrieved values from this study with comparison to ground measurements over SURFRAD sites

Site Name	Bias	RMSE	R ²
Bondville	-0.0097	0.0615	0.6268
Boulder	0.0245	0.0781	0.0086
Desert Rock	-0.0033	0.0271	0.0013
Fort Peck	0.0241	0.0541	0.9714
Goodwin Creek	-0.0403	0.0581	0.1035
Penn State	-0.0135	0.0390	0.4537
Sioux Falls	-0.0031	0.0762	0.7884
All sites for no snow	-0.0016	0.0268	0.0783
All sites for snow	0.0324	0.1319	0.3855

(a)

Site Name	Retrieved AOD vs ground measurements		MODIS AOD vs ground measurements	
	Bias	RMSE	Bias	RMSE
	Bondville	0.0529	0.1283	0.0579
Boulder	-0.0059	0.0567	0.0025	0.0612
Desert Rock	0.0186	0.0451	n/a	n/a
Fort Peck	0.0330	0.0654	0.0357	0.0986
Goodwin Creek	0.0095	0.1271	-0.0445	0.1290
Penn State	n/a	n/a	n/a	n/a
Sioux Falls	0.0232	0.0901	-0.0480	0.1210
All sites	0.0243	0.0984	-0.0009	0.1187

(b)

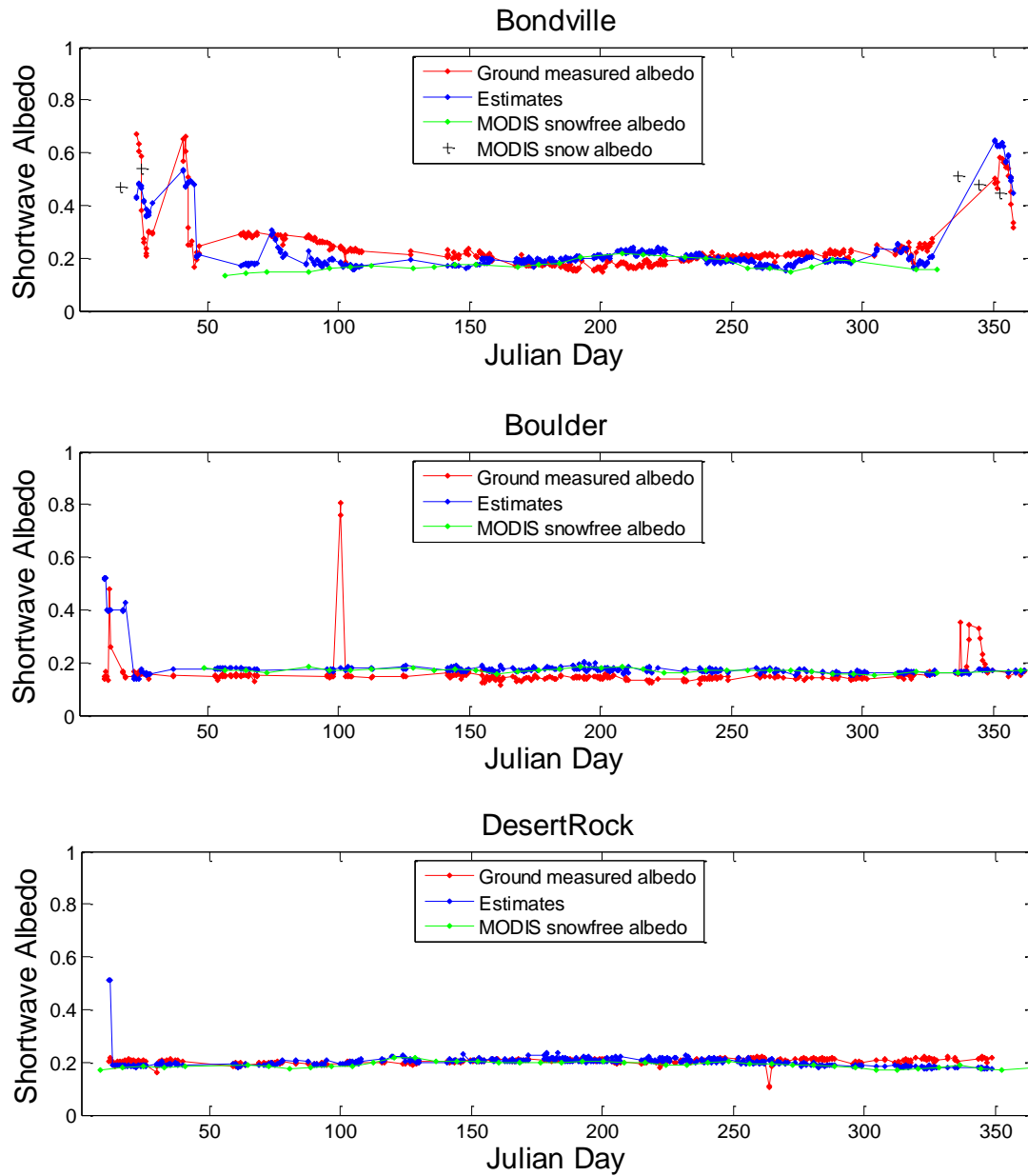


Figure 2-4 Verification of time series shortwave albedo from MODIS observations in 2005 over seven SURFRAD sites (red diamond: ground measured shortwave albedo; blue diamond: estimated albedo from MODIS observations; green diamond: MODIS 16-day snow-free albedo; black cross: MODIS 16-day snow albedo)

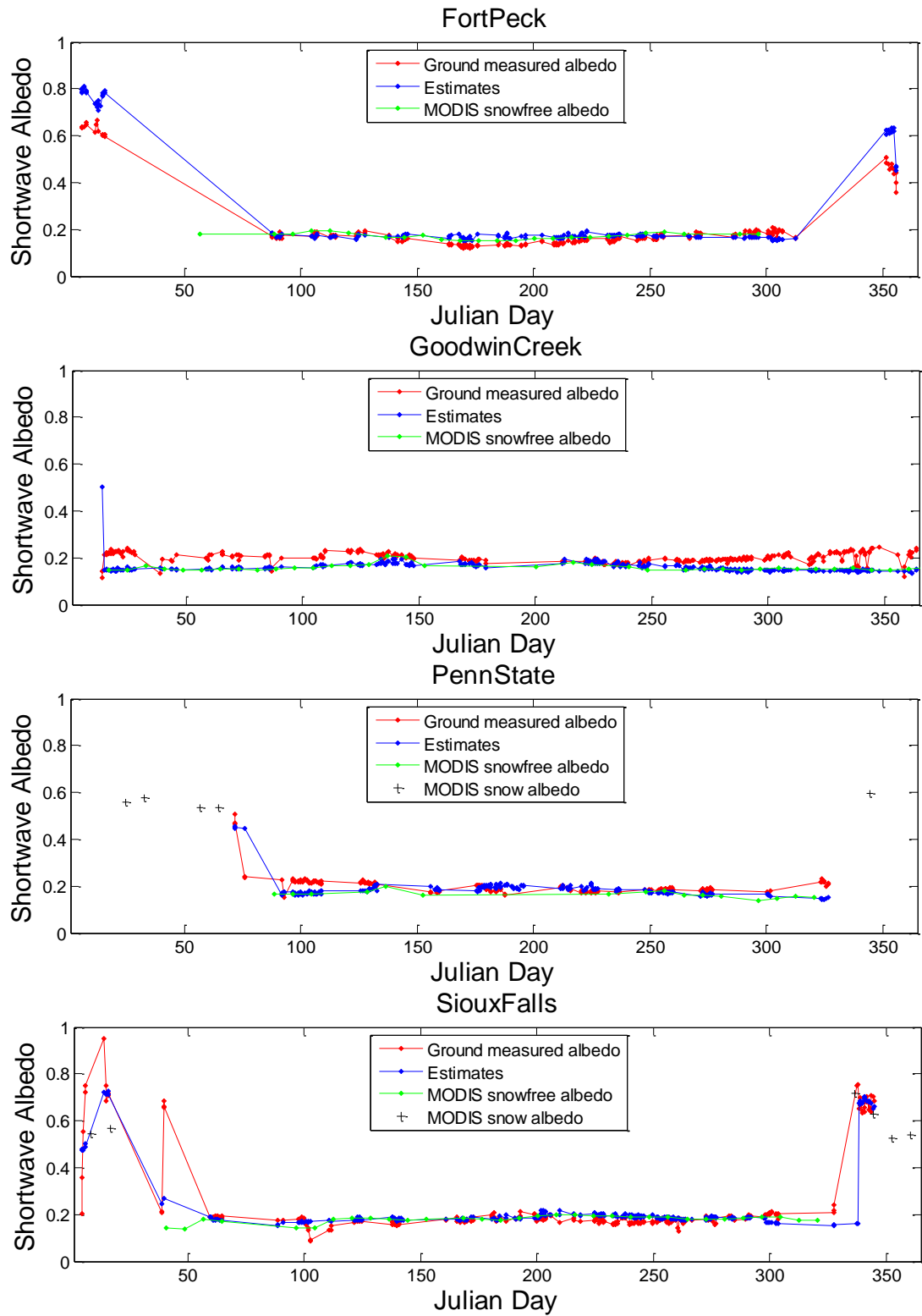


Figure 2-4 (continued)

Generally, the retrieved albedo values have a good match with the field measurements and MODIS albedos. The proposed algorithm in this study generates albedo estimates, which are very close to the MODIS data since large albedo changes are rarely encountered over the snow-free period especially for these vegetated sites. For the non-snow cases (Desert Rock and Goodwin Creek), the Root Mean Square Errors (RMSE) are quite small, although the R^2 values are rather low due to the small range of albedo variations. At Goodwin Creek, both our estimations and the MODIS products are slightly lower than the field measurements.

Both our retrievals and the MODIS albedo data can represent the seasonal snow albedo over Bondville and Sioux Falls reasonably well. However, due to the failure of the MODIS albedo algorithm, the albedo values cannot reflect the snow covered situations in some cases, either due to a mismatch of the snow or a non-snow condition (e.g., around DOY 40 over Bondville) or to having filled values in winter (e.g., over Fort Peck).

The proposed algorithm has difficulty deriving surface albedo over the site of Penn State in winter and early spring because of lack of available clear sky observations within the sliding window while the MODIS magnitude algorithm can produce some estimates.

Overall, the proposed algorithm in this study provides good estimations at all the seven sites with a small bias (-0.0016) and RMSE (0.0268) for no snow conditions, and reasonable results for snow events (bias: 0.0324, RMSE: 0.1319, R^2 : 0.3855). Besides residual cloud contamination, the pixel mixture (e.g., partial snow and surface heterogeneity during the non-snow season) problem could be one of the main reasons for

the bias found at Fort Peck and Goodwin Creek. It should be noted that the surface condition is very stable over some sites mainly covered by grass (e.g., Boulder, Desert Rock and Goodwin Creek). In these cases, the R^2 can be quite low due to the small change in surface albedo and the reduced RMSE is observed as well.

Comparisons of AOD estimations from the proposed algorithm and the MODIS algorithm with ground measurements are provided along with the statistics in Table 2-5(b). MODIS instantaneous AOD data (Collection 5) from both Terra (MOD04_L2) and Aqua (MYD04_L2) observations were used in this comparison. For Bondville, significant positive bias and RMSE are found for both the retrieved AODs and MODIS estimations. The site's close vicinity to the urban area could be a main reason for the large aerosol variations, which may contribute to an underestimation of the albedo. The slight underestimation over Boulder is one of the possible reasons for the introduction of the positive bias in the albedo estimation. There are some overestimations over Desert Rock where the RMSE (0.0451) is the smallest among all the sites, indicating accurate surface albedo estimations and non-significant surface changes. However, the MODIS aerosol algorithm generates very few values over Desert Rock, which makes the comparison impossible. This is probably caused by the increased surface reflectivity, which its algorithm is not capable of processing. Both Fort Peck and Goodwin Creek have large AOD variations; the uncertainty of aerosol retrievals may have deteriorated the albedo estimations. Due to the lack of ground measurements over Penn State, no comparison is made for this dataset. For Sioux Falls, the positive bias (0.0232) corresponds to the slight underestimation of albedo, while the impact is not very significant. Combining the comparisons for all the sites, the AOD values generated by the

proposed algorithm have accuracy levels similar to those of the MODIS aerosol products. A positive bias (0.0243) is found for the retrievals with a slightly smaller RMSE (0.0984) compared to that of the MODIS AOD (RMSE: 0.1187). The positive biases of the MODIS AOD data over Bondville (0.0579) and Fort Peck (0.0357) are offset by the negative ones over Goodwin Creek (-0.0445) and Sioux Falls (-0.0480) leading to a small bias (-0.0009).

2.3.2 GC-Net sites

Similar to the comparisons made over the SURFRAD sites, the MODIS 1-km albedo and quality data were processed for the GC-Net sites. Time series comparisons of ground measurements, retrieved albedo values, and MODIS albedo products over the GC-Net sites are given in Figure 2-5. From the results shown here, snow and snow-melt events were clearly captured by the retrievals of our proposed algorithm. The results based on daily observations show variations in ground measurements and retrieved albedo data whereas the 16-day MODIS albedo curves are smooth over most cases. The albedo variations are caused by the changes in solar zenith angle, since MODIS can have multiple overpasses over Greenland in one day (combined Terra and Aqua). As more observations can be obtained over Greenland compared to those of the SURFRAD sites, the time range for collecting the cloud free observations becomes shorter over the Greenland sites, which gives the algorithm better capability for capturing rapid changes.

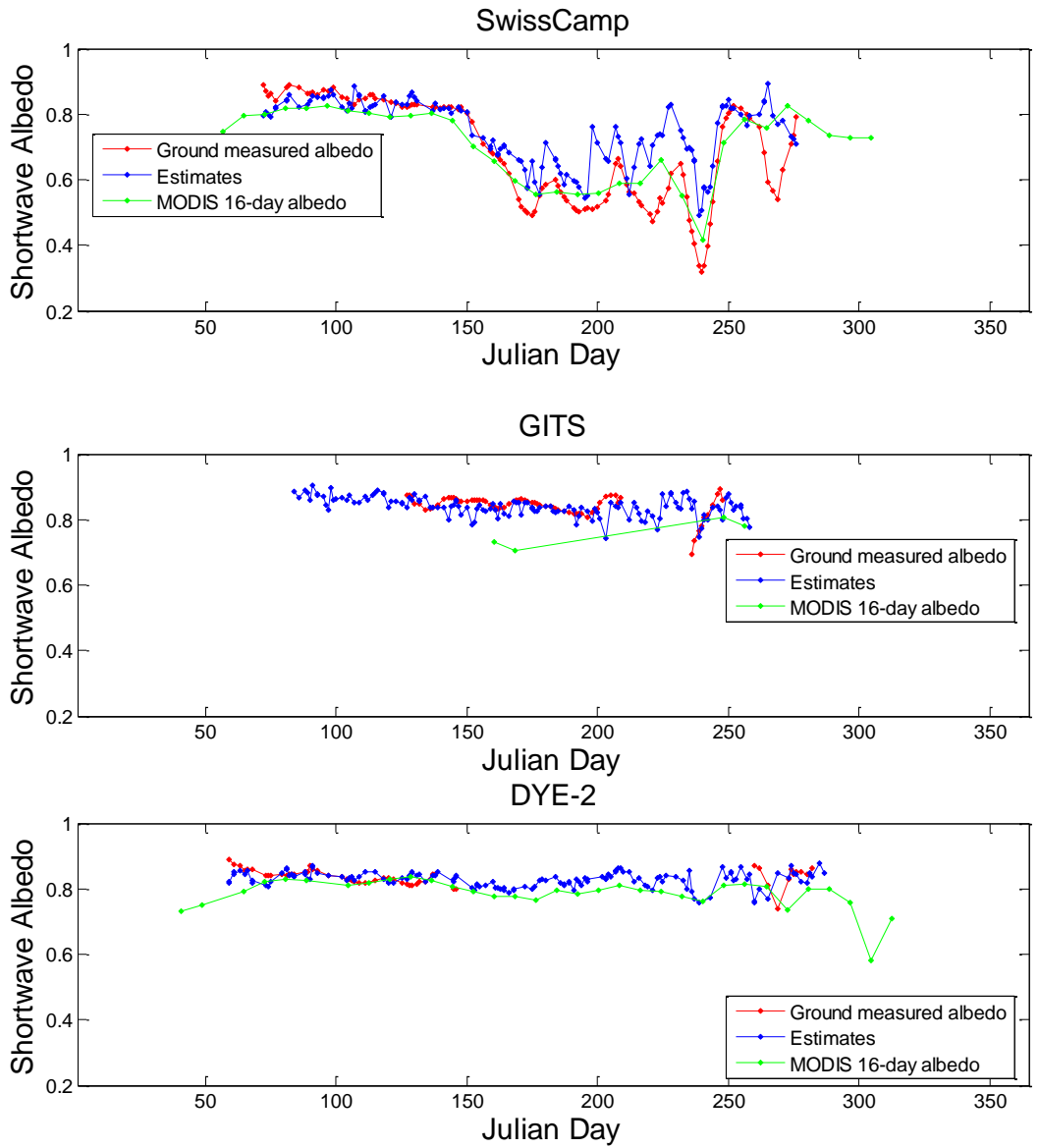


Figure 2-5 Verification of time series total shortwave albedo from MODIS observations in 2003 over six GC-Net sites (red diamond: ground measured visible albedo; blue diamond: estimated albedo from MODIS observations; green diamond: MODIS 16-day albedo)

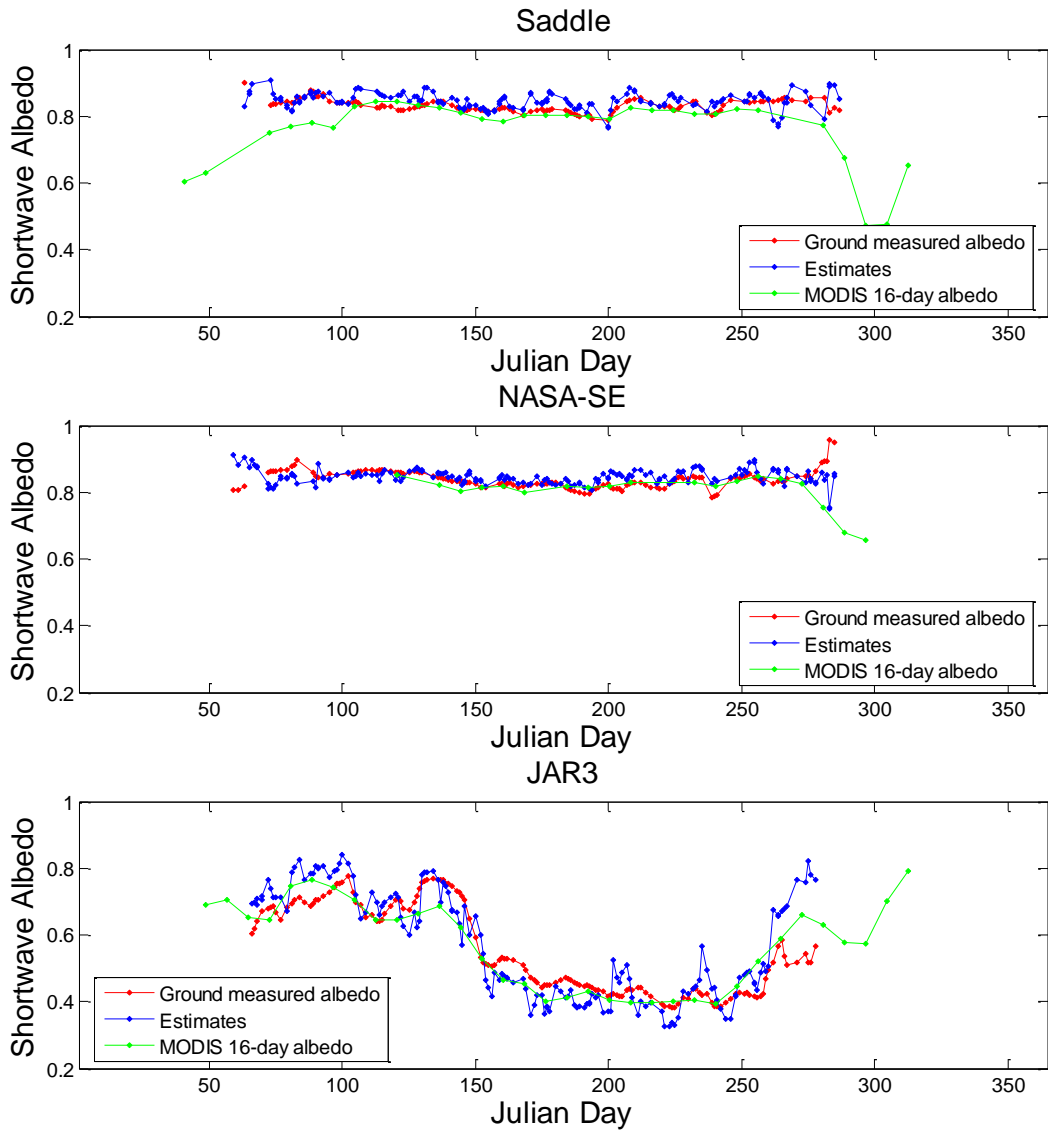


Figure 2-5 (continued)

The statistics of the comparisons between the instantaneous retrievals and ground measured albedo data over all the sites are given in Table 2-6. This algorithm gives a satisfactory result over all sites with a small positive bias (0.012). The overall R2 (0.842) shows that the albedo retrievals have a good correlation with the ground measurements indicating that the snow surface changes can be well captured, although sometimes the sliding window size is still larger than the real situation given that the RMSEs are higher

than 0.05 over some sites. Figure 2-6 shows the comparison of the 16-day MODIS products and averaged retrievals and ground measurements over the same time period. The MODIS albedo data have a negative bias (-0.027) while the retrieved values here have a much smaller bias of 0.013. Furthermore, the retrieved albedos have a higher correlation with the ground measurements (R^2 : 0.838) and a smaller RMSE (0.0589) than those from MODIS (R^2 : 0.773, RMSE: 0.076). Unlike the seasonal albedo changes at the sites close to the seashore (e.g., Swiss Camp, JAR1, and JAR3), the snow albedo does not change significantly at the rest of the chosen sites due to fewer snow fall/melt events. The values of R^2 and RMSE are much lower for sites close to the center of Greenland due to the small albedo variation and possible misidentification of clouds over snow surface.

Table 2-6 Statistics of the retrieved values from this study with comparison to ground measurements over GC-Net sites

Site Name	Bias	RMSE	R^2
Swiss Camp	0.062	0.1110	0.700
GITS	-0.011	0.0356	0.077
Summit	0.0098	0.0467	0.027
DYE-2	-0.0039	0.0333	0.006
JAR1	0.015	0.0910	0.872
Saddle	0.015	0.0304	0.060
NASA-E	-0.024	0.0341	0.002
NASA-SE	0.0074	0.0351	0.001
JAR3	0.0012	0.0767	0.774
All sites	0.012	0.0654	0.842

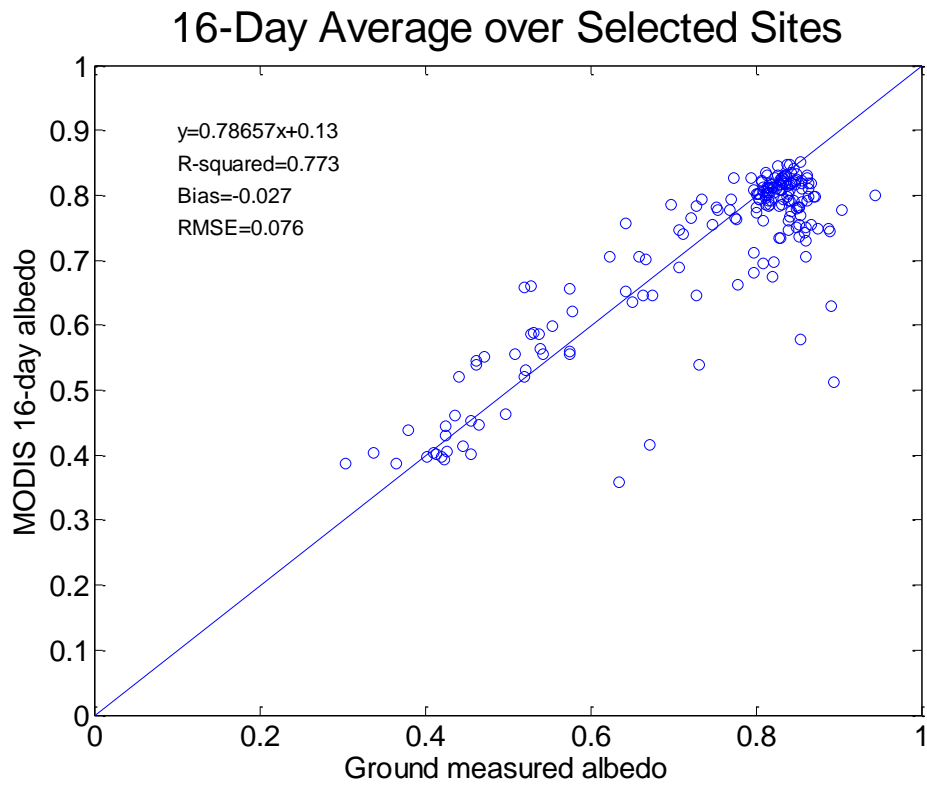
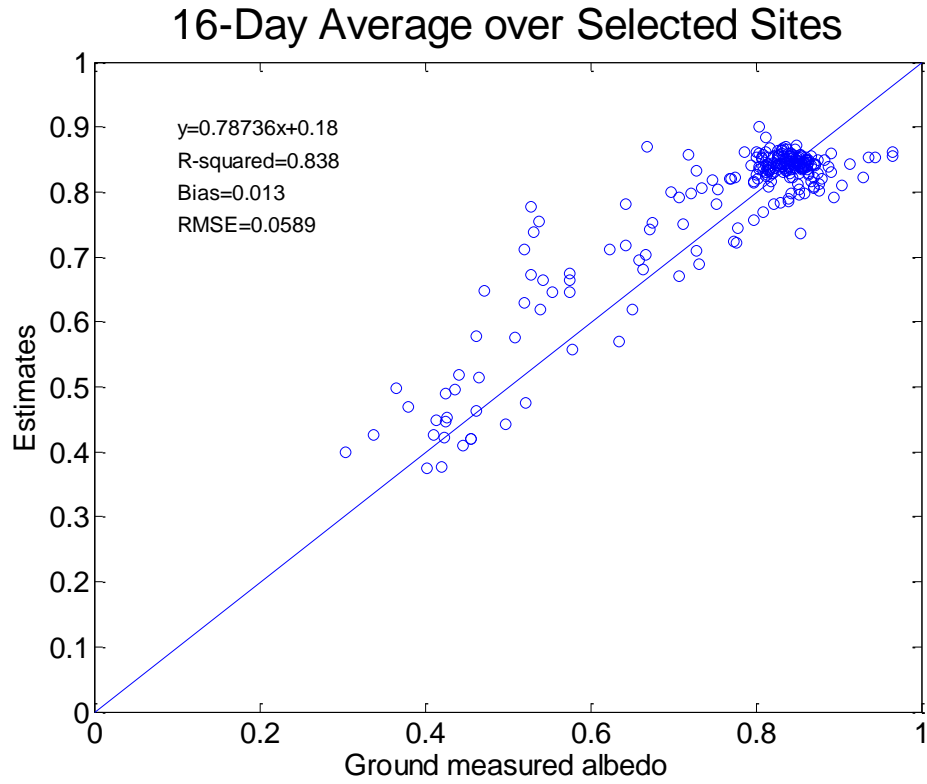


Figure 2-6 Scattering plots of the 16-day averaged albedo values over nine GC-Net sites

2.3.3 Comparisons with MODASRVN data set

Sixteen sites were chosen for validation of the surface reflectance using the MODASRVN data set. Time series comparisons of the red band and near-infrared band data over six vegetation sites are given in Figure 2-7. The retrieved surface reflectances in these two bands capture the seasonal trends and match the MODASRVN instantaneous reflectance products very well. The difference plot in Figure 2-7 shows that most of the errors lie in the range of ± 0.05 for both bands and the errors are randomly distributed for a short time period. However, since in most cases the MODASRVN data failed to provide the reflectance over the snow covered surfaces, it is difficult to validate the proposed algorithm over bright surfaces using this dataset. Moreover, as this dataset relies only on the MODIS sensor onboard Terra, fewer retrievals are available than those in our results presented in this study.

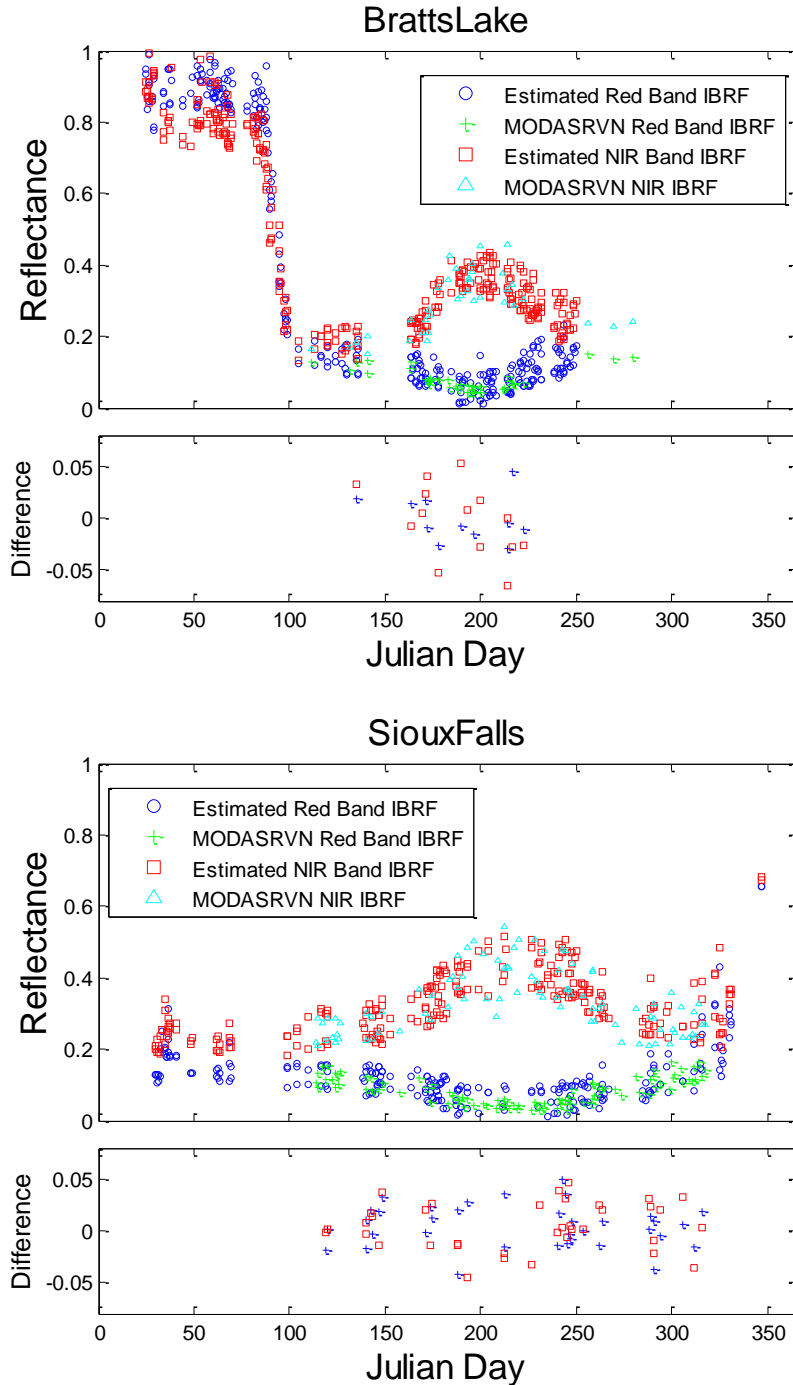


Figure 2-7 Verification of time series instantaneous reflectance from MODIS observations in 2005 over six AERONET sites (dark blue circle: estimated red band reflectance; green cross: MODASRVN red band reflectance; red square: estimated near-Infrared band reflectance; light blue triangle: MODASRVN near-Infrared band reflectance) and time series of differences between the retrieved values and MODASRVN data (red square: difference for red band; blue cross: difference for near-Infrared band)

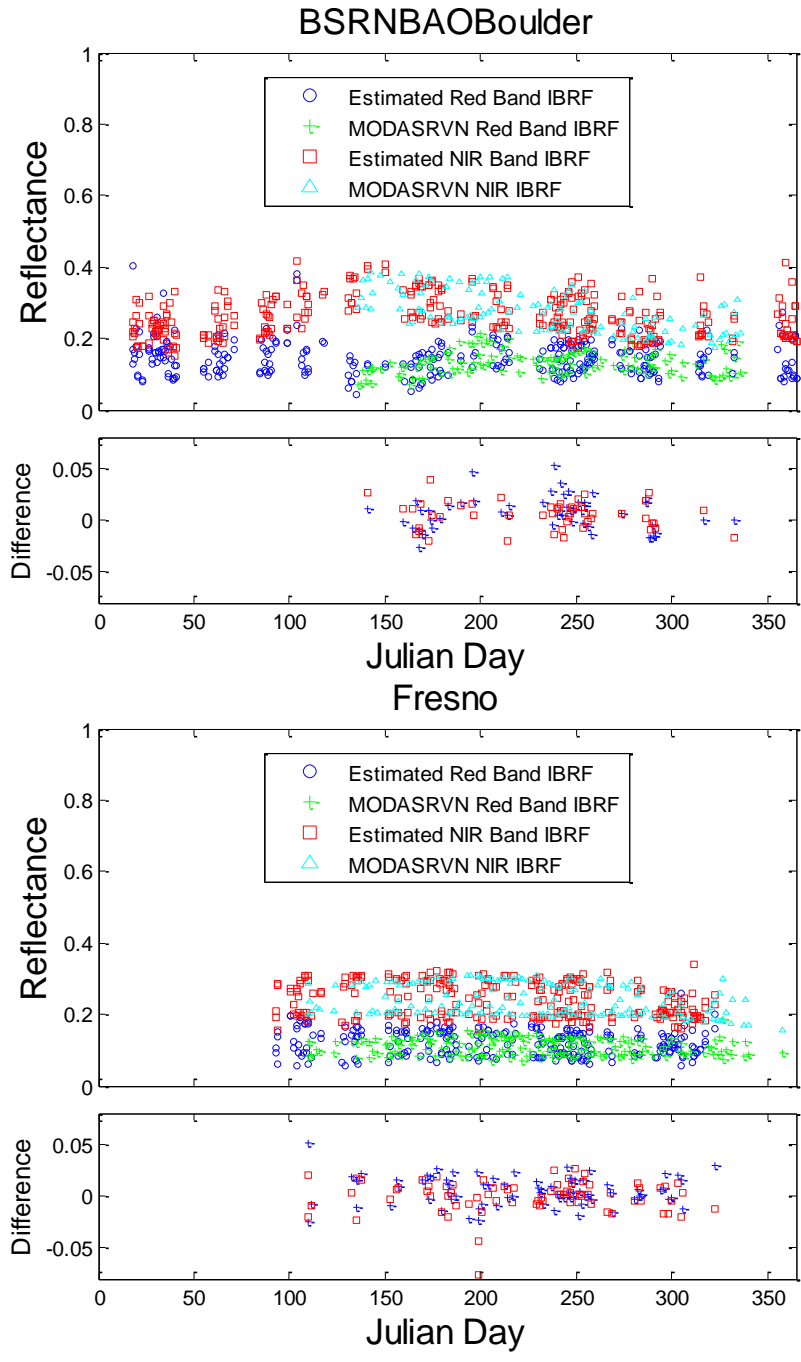


Figure 2-7 (continued)

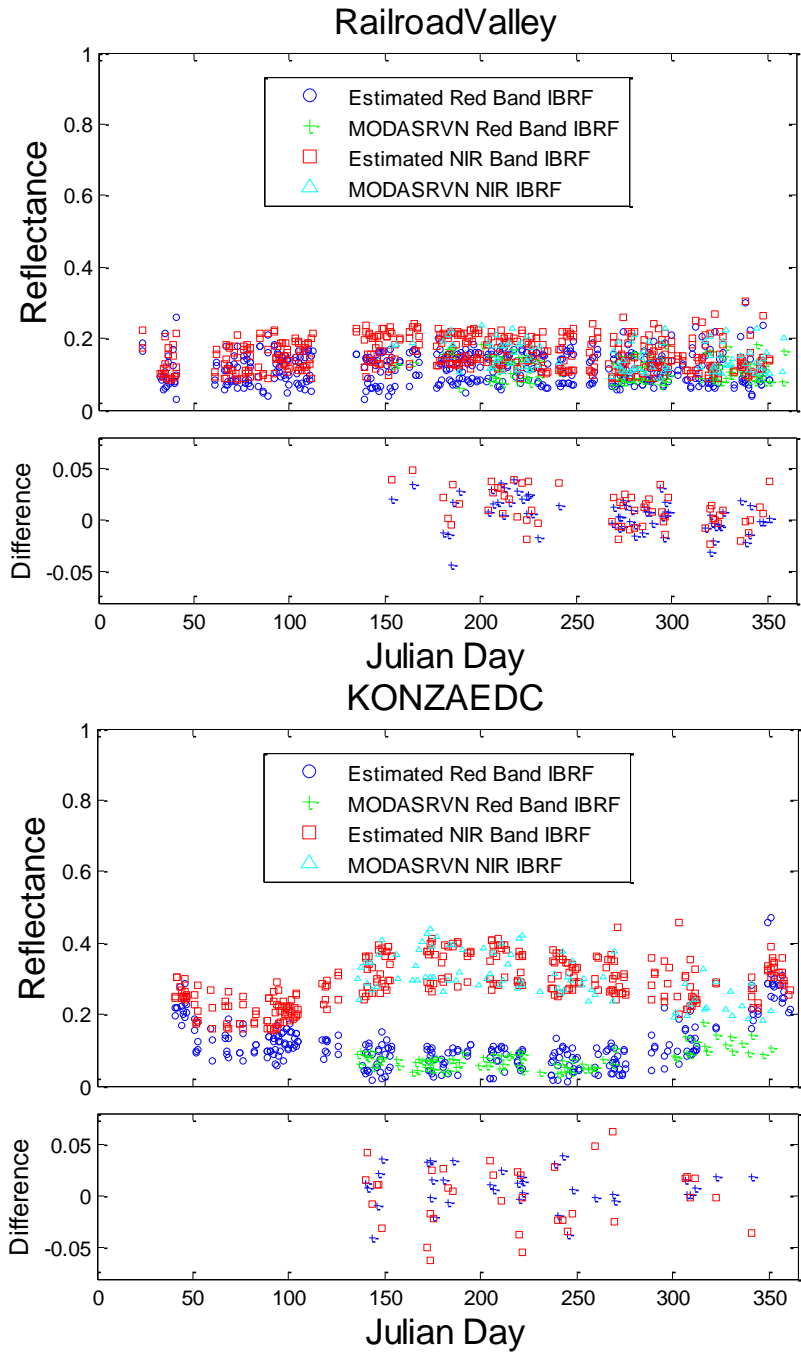


Figure 2-7 (continued)

Direct comparisons are given in Figure 2-8 (statistics listed in Table 2-7) over all sixteen sites for all 7 MODIS bands. The overall correlation of the retrievals and the MODASRVN data is very good for each individual band and the bias and RMSE are

small. The R^2 values are relatively small for band 3 and band 4 because there is only a narrow range for the reflectances (0–0.2). Some outliers are found in the comparison, probably due to the misclassification of the cloud mask, which is one of the major input components for this algorithm. Given the variability of surface cover types over all the sixteen sites, the results show that the algorithm proposed here is capable of handling different types of land cover regardless of its homogeneity.

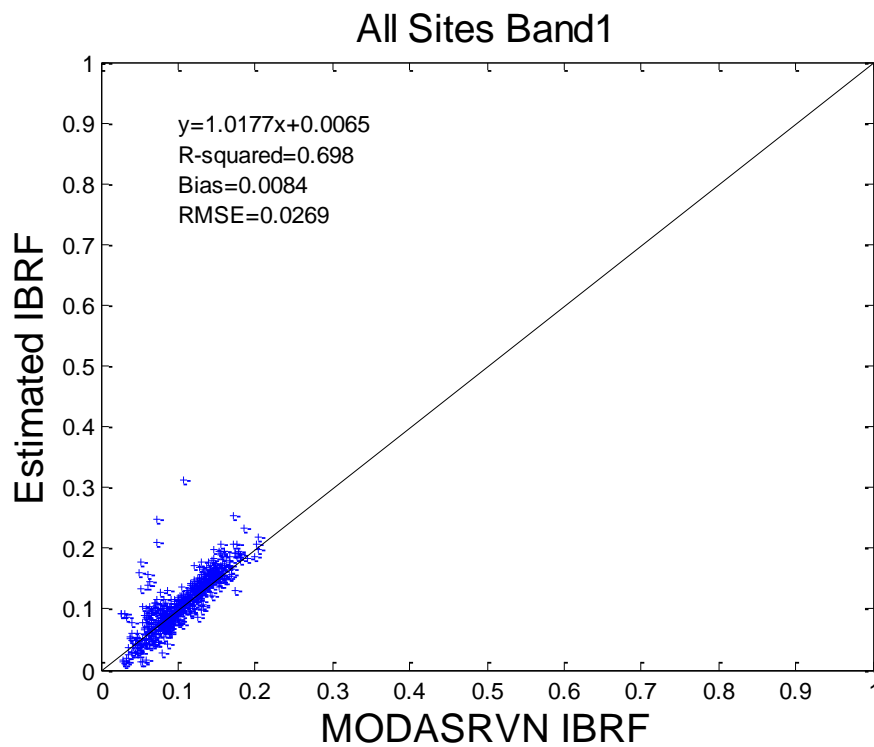


Figure 2-8 Scatter plot of estimated and MODASRVN instantaneous bidirectional reflectance for each of the seven MODIS bands over all the selected AERONET sites during 2005

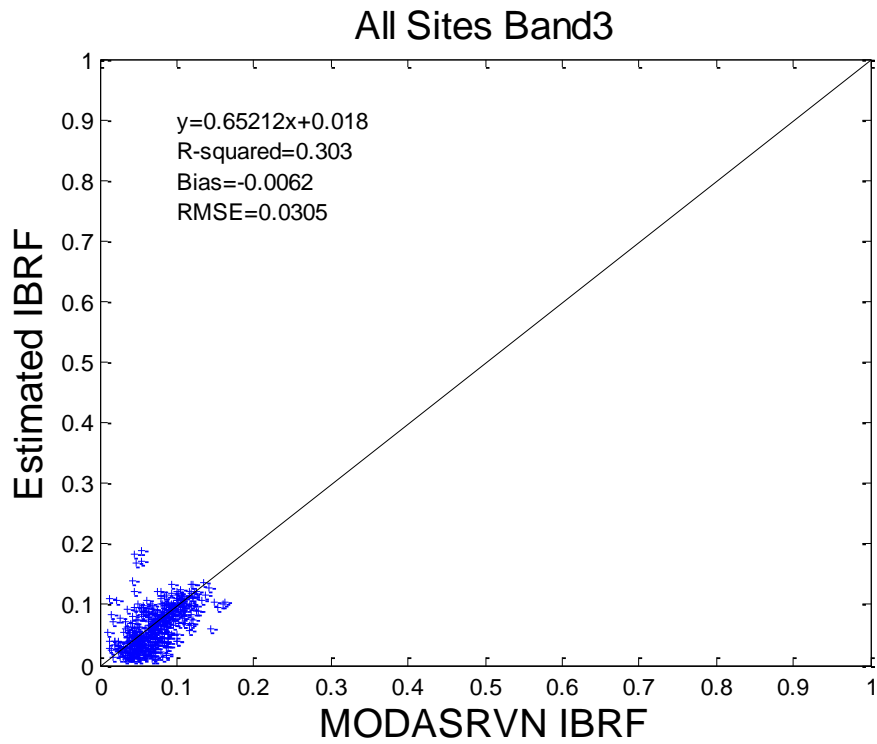
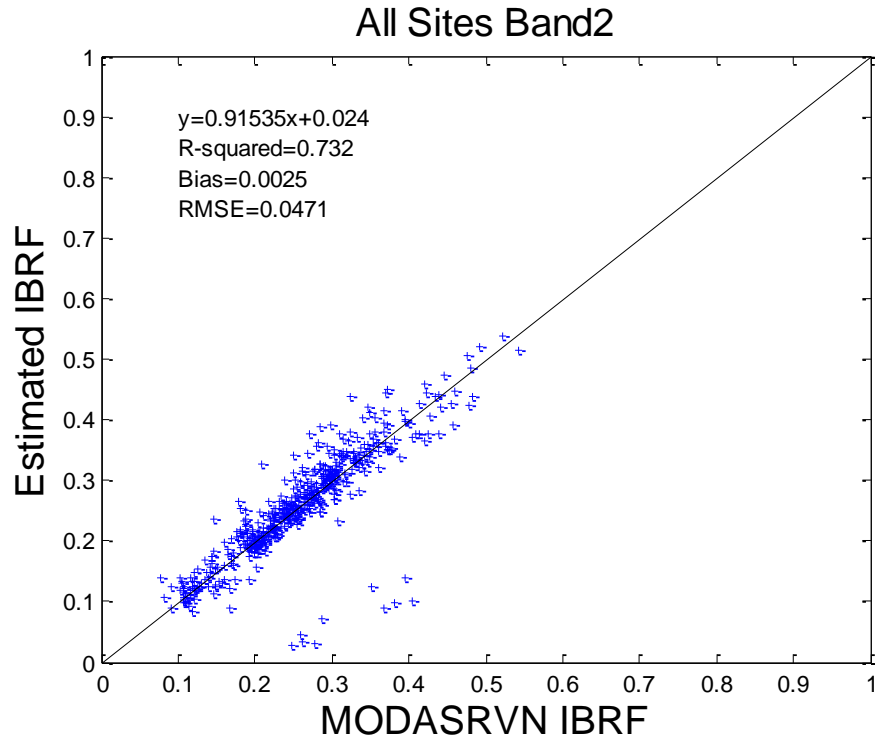


Figure 2-8 (continued)

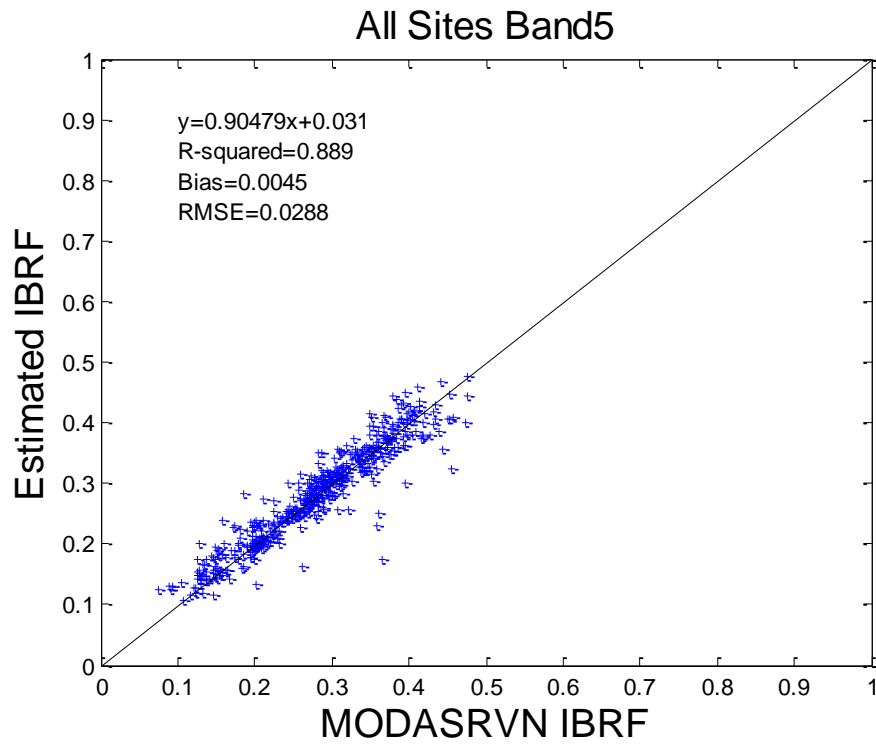
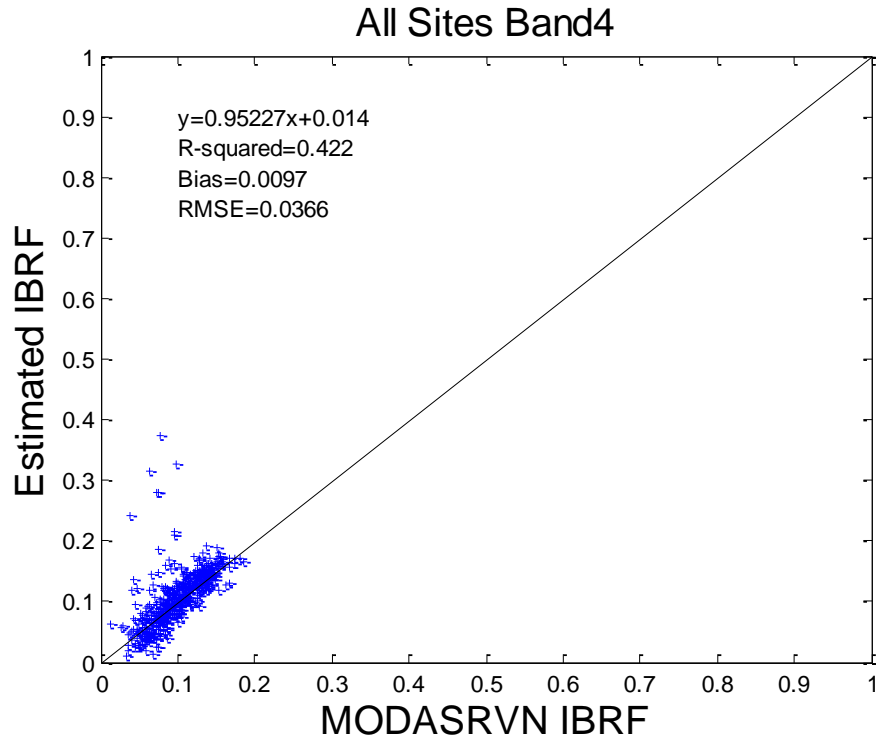


Figure 2-8 (continued)

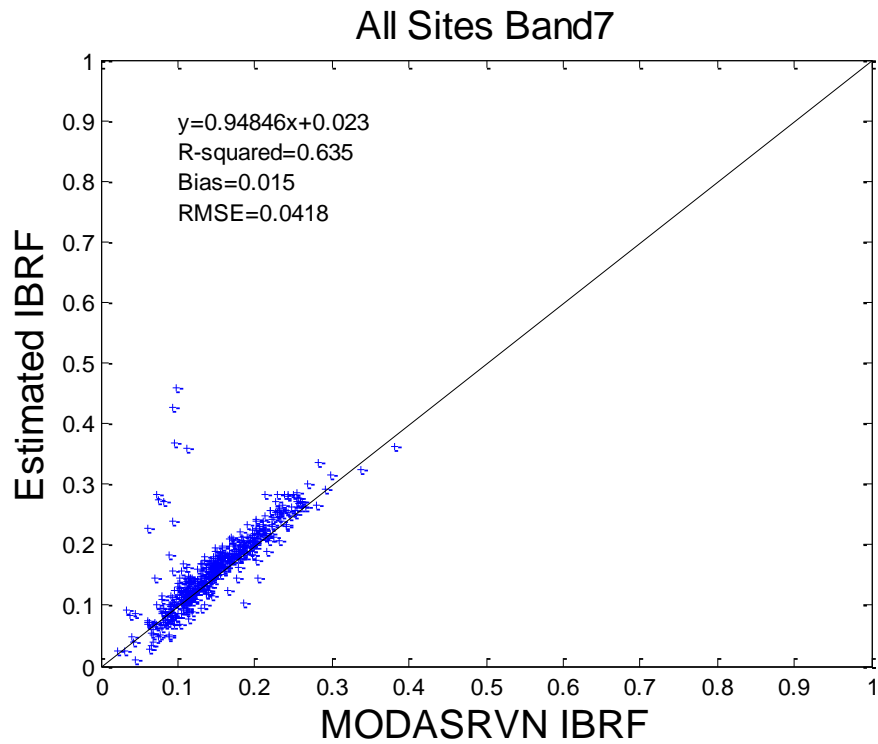
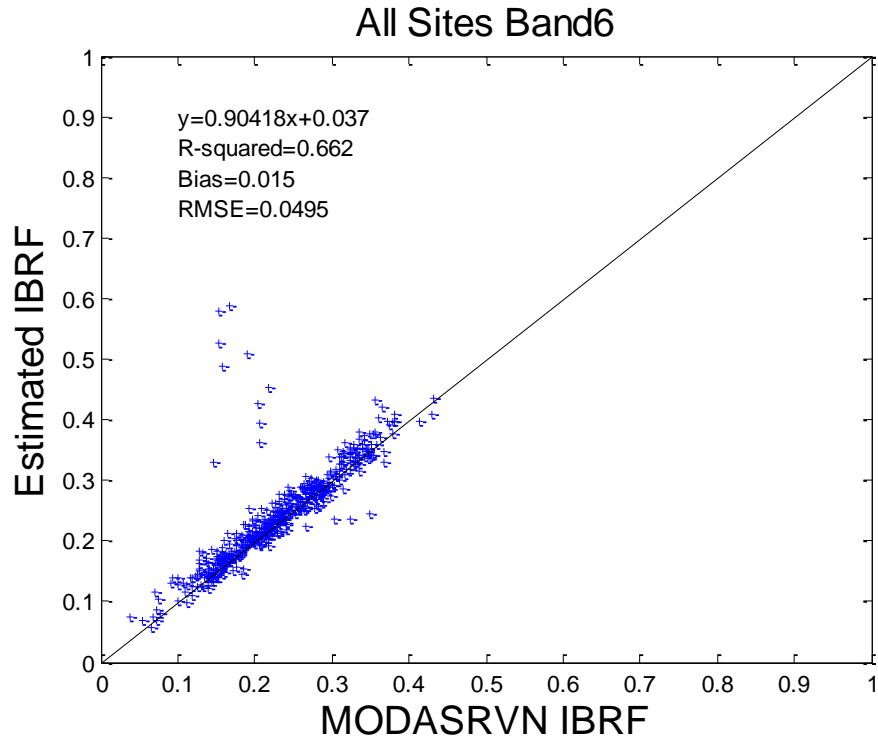


Figure 2-8 (continued)

Table 2-7 Statistics of the retrieved reflectance values from this study with comparison to MODASRVN reflectance products ground measurements over sixteen AERONET sites

Band No.	Bias	RMSE	R ²
1	0.0084	0.0269	0.698
2	0.0025	0.0471	0.732
3	-0.0062	0.0305	0.303
4	0.0097	0.0366	0.422
5	0.0045	0.0288	0.889
6	0.015	0.0495	0.662
7	0.015	0.0418	0.635

Table 2-8 Impacts of solar zenith angle and estimation accuracies of AOD on surface reflectance estimations

(a) SZA on AOD and reflectance

SZA	15°-25°	25°-35°	35°-45°	45°-55°	55°-65°	65°-75°
Mean(E _{AOD} [*])	0.0311	0.0428	0.0333	0.0120	0.0079	0.0022
STD(E _{AOD} [*])	0.1204	0.1238	0.1015	0.0324	0.0251	0.0495
Mean (E _{B1} ^{**})	0.0121	0.0107	0.0186	-0.0017	-0.0139	n/a
STD(E _{B1} ^{**})	0.0142	0.0190	0.0262	0.0128	0.0204	n/a
Mean (E _{B2} ^{***})	0.0347	0.0292	0.0075	0.0016	-0.0136	n/a
STD(E _{B2} ^{***})	0.0318	0.0442	0.0301	0.0226	0.0178	n/a

(b) AOD on reflectance

Abs(E _{AOD} [*])	<0.05	0.05-0.10	0.10-0.15	0.15-0.20	>0.20
Mean (E _{B1} ^{**})	0.0035	0.0066	0.0204	0.0289	0.0184
STD(E _{B1} ^{**})	0.0189	0.0224	0.0204	0.0347	0.0246
Mean (E _{B2} ^{***})	0.0049	0.0278	0.0604	0.0278	-0.0221
STD(E _{B2} ^{***})	0.0254	0.0348	0.0534	0.0571	0.0394

E_{AOD}^{*}: Estimated AOD – AERONET AOD

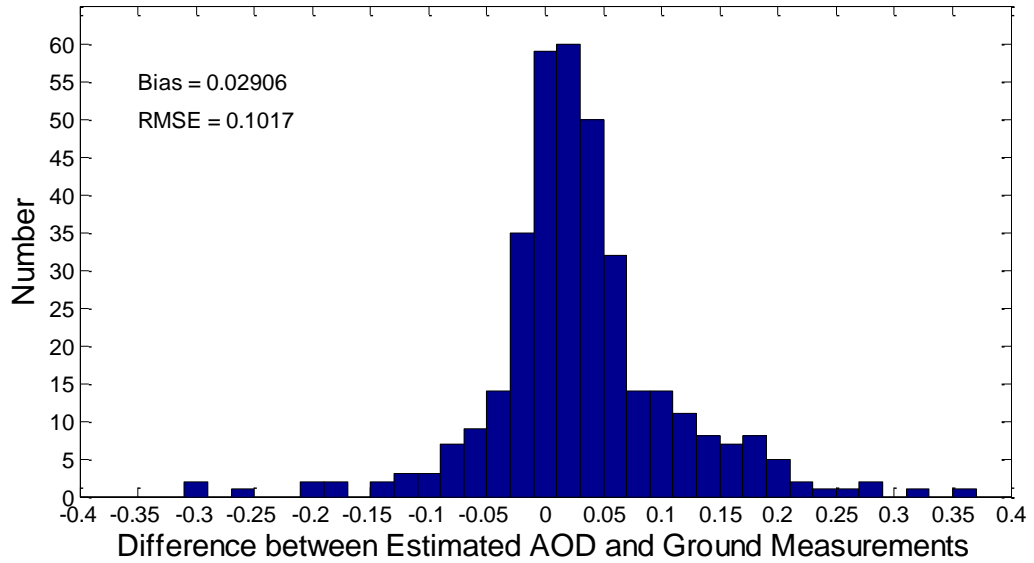
E_{B1}^{**}: Estimated reflectance – MODASRVN reflectance for MODIS Band 1

E_{B2}^{***}: Estimated reflectance – MODASRVN reflectance for MODIS Band 2

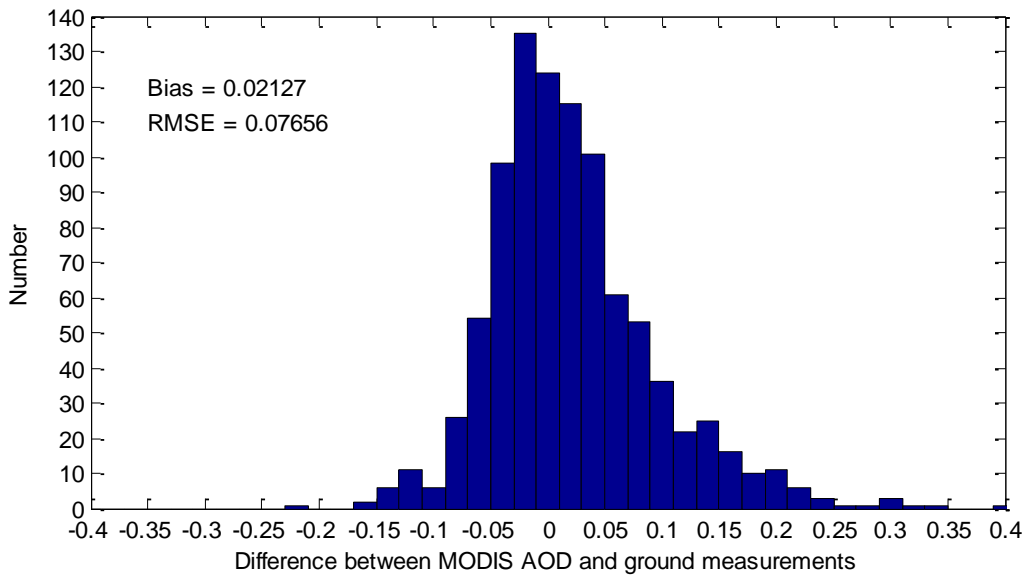
The direct comparison of retrieved instantaneous AOD values with AERONET observations is shown in Figure 2-9(a). The errors in the AOD estimates follow a normal distribution which shows a positive bias less than 0.03. The overall results have a large RMSE (0.1017) which is larger than the MODIS AOD products shown in Figure 2-9(b). Analysis has been carried out to investigate the performance of the algorithm in estimating AOD and therefore surface reflectance, and the statistics listed in Table 2-8. As MODIS passes over the same location only twice a day around local noon for mid-latitude sites (including Terra and Aqua), solar zenith is used here as the inference of the season – small values in summer and large values in winter. Solar zenith is divided into 6 segments: 15°–25°, 25°–35°, 35°–45°, 45°–55°, 55°–65°, and 65°–75°. The AOD estimation accuracies generally decrease with the increase of solar angles, which means better accuracies can be achieved during winter. There are two reasons for this. One is that summer has lower solar zenith but more variation of aerosol, while winter has large solar zenith with small aerosol accumulation. The other is that a large solar zenith angle provides a longer path from earth's surface to the satellite as well as more information on aerosol. The uncertainties of reflectance estimates also generally decrease with the increase of solar zenith when it is less than 55°. When the solar angle increases to 55°–65°, there is a negative bias for each of the two bands. The underestimation may result from the difference of the two algorithms in accumulating the observations in the time period of partial snow.

Table 2-8(b) shows the impacts of AOD estimation errors on the surface reflectance retrieving accuracies. Absolute AOD error values are divided into five ranges: <0.05, 0.05–0.10, 0.10–0.15, 0.15–0.20, and >0.20. According to the statistics, the algorithm

generates larger errors in reflectance for both bands when the AOD uncertainties become larger. As most of the AOD errors lie within the range of ± 0.05 , the overall reflectance retrievals can have good accuracies in terms of the averaged errors.



(a)



(b)

Figure 2-9 AOD estimation accuracies from (a) the proposed algorithm and (b) the MODIS algorithm at MODASRVN sites during 2005

2.3.4 Summary and conclusions

Based on the integration of the land-atmosphere radiation interaction framework, this study focuses on estimating the MODIS surface albedo and directional reflectance. The major contributions of this study are as follows:

1) As existing algorithms deriving albedo products from geostationary satellite data mainly focus on the partitioning the contributions from atmosphere and surface, the “dark object” algorithm may bias the estimation of surface anisotropy. The proposed approach in this study is designed to mitigate this problem. This is the first prototype algorithm that estimates the surface albedo and reflectance for use with the future geostationary satellite Geostationary Operational Environmental Satellite-R Series (GOES-R) Advanced Baseline Imager (ABI) sensor. This study provides the complete algorithm framework for the albedo retrieving procedure using MODIS observations as proxy data.

2) By using different “truth” datasets, this study provides extensive validation of the proposed algorithm by comparing the broadband albedos, spectral reflectances and instantaneous AODs. The overall results show that the retrievals are a good representation of the seasonal curves of the albedo and reflectance changes all year round. Compared with the MODIS albedo algorithm and MODIS AOD products, this proposed algorithm with a smaller sliding window provides reasonable results with relation to ground measurements for both surface albedo and AOD, while the capabilities in terms of handling rapid surface albedo changes caused by snowfall and snow-melt situations still need further investigations. This will help climate models in the simulation and forecast applications.

Future work will focus on several major problems. First, efforts will be made on the mitigation of cloud effects and improvements over rapid change surfaces. Time series of previous retrievals/observations can be better used if clouds are persistent in the sliding window. Temporary cloud contamination or partial snow cover impacts can also be mitigated by introducing the previous retrievals as constraints in the current retrieving procedure. Since direct broadband albedo estimation can be carried out when limited clear skies are available, efforts will be made to incorporate and extend this algorithm to estimate both the broadband and spectral band albedos.

Second, the retrieved albedo values have some correlation with the climatology used in this study. While the observation data and climatology maps come from the same data source – MODIS, further efforts should be made to derive an unbiased climatology from multiple data sources. In addition, factors such as disturbance, precipitation and soil moisture changes, will be taken into account in building the climatology. More efforts will be made on analyzing the covariance between different input data in the cost function.

Finally yet importantly, extensive validations need to be carried out using various sources of data that include finer-resolution satellite products. In addition, proxy data from a geostationary satellite (e.g., MSG/SEVIRI) will be used in evaluating this retrieving procedure in Chapter 3.

CHAPTER 3 ESTIMATION OF SURFACE ALBEDO FROM SEVIRI OBSERVATIONS

3.1 Methodology

3.1.1 Optimal estimation

In the last chapter, a method is proposed relying on both the albedo prior information and the satellite observations to estimate properties of surface and atmosphere simultaneously from MODIS data. As SEVIRI provides observations every 15-30 mins, around 20-50 clear sky observations can be available per day that make the angular samplings sufficient to capture both aerosol and surface anisotropy. The surface invariability assumption can be shortened to one in this study. Another assumption needs to be made on the aerosol type and its properties (e.g., Angström exponent): that they do not change within one day, but AOD varies from time to time.

3.1.2 Broadband shortwave albedo calculation

In this study, the major objective is to generate the shortwave albedo that is required by many land surface models and weather forecast applications to quantify the overall solar shortwave net radiation. From the BRF models, albedo from spectral bands can be easily estimated through the polynomial function, as mentioned in the last chapter. As the broadband albedo quantifies the ratio of the total reflected and incident radiation for a wide range of wavelengths, it can be expressed as the linear combination of spectral albedos with the weights from the distribution of the incident energy. Variation of atmospheric aerosol loading will scatter and/or absorb the solar radiation and reflected

radiation from the surface. Aerosol tends to scatter more in the shorter wavelength, thus changing the spectral distribution of solar radiation that reaches the surface. To simplify the estimation of broadband albedo, a general equation needs to be worked out to express the relationship between the spectral albedo and the integrated broadband shortwave albedo, accounting for various aerosol loadings over different surfaces (Liang 2001). The relationship can be established using the following linear equation:

$$\alpha_{sw} = \sum_{\lambda=1}^n Reg_{\lambda} \alpha_{\lambda} + Reg_0 \quad (3-1)$$

where α_{sw} is the total shortwave albedo, α_{λ} ($\lambda \in [1, n]$) is the albedo from spectral band, Reg_i ($i \in [0, n]$) is the regression coefficients.

Samples from the U.S. Geological Survey (USGS) Digital Spectral Library (Clark et al. 2007) were used in this study for the representation of spectral albedo for various surfaces (Table 3-1). The Second Simulation of a Satellite Signal in the Solar Spectrum (6S) software (Kotchenova et al. 2006) is able to simulate the both incoming and outgoing radiation data at the surface with the inputs of surface albedo and AOD at 550 nm. The simulations were carried out by varying the AOD from 0.01 to 0.5 with the albedo spectrum as input. Albedos from spectral bands and the total shortwave band were calculated from the simulated radiation data and then put into the linear regression. Results are shown in Equation (3-2):

$$\alpha_{short} = 0.4331\alpha_1 + 0.3939\alpha_2 + 0.1136\alpha_3 - 0.0084 \quad (3-2)$$

Only one equation was generated while not separating the snow surface from non-snow ones because good agreement was found using these coefficients for high albedo values (Figure 3-1). Moreover, with SEVIRI's 3-km resolution, a lot of pixels are mixtures of multiple land cover types.

Table 3-1 Albedo spectrum samples from USGS library

Surface type	Vegetation	Soil	Water	Snow/Ice	Rock	Manmade
Samples	118	50	7	21	18	31

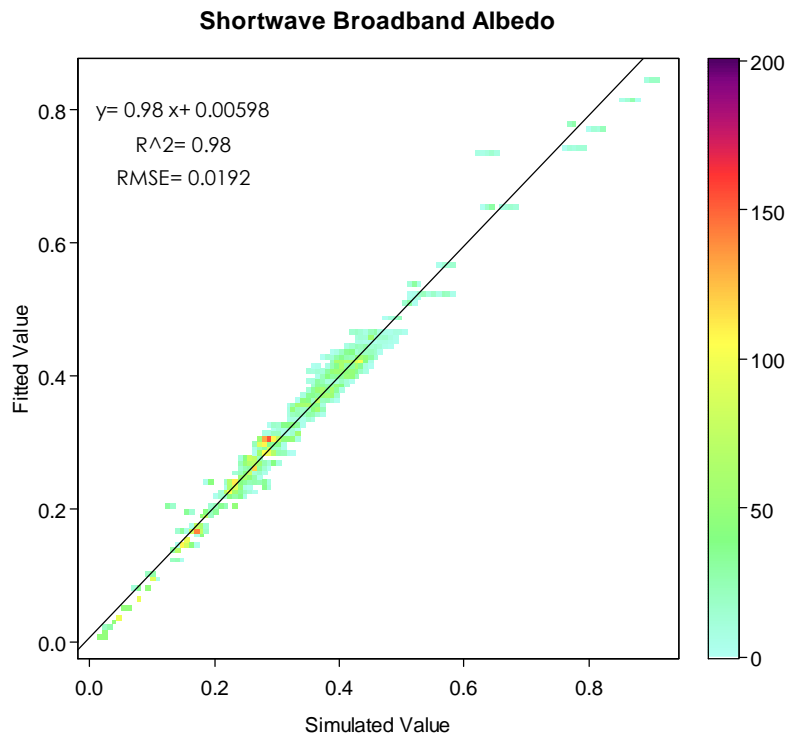


Figure 3-1 Narrowband-to-broadband conversion accuracy from all the samples

The limited number of spectral bands on SEVIRI limits the band conversion accuracy. The RMSE using Eq. (3-2) is around 0.02, while based on the same surface spectrum the RMSE for MODIS is lower than 0.001. This is caused by the reduced bands in visible

range on SEVIRI which results in lower accuracy capturing the high reflectivity over soil and snow.

3.2 Data and retrieving procedure

3.2.1 MSG/SEVIRI data

Meteosat-8 SEVIRI level 1.5 data stores the TOA radiance covering the continent of Africa, east of South America, and a large portion of Europe. Data for the year of 2005 was used in this study. The radiance data was converted to reflectance by dividing the incoming solar radiation reaching at TOA. Local solar illumination angles (zenith and azimuth) for the observing time were calculated by the solar positioning algorithm (Reda and Andreas 2004). Source code is available at <http://rredc.nrel.gov/solar/codesandalgorithms/spa/>. Since the viewing geometry is fixed for the same location, the relative azimuth angle is easy to calculate with the solar azimuth.

The SEVIRI cloud mask (Derrien and Le Gleau 2005) distributed along with the radiance data was used to remove the TOA observations affected by cloud cover. As the cloud mask algorithm has difficulties identifying the clouds in low-sun conditions (Derrien and Le Gleau 2010), the TOA observations in early-morning or late-afternoon were not used in this study.

3.2.2 Albedo climatology

Albedo climatology was calculated from ten years' MODIS shortwave albedo product (2000-2009). MODIS 0.05° albedo data set (MCD43C3) was used in this study because the spatial resolution is similar to that of SEVIRI data. The shortwave albedo data in MCD43C3 data set is stored in the lat/lon projection. MODIS data was reprojected to the SEVIRI projection. To reduce the data volume and the dependence of solar angle, white-sky albedo was used here. Ten years' mean and standard deviations (Figure 3-2) were calculated with only the “best quality” MODIS albedo products. In the climatology maps, albedo in the Amazon and central Africa is generally small and stable because of large forests. Usually cloud contamination can be the major reason for gaps over these areas; therefore, surface albedo algorithm may still get reasonable estimations from this prior information with limited instantaneous cloud-free observations. North Africa is largely covered by desert, which causes the major failure of the “dark object” algorithms. Since the ten years' albedo variation is not huge, the multi-year mean data can serve as the prior information very well in this area. Large values are found for both albedo mean and standard deviation over east Europe, which suggests inter-annual variation of snow events. This also implies that the accurate estimates may rely on the instantaneous observations more if its error is lower over this area during winter.

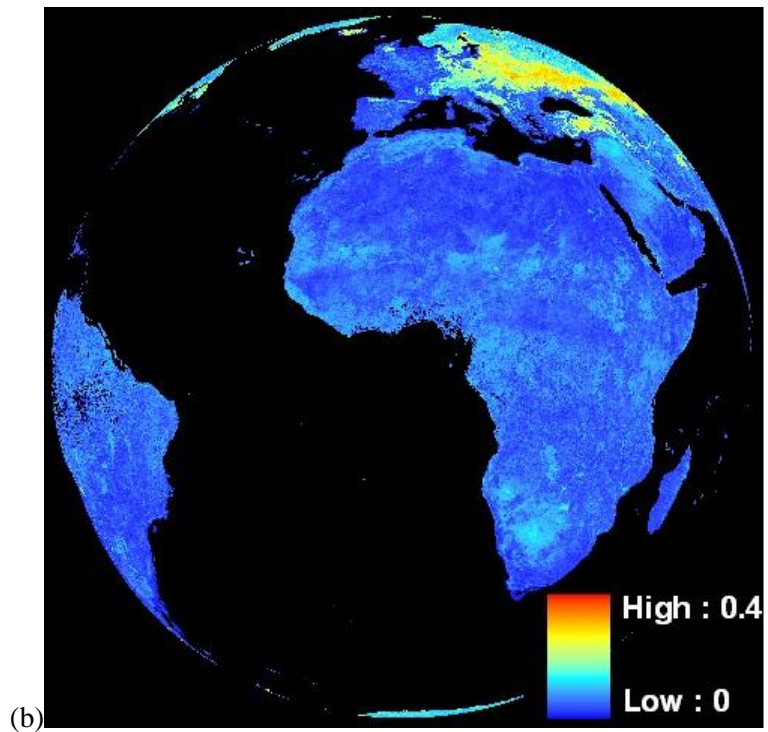
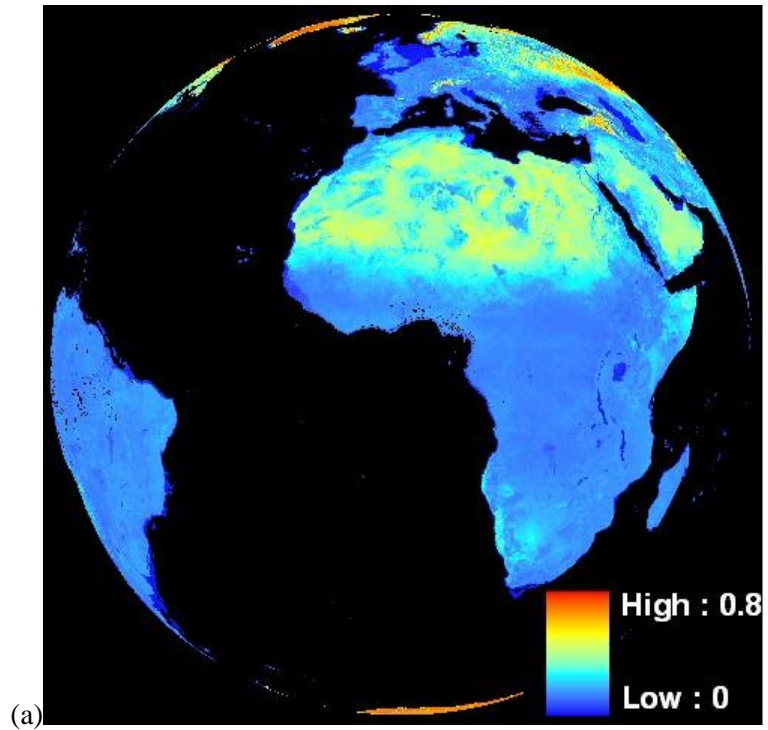


Figure 3-2 Albedo climatology for day of year (DOY) 065 in SEVIRI projection from ten years' MODIS shortwave albedo: (a) mean value of MODIS white-sky albedo; (b) standard deviation of MODIS white-sky albedo in ten years

3.2.3 Atmospheric look-up table (LUT)

The atmospheric LUT was created before the algorithm implementation to expedite the online calculation of the atmospheric variables needed in the radiative transfer and the estimation of all-sky surface albedo. Again, 6S software was used to do the atmospheric radiative transfer simulations. With the spectral response functions for all three SEVIRI bands as input, 6S can generate the atmospheric variables through the settings on geometries, and aerosol type, etc.

3.2.4 Algorithm implementation

All the TOA observations within the same day were collected. Before the ingestion of the data into the retrieving procedure, TOA reflectances were masked with the cloud data to insure that only clear sky information was used to derive the BRF. With only three spectral bands on SEVIRI, the minimum requirement for clear sky observations should be at least five in order to retrieve all the unknown variables in one retrieving procedure. 0.1 of AOD at 550 nm and the BRF kernel parameters from the preceding day provide the “first guess” in the retrieving process. The albedo climatology plays a vital role in matching it with the simulated broadband shortwave white-sky albedo to constrain the estimated surface BRF. Through minimization of Eq. (2-1), the retrieved BRF models and AOD were balanced with the albedo climatology and the satellite observations according to their uncertainties.

Once the surface BRF models were obtained through minimization of the cost function, the instantaneous bidirectional surface reflectance can be calculated. Given the

surface BRF and AOD retrievals, the instantaneous “blue-sky” albedo can be calculated based on the black-sky and white-sky albedo using diffuse skylight ratio f_{dif} using Eq. (2-3) which were used for the comparison with the ground measurements:

3.3 Results and discussion

3.3.1 Albedo comparison at IMECC sites

The network of IMECC is designed to provide dataset for characterizing the carbon balance of Europe. The IMECC Terrestrial Carbon Data Center (TCDC) maintains the access to the radiation measurements. Downward and upward surface radiation data are measured at a 30-min interval. Quality flags are provided along with the radiation measurements. There are four levels of quality flags: best, medium, bad, and missing. Only the data with “best” quality were used in this study. According to the availability and the quality of the data and the surface homogeneity, eight sites (listed in Table 3-2) were chosen here to compare our estimations with the ground measurements. The 16-day MODIS 5 km albedo products are provided through their website at an 8-day interval. To get comparable results, MODIS data with the best quality were used here in the comparisons at the chosen sites.

Daily-aggregated comparisons between the retrieved albedos from SEVIRI, the ground observations, and the MODIS 16-day averaged albedo values are given in Figure 3-3 (statistics listed in Table 3-3). The albedo estimates from this study are generally very close to MODIS values. One reason for this is that the albedo climatology is generated

from multi-year MODIS data. The other one is possibly the scale difference between the satellite pixel and the ground point.

Table 3-2 Information of the chosen IMECC sites

Site name	Latitude	Longitude	Surface cover type
CZ-Bk2	49.4953	18.5448	GRA
CH-Oe2	47.2863	7.7343	CRO
CZ-Wet	49.025	14.7722	WET
DE-Hai	51.0793	10.452	DBF
DK-Sor	55.4859	11.6446	MF
CH-Oe1	47.2858	7.732	GRA
DE-Geb	51.1001	10.9143	CRO
DE-Me2	51.2754	10.6556	GRA
DE-Meh	51.2753	10.6554	MF

GRA: grassland; CRO: cropland; WET: wetland; DBF: deciduous broadleaf forest; ENF: evergreen needleleaf forest; MF: mixed forest; EBF: evergreen broadleaf forest.

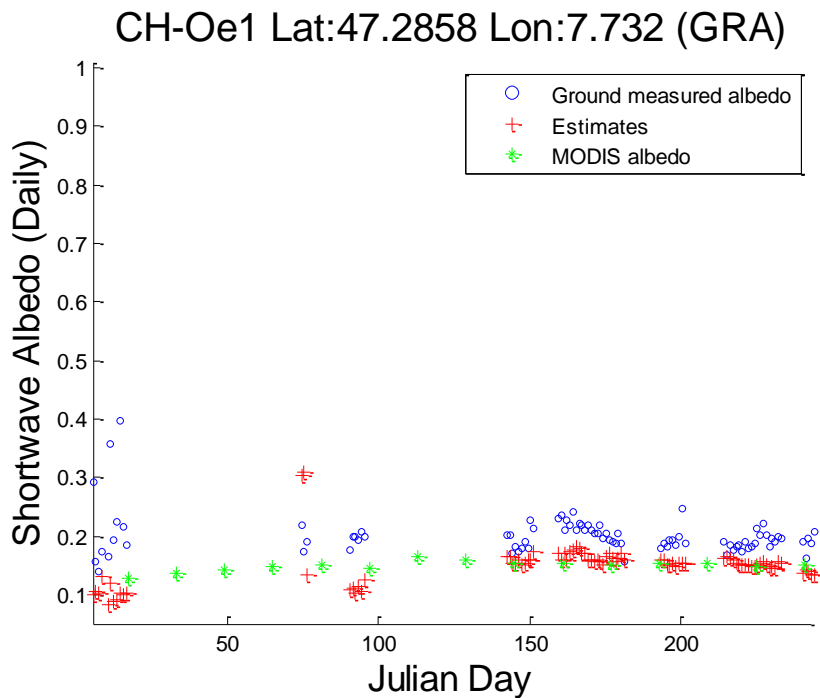
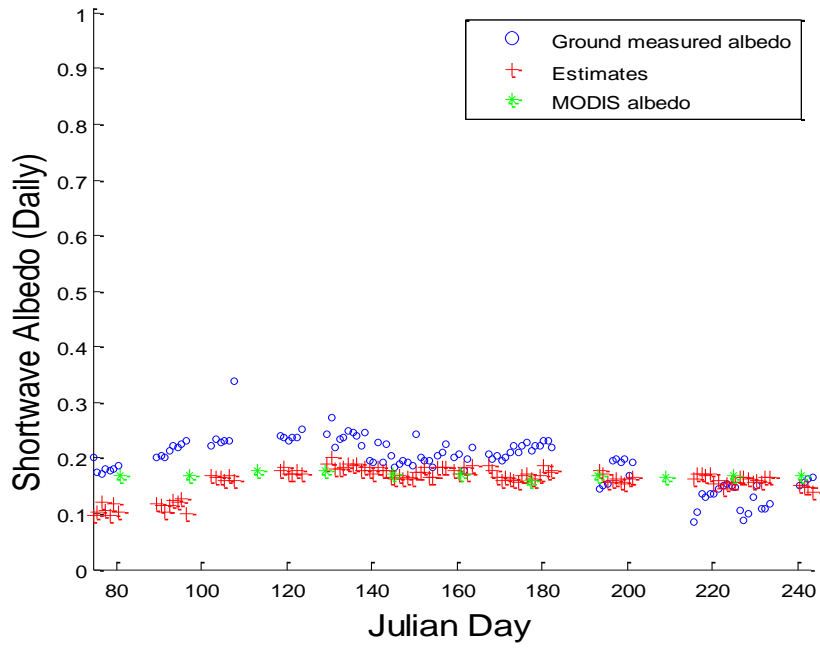


Figure 3-3 Comparison of daily-aggregated albedo from estimates in this study and ground measurements with MODIS 5 km products as reference at the IMECC sites

CH-Oe2 Lat:47.2863 Lon:7.7343 (CRO)



CZ-Bk2 Lat:49.5047 Lon:18.5411 (GRA)

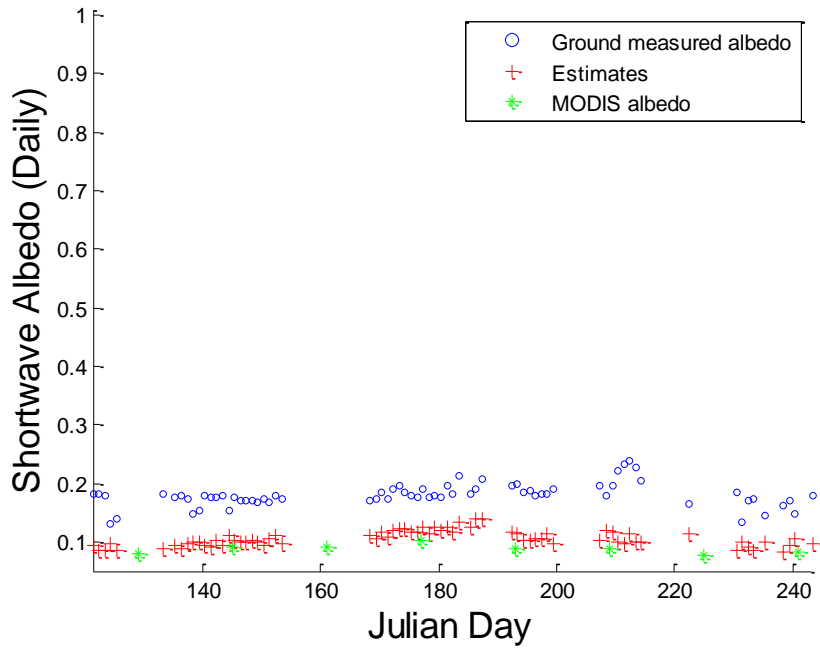
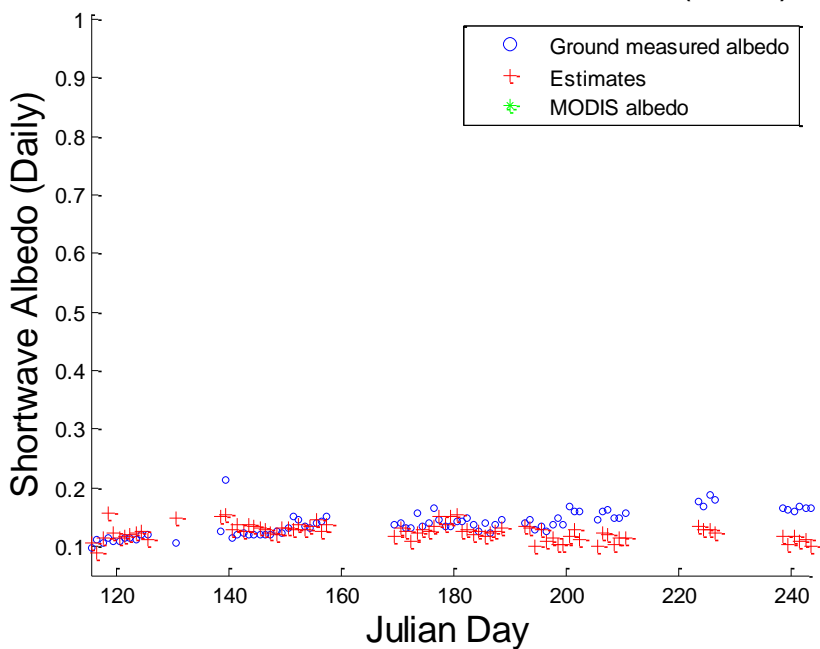


Figure 3-3 (continued)

CZ-Wet Lat:49.025 Lon:14.7722 (WET)



DE-Geb Lat:51.1001 Lon:10.9143 (CRO)

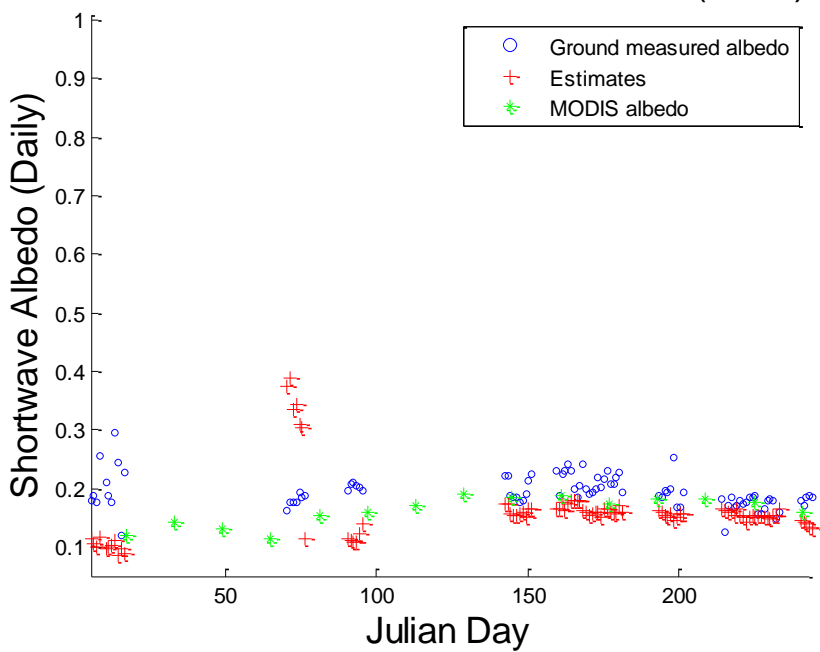
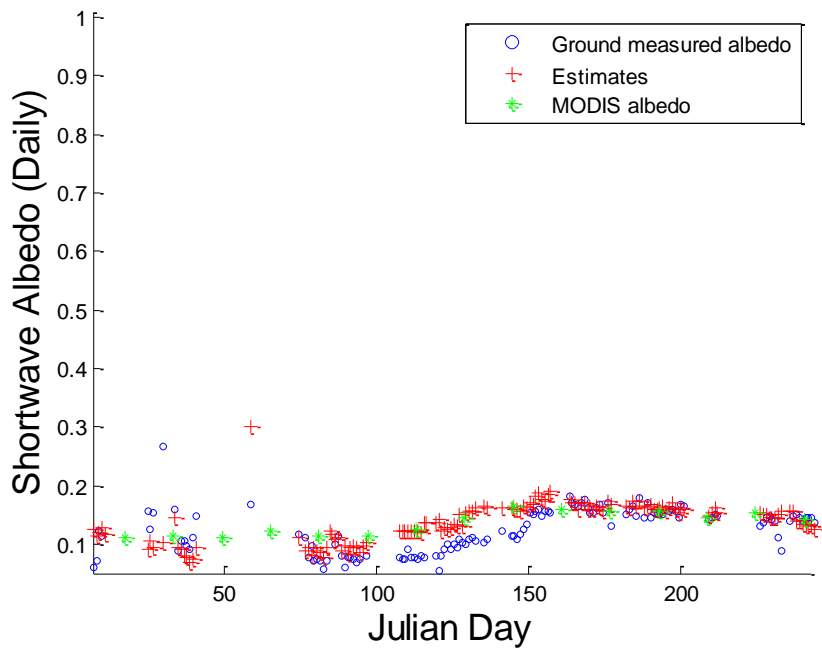


Figure 3-3 (continued)

DE-Hai Lat:51.0793 Lon:10.452 (DBF)



DE-Me2 Lat:51.2754 Lon:10.6556 (GRA)

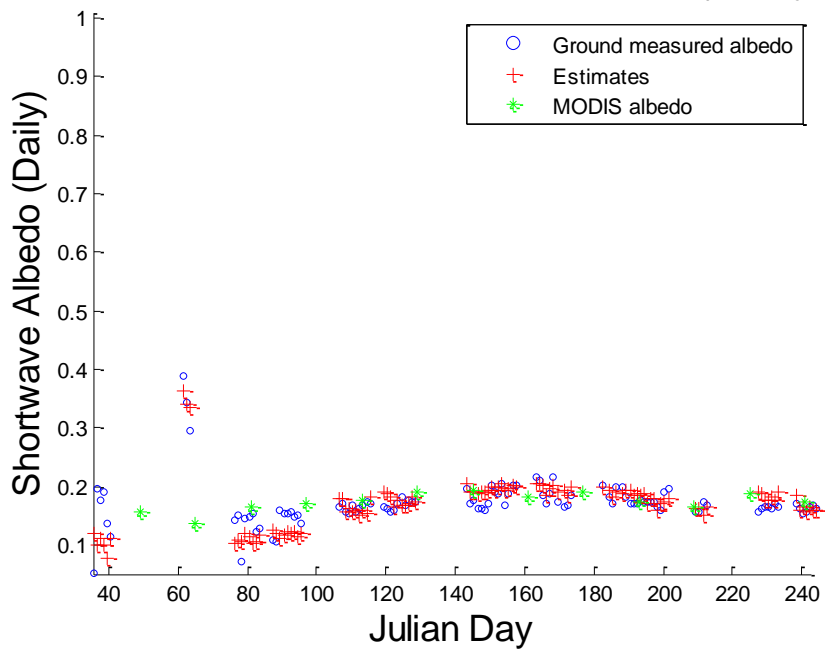


Figure 3-3 (continued)

DK-Sor Lat:55.4859 Lon:11.6446 (MF)

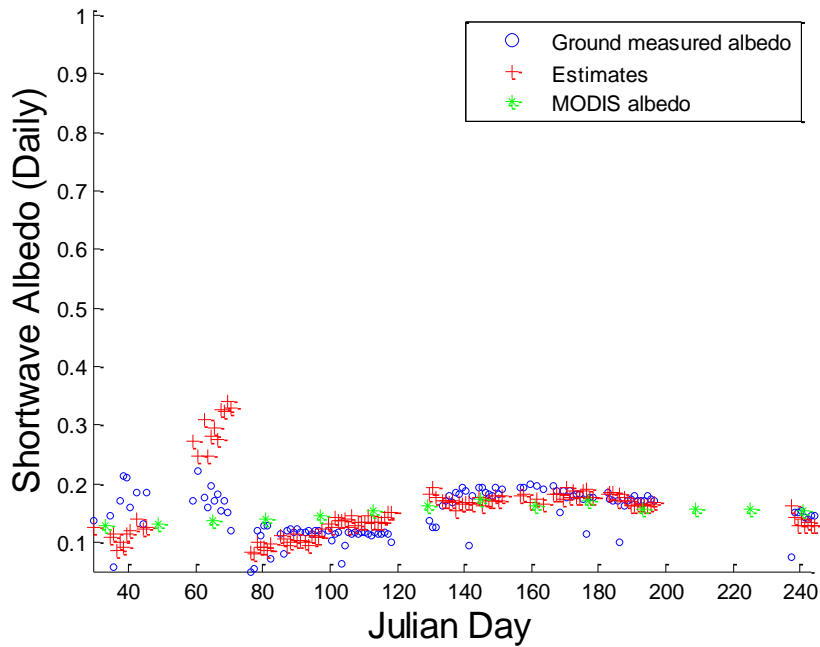


Figure 3-3 (continued)

Table 3-3 Statistics of daily-aggregated albedo estimation accuracies with comparison to ground measurements

Site name	Bias	RMSE	Site name	Bias	RMSE
CH-Oe1	0.0644	0.0802	DE-Geb	0.0289	0.0629
CH-Oe2	0.0483	0.0694	DE-Hai	-0.0066	0.0375
CZ-Bk2	0.0819	0.0857	DE-Me2	0.0174	0.0397
CZ-Wet	0.0289	0.0437	DK-Sor	-0.0029	0.0492

With the unique characteristics of angular samplings from SEVIRI, it is very important for the proposed algorithm to be able to generate diurnal surface albedo estimations. Figure 3-4 provides comparisons of the instantaneous albedo retrievals and the ground measurements. The time-series data comparisons were chosen based on the availability of ground measurements and satellite observations. In addition, it is found that around DOY 182 to DOY 200 MODIS albedo products agree well with ground measurements at all the chosen sites. This time period is chosen to examine the instantaneous albedo estimations from the proposed algorithm. The number of “best

quality” ground data was restricted to 80% for a whole day when the downward solar radiation is larger than 10 W/m^2 . The comparisons show that the retrieved albedo can well capture the diurnal change caused by the solar illumination angle. In addition, the day-to-day variation can be well represented by the retrievals in this study since the variation can be observed which the 16-day MODIS products do not have. In order to match the MODIS albedo data with the ground measurements, MODIS 0.05° BRDF dataset is used to calculate the instantaneous albedo value. Only the BRDF values with the “best quality” are used to do the calculation.

The day-to-day albedo variation can be caused by the soil moisture change resulting from precipitation. Results show that the proposed algorithm works reasonably good for SEVIRI data and the day-to-day variation can be captured even when the 16-day albedo climatology is not very accurate. For some sites, the albedo changes differently in the morning and in the afternoon, which some researches have proven that the dew in the morning and the wind near the ground can be the reason (Minnis et al. 1997; Song 1998). However, in this study, the surface BRDF shape was assumed to be invariant within a day which would therefore limit the capability to capture this phenomenon. Sometimes, the proposed algorithm here even generates the opposite shape.

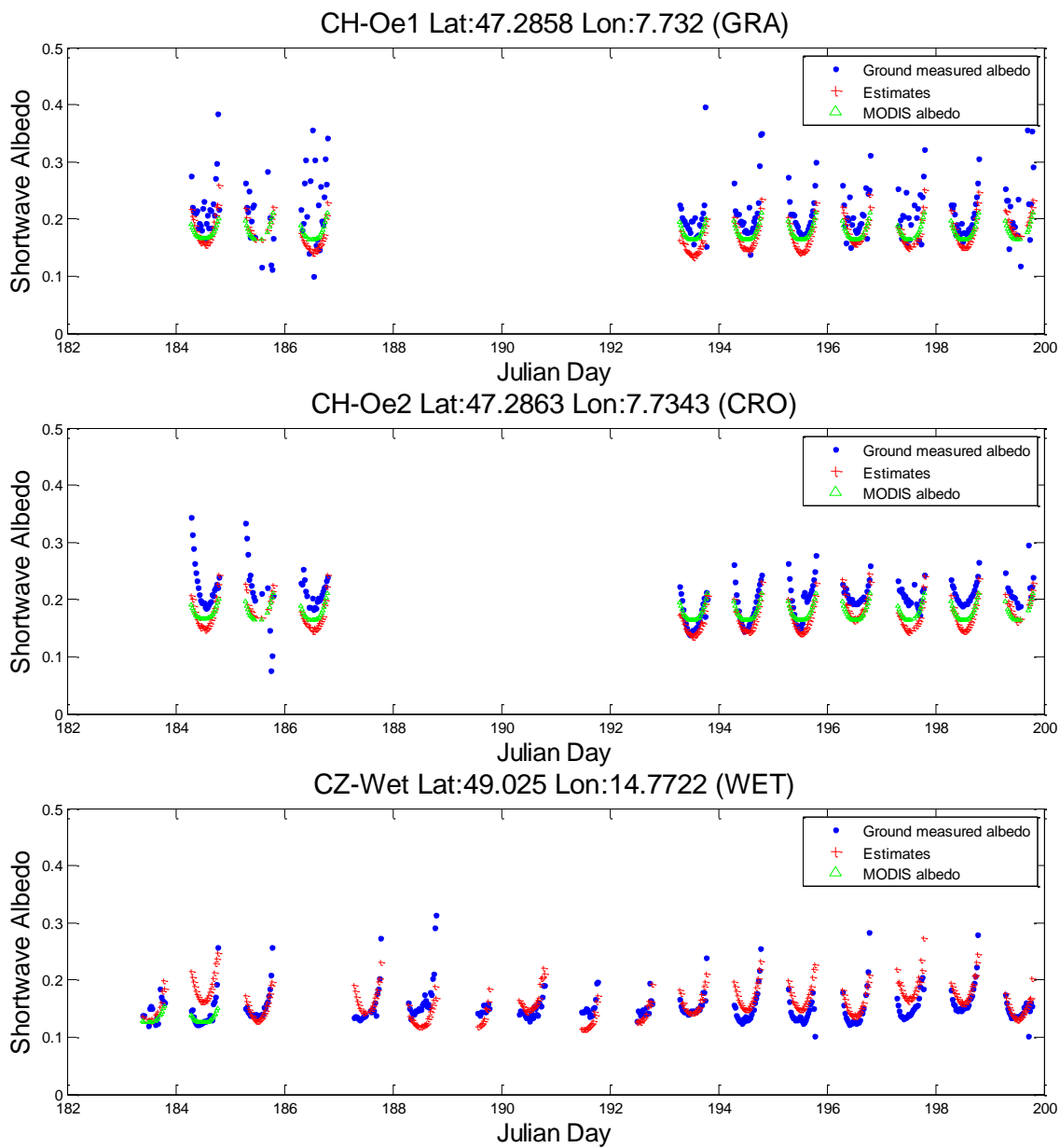


Figure 3-4 Comparison of instantaneous albedo from estimates in this study and ground measurements with MODIS 5 km products as reference at the IMECC sites

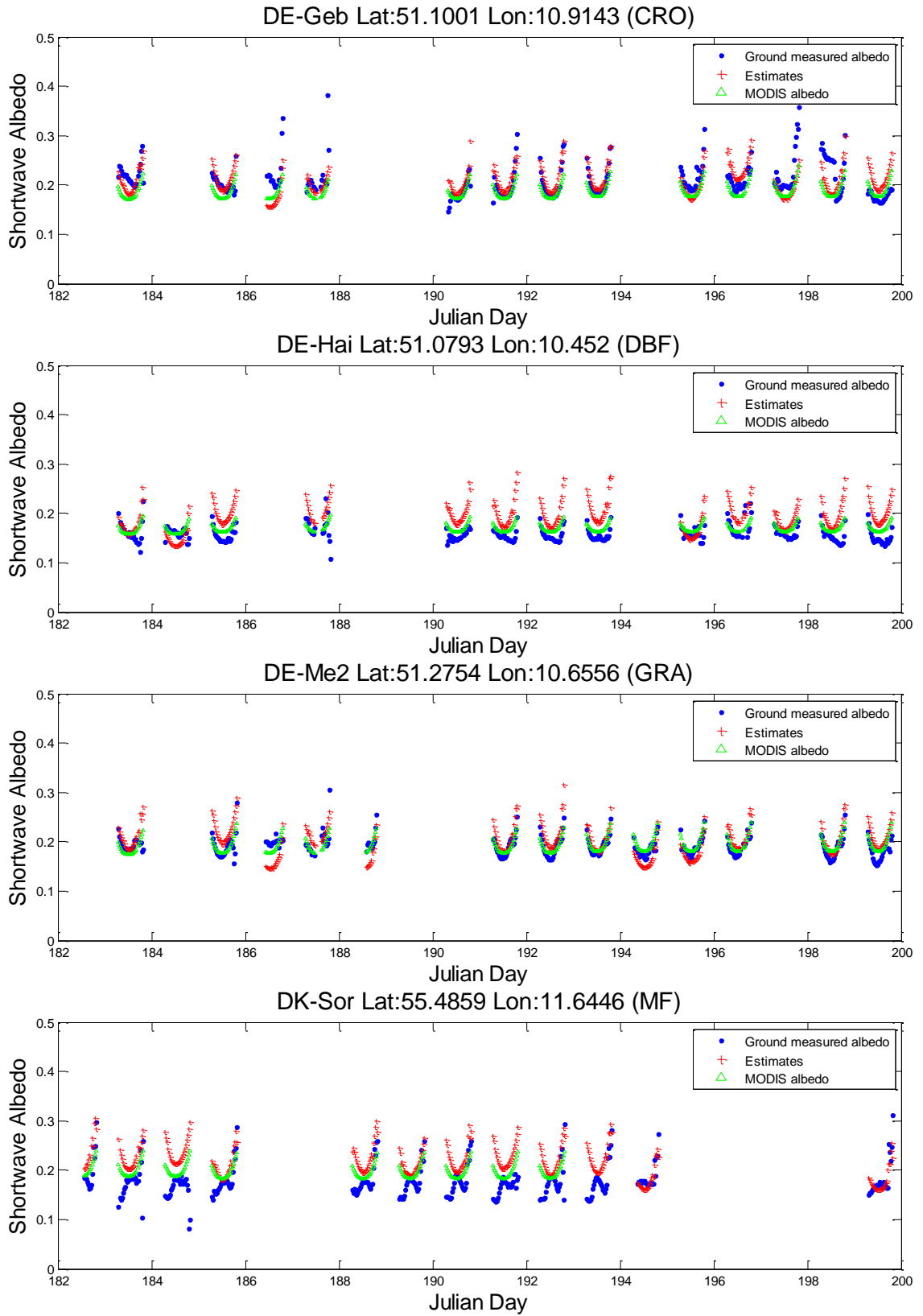


Figure 3-4 (continued)

An interesting phenomenon found at the site of DK-Sor is that the diurnal shape of ground-measured albedo is not convex but concave. The land cover type for this site is mixed forest. This might be the reason sunlight tends to penetrate from the gaps of the trees and is then reflected by the ground soil (which has higher reflectivity than vegetation in visible range) when the solar zenith is small. As the solar zenith becomes larger, more energy is absorbed by the forest while less energy can be reflected to the sensor. However, the basic assumption that the kernel parameters are non-negative otherwise similar albedo shapes as observed by the ground instrument cannot be generated.

Statistics in Table 3-4 suggest that good agreement has been achieved between the instantaneous albedo estimations from our algorithm and the MODIS algorithm, and the ground measurements. The proposed algorithm tends to generate larger albedo than the MODIS algorithm does when solar zenith angle is large, which may result from the wider angular sampling from SEVIRI than that from MODIS. It has been found that for MODIS albedo products, the absolute bias and RMSE increase with the solar zenith angle (Liu et al. 2009). Similar trend is found in this study that both bias and RMSE of our retrieved albedo values increase with the solar zenith angle. When the solar zenith is smaller than 55° , there is a small positive bias of 0.0009 with an RMSE of 0.0336. As the solar zenith increases beyond 55° , the bias and the RMSE increase to 0.0140 and 0.0414 respectively. The increase of the albedo standard deviation from 0.0253 ($<55^\circ$) to 0.0329 ($\geq 55^\circ$) is the major reason for the decrease of the albedo estimation accuracy while the bias may come from the problem of the kernel models that are with less accuracy for large solar angles.

In surface radiation budget studies, surface albedo is an indicator of how much energy is reflected by the surface, from which the remained downward solar radiation is absorbed. Net radiation quantifies the solar radiation absorbed by Earth’s surface. Unlike the polar-orbiting satellites, SEVIRI can obtain observations under different solar angles during the daytime thus provides better capability of monitoring the net radiation at the surface. Net shortwave radiation R_{Net} estimations from this study is calculated from ground measured downward shortwave radiation R_{\downarrow} and surface albedo α_{blue} using Eq. (3-3):

$$R_{Net} = R_{\downarrow} - R_{\uparrow} = (1 - \alpha_{blue}) R_{\downarrow} \quad (3-3)$$

Table 3-4 Statistics of instantaneous albedo estimation accuracies with comparison to ground measurements

Site Name	Our retrievals			MODIS albedo from BRDF		
	Bias	STD	RMSE	Bias	STD	RMSE
CH-Oe1	-0.0379	0.0262	0.0562	-0.0337	0.0129	0.0545
CH-Oe2	-0.0301	0.0260	0.0404	-0.0247	0.0131	0.0389
CZ-Wet	0.0077	0.0278	0.0286	-0.0125	0.0083	0.0244
DE-Geb	0.0013	0.0277	0.0327	-0.0199	0.0145	0.0341
DE-Hai	0.0344	0.0294	0.0446	0.0109	0.0086	0.0187
DE-Me2	0.0099	0.0318	0.0278	0.0018	0.0158	0.0146
DK-Sor	0.0396	0.0320	0.0549	0.0215	0.0147	0.0358
All sites	0.0056	0.0351	0.0414	-0.0075	0.0181	0.0341

Table 3-5 lists the accuracy of net shortwave radiation estimations for all the chosen sites. A negative bias in surface albedo estimation causes an underestimation of upward radiation thus an overestimation of net radiation. When there is a larger error in the surface albedo estimation, there is greater uncertainty in the net radiation calculation. Combining all sites together, there is a small negative bias of -2.2023 W/m^2 (RMSE: 18.2900 W/m^2) in net radiation estimations. Unlike the solar angle's impacts on surface albedo estimations, the accuracy of net radiation estimations does not change much under different solar angles ($<55^\circ$ and $\geq 55^\circ$) in terms of the bias and the RMSE. This is probably because that the downward radiation decreases with the solar angles.

Table 3-5 Accuracy assessment of net radiation estimations

Site Name	Net shortwave radiation (W/m^2)	
	Bias	RMSE
CH-Oe1	16.7390	21.4240
CH-Oe2	-4.9975	12.0180
CZ-Wet	-15.2350	19.7850
DE-Geb	-17.8170	23.5220
DE-Hai	17.9830	24.0860
DE-Me2	-0.0007	13.6960
DK-Sor	-4.6793	11.6970
All sites	-2.2023	18.2900
All sites $<55^\circ$	-1.3520	20.1900
All sites $\geq 55^\circ$	-3.7125	14.3080

3.3.2 AOD comparison with MISR products

The MISR on board Terra is one of the most successful polar-orbiting sensors designed for the aerosol monitoring. It has some unique advantages to accurately estimate the AOD with multiple bands in the shortwave range (especially the blue band) and observations from nine viewing angles. The MISR Level 2 aerosol products (Diner et al.

2005) with the most recent version (V22) are used in this study. This dataset is reported at a spatial resolution of 17.6 km using a 16×16 array of 1.1 km radiance pixels. Extensive validations of the MISR AOD with ground measurements (Kahn et al. 2010; Kahn et al. 2005) show that the error of AOD at 550 nm is less than 0.03-0.05. Comparisons made between our AOD estimations and MISR AOD products are given in Figure 3-5 at all the chosen IMECC sites. To match SEVIRI data with MISR data and to reduce the temporal fluctuation of our retrieved values, averages of our AOD retrievals are calculated if the SEVIRI observation time is within the ± 30 -min window of the MISR overpass. A slight underestimation of AOD is found in this comparison, with 68% of our retrievals falling within $20\% \times \text{AOD}$.

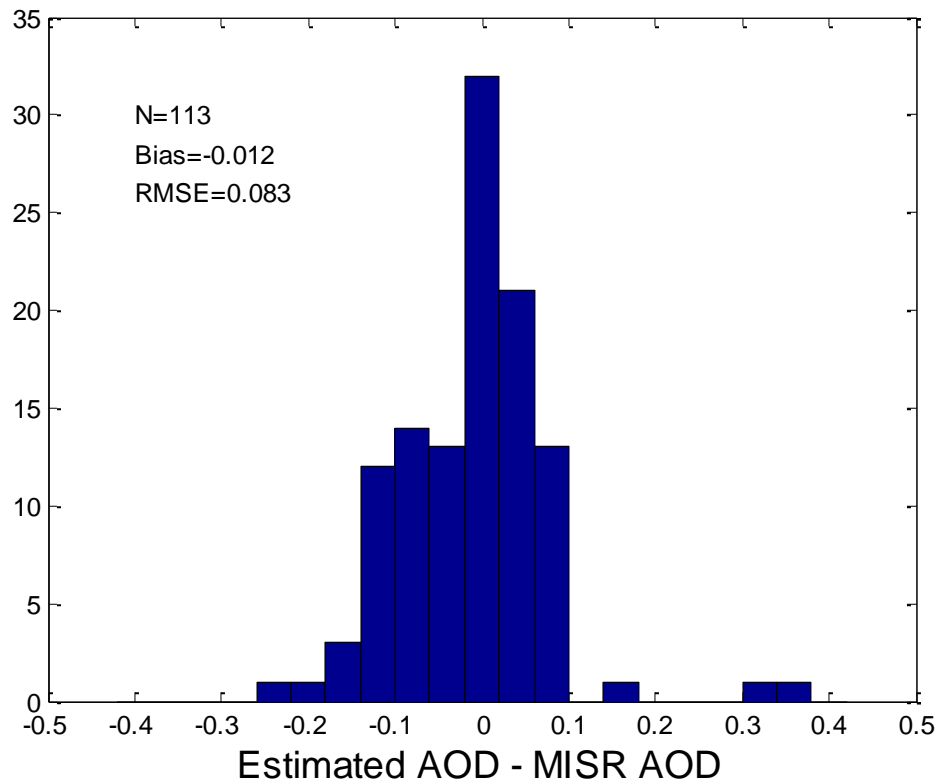


Figure 3-5 Histogram of the AOD estimation error

3.3.3 Albedo map

The major objective of this algorithm is to generate the surface albedo from SEVIRI data. At SEVIRI's spatial resolution, it's difficult to find homogeneous ground truth from the ground measurements. Therefore, albedo products from other satellite data are needed to help verify the performance and validity of the albedo estimations from this algorithm under different atmosphere and surface conditions over a large area. In this study, MODIS albedo products are reprojected and resampled into the SEVIRI projection. Comparison is made between the retrieved albedo here and the reprojected MODIS albedo map on DOY 121, 2005 (Figure 3-6). Similar spatial patterns can be found in both maps. However, our results show greater spatial variations in surface albedo over the deserts and the sparsely vegetated area in North Africa and the Middle East, which suggests that the algorithm used in this study may have better capabilities in monitoring aerosol variation over bright surfaces. Over the east part of South America which is covered mainly by rain forests, our algorithm generates some higher albedo values. This overestimation is probably caused by undetected clouds. The viewing path is longer for the pixels close to the edge of the scene, which gives a higher possibility of cloud contamination. Moreover, other than the 16-day composition method used in the MODIS algorithm, the daily basis albedo estimation in this study can sometimes suffer from the undetected sub-pixel clouds. Due to the reduced spatial coverage of the cloud mask products, our algorithm do not have albedo estimations over the areas (Greenland and Central Asia, etc.) close to the edge of the scene. The overall statistics shown in Figure 3-7 suggest that our results are comparable to MODIS products, though with a small positive bias.

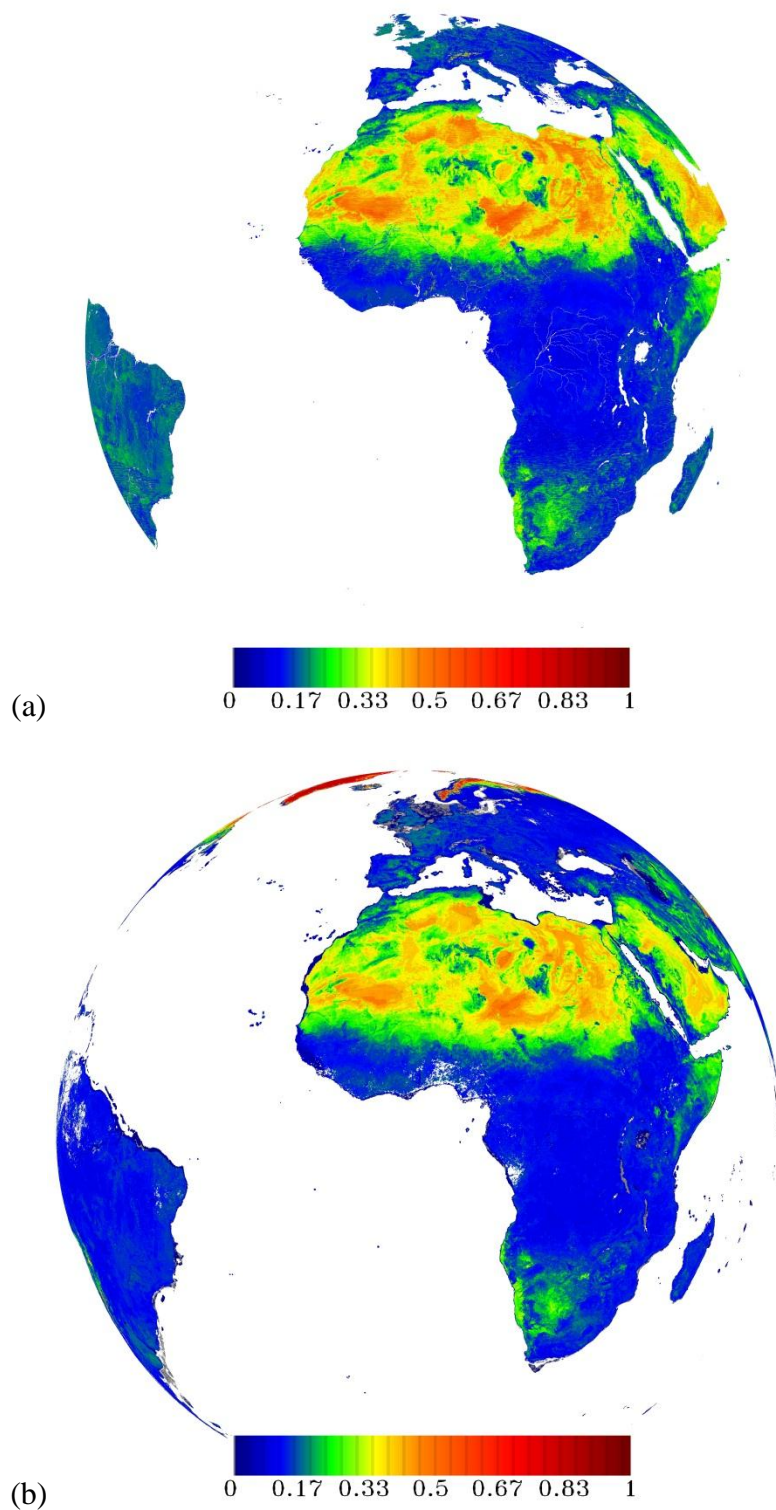


Figure 3-6 Comparison of shortwave albedo in MSG2/SEVIRI projection on DOY 121, 2005: (a) black-sky albedo estimations from SEVIRI proxy data; (b) reprojected MODIS black-sky albedo products (white color means no data or water)

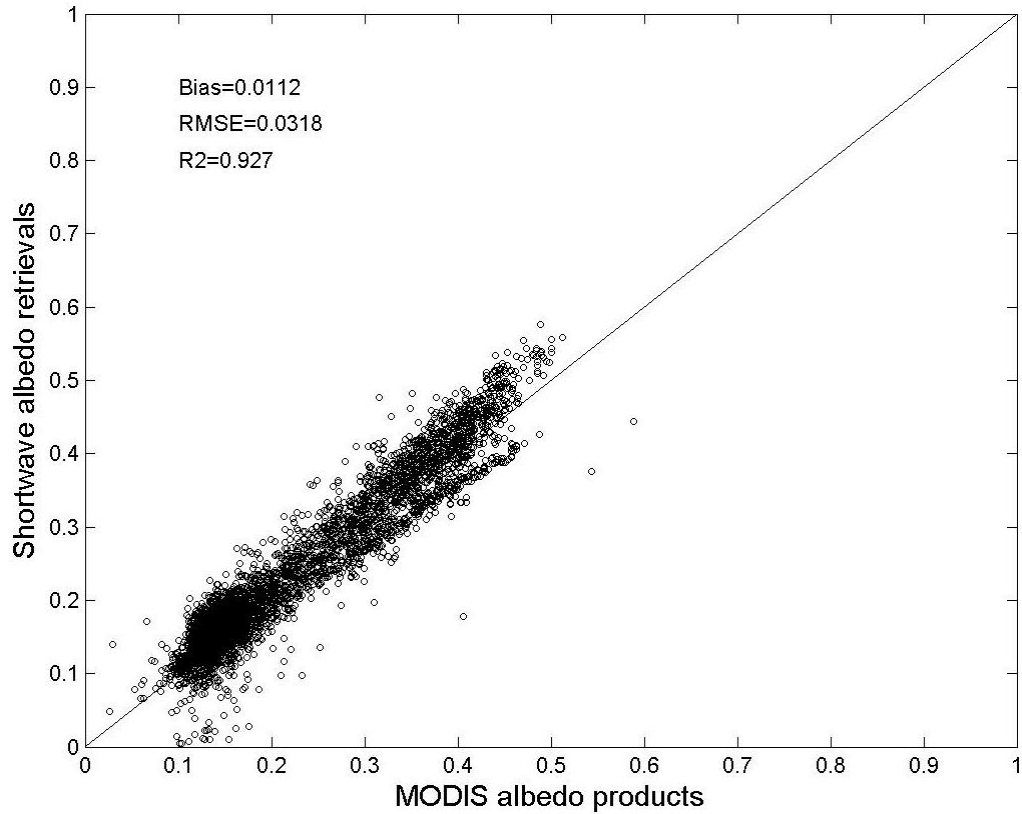


Figure 3-7 Statistics of the comparisons over the scene

3.4 Summary and conclusions

The geostationary satellite provides a unique means to observe the Earth's surface at very high temporal resolution that can better capture the surface anisotropy within a short time period while the polar orbiting satellites cannot. As a prototype for the GOES-R ABI surface albedo algorithm, the approach proposed in this study used the MSG/SEVIRI as proxy data to evaluate its performance. Generally, this study showed reasonably results while comparing the retrieved albedo from this approach with the ground measurements and satellite-derived products. Given the limitation of the SEVIRI spectral bands, the aerosol loadings could not be estimated accurately due to lack of a

blue band and the narrow-to-broadband albedo conversion accuracy suffered from the limited number of spectral bands in the visible range. In addition, the residual cloud contamination, which was not successfully identified by the current cloud mask algorithm, influenced the retrieving procedure by either overestimating or underestimating the surface albedo due to cloud or cloud shadow.

With the development of the GOES-R ABI, which has more bands in the shortwave range (similar to MODIS), the estimation accuracy will probably be improved through better characterization of aerosol and broadband albedo conversion.

CHAPTER 4 GENERATING CONSISTENT SURFACE ALBEDO PRODUCTS ACROSS SCALES FROM DIFFERENT SATELLITE SENSORS USING A MULTI-RESOLUTION TREE (MRT) METHOD

4.1 Introduction

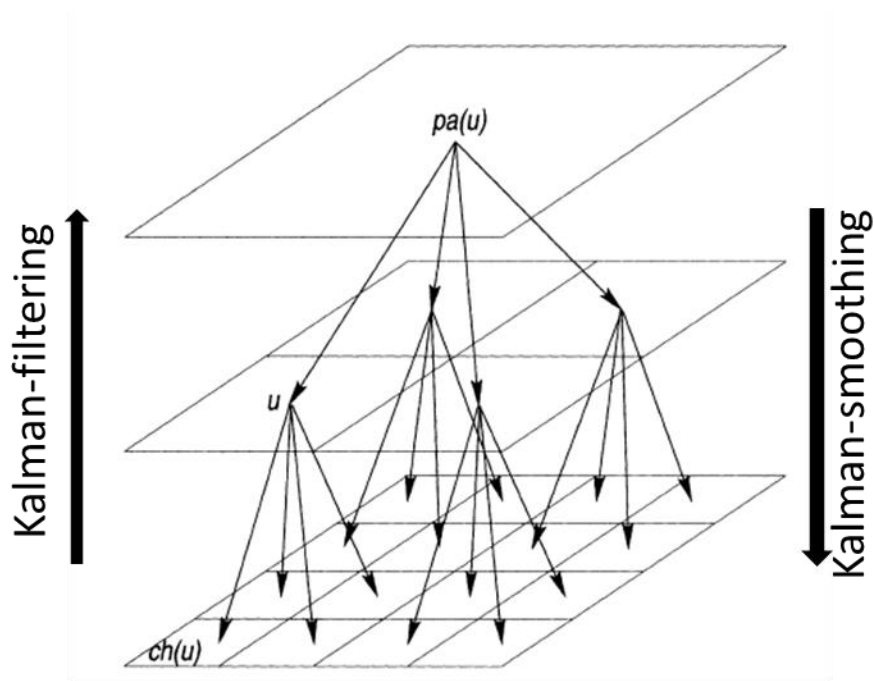
The framework of the MRT method has been developed in recent years to make predictions consistent across different spatial resolutions by assuming a statistical model that is autoregressive in levels of resolution (Chou et al. 1994). The MRT method has been widely used on large datasets to overcome the computational difficulties which the other existing methods (optimal interpolation, kriging, etc.) may have (Yue and Zhu 2006). Many researchers have been applying this method to interpolate and to smooth data over various satellite products (Huang et al. 2002; Wang and Liang 2010; Yue and Zhu 2006; Zhu and Yue 2005; Zhu et al. 2010). Based on its time efficiency and capability of generating interpolations with minimal bias, this method is chosen to do the albedo data fusion from multiple satellite datasets.

4.2 Methodology

The theoretical basis of the MRT is to assume that data at different spatial resolutions are autoregressive and can be organized in the tree structure (Figure 4-1). The linear tree-structure model can be expressed using (4-1):

$$y_u = A_u y_{pa(u)} + w_u \quad (4-1)$$

where y_u is the variable to estimate at the scale u and $y_{pa(u)}$ is the variable at the parent node. w_u is the spatial stochastic process that follows a Gaussian normal distribution with a variance of W_u . A_u is the state conversion matrix that estimates the variable at scale u from its parent node. There is a similar formulation that transfers the variable at scale u from its child node $ch(u)$. To determine the state conversion matrix, the “change-of-support” problem has been widely discussed in much research (Huang et al. 2002; Plumejeaud et al. 2011; Wikle 2003). A simple aggregation method is used in this study.



Source: Huang, et al. 2002

Figure 4-1 MRT data structure

Besides the state conversion model, an observation model is also used in this method by converting the satellite products to the “truth” data:

$$z_u = C_u y_u + \varepsilon_u \quad (4-2)$$

Here, z_u is the satellite product with a white noise ε_u that follows a normal distribution $N(0, \Phi_u)$. C_u is the observation matrix that converts the variable of interest to the satellite data. Since both the variable and the satellite data are surface albedo, the observation matrix C_u is set to be one.

The MRT algorithm consists of two-steps, the leaves-to-root filtering step and the root-to-leaves smoothing step. The basic assumption of the tree models is that the tree-structure follows a Markov chain process which means that the state variable is only related to its instant child nodes and instant parent node(s). The first step is a high-to-low resolution filtering to estimate state variable from higher resolution data (Eq. (4-3)). The major purpose of this step is to fill in the gaps at different resolutions. In the leaves-to-root filtering step, the Kalman filter is used here to deal with the Markov process. The second step is a low-to-high resolution smoothing to update the state variable with the information at a coarser resolution (Eq. (4-4)). This step generally assumes that the process at the parent scale provides the foundation of the process at current scale. After the Kalman-smoothing step, the datasets at different spatial scale will become smooth and consistent. For details of the Kalman filter derivations please refer to Huang et al. (2002).

$$\hat{y}_u = E(y_u | \mathbf{Z}_u, \mathbf{Z}_{ch(u)}) \quad (4-3)$$

$$\hat{y}_u = E(y_u | \mathbf{Z}_u, \mathbf{Z}_{pa(u)}) \quad (4-4)$$

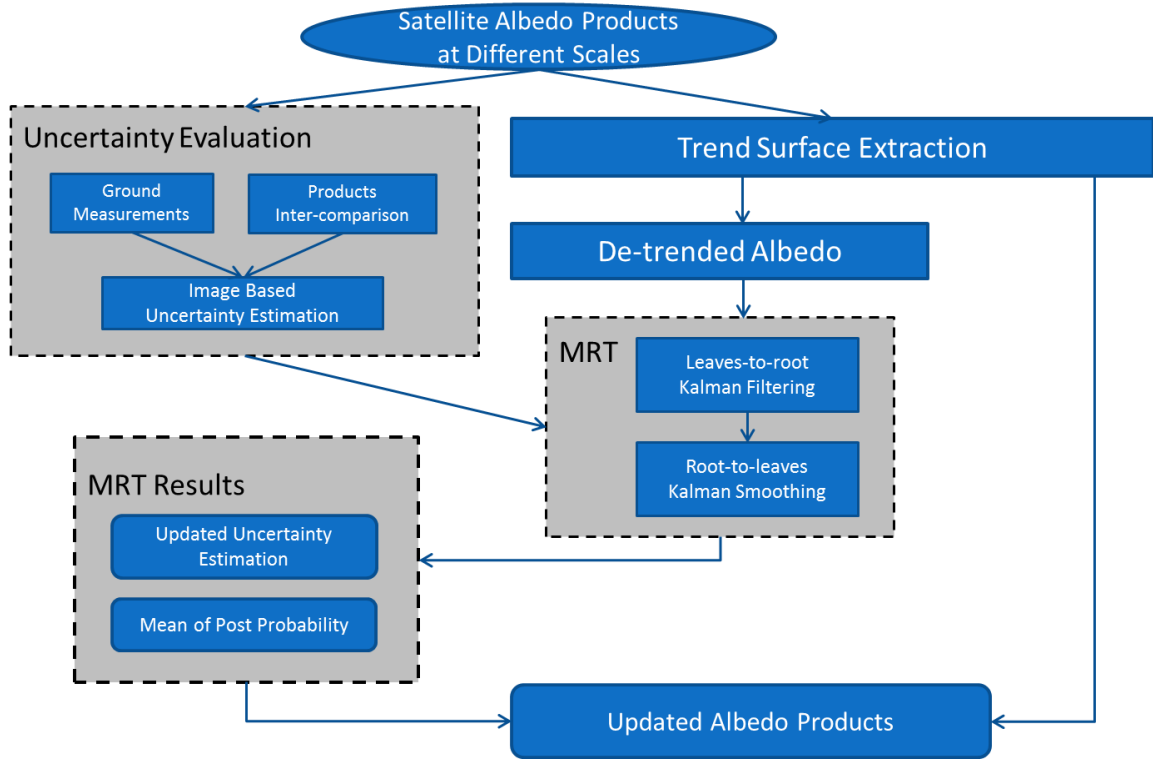


Figure 4-2 Framework of MRT albedo data fusion from multiple satellite products

To implement the MRT using multiple satellite products, there are generally several steps (Figure 4-2). First, the data uncertainties of different satellite products need to be evaluated and quantified. To do this, the ground measurements of surface albedo are collected to verify the satellite albedo products. Inter-comparison between different satellite datasets also provides the accuracy information. Second, there is one basic assumption of zero mean in the spatial process of the variable used and predicted in the MRT. Therefore, the spatial trend surface for each of the satellite products needs to be extracted so that the de-trended albedo datasets can be used in the data fusion process. Third, the leaves-to-root Kalman filtering and the root-to-leaves Kalman smoothing are implemented recursively to get the updated probability estimation of the data at each

scale. Finally, the updated spatial residual “albedo” is added back to the trend surface to get the real updated albedo maps at all the scales involved. In this study, satellite albedo products from MISR, MODIS, and Landsat are used to apply the MRT method.

4.3 Characterization of the data uncertainties of different satellite products

4.3.1 Ground measurements

The study area is located in the middle north of the United States. The land cover types are mainly cropland, grassland, forest, and some water bodies. Data are collected at nine AmeriFlux sites in the study area. Site information is listed in Table 4-1.

4.3.2 Landsat data

Landsat L1T dataset is geometrically and radiometrically calibrated and projected in the Universal Transverse Mercator (UTM) coordinate system from the original Landsat data. This dataset is available on the USGS website (<http://earthexplorer.usgs.gov>).

Table 4-1 AmeriFlux sites

Site_Name	State	Latitude	Longitude	Elevation	IGBP	Landsat Scene
Bondville	IL	40.006	-88.290	219	CRO	p023r032
Bondville Companion Site	IL	40.009	-88.290	219.3	CRO	p023r032
Brookings	SD	44.345	-96.836	510	CRO	p029r029
Fermi Agricultural	IL	41.859	-88.223	225	CRO	p023r031
Fermi Prairie	IL	41.841	-88.241	226	CRO	p023r031
Fort Peck	MT	48.308	-105.102	634	GRA	p035r026
Lost Creek	WI	46.083	-89.979	480	DBF	p025r028
Willow Creek	WI	45.806	-90.080	515	DBF	p025r028
nstl10	IA	41.975	-93.691	315	CRO	p027r031

CRO: cropland; GRA: grassland; DBF: deciduous broadleaf forest.

To get the surface reflectance, the LEDAPS tool (Masek et al. 2006) is here used to do the atmospheric correction on Landsat L1T data for the year of 2005. The LEDAPS tool relies on 6S software (Kotchenova et al. 2006) to do the atmospheric correction based on some atmospheric ancillary dataset from reanalysis data. To mitigate the cloud contamination on the atmospheric correction, only the scenes with no more than 30% cloudy pixels are used in this study.

If we assume the surface is lambertian on the Landsat 30m scale, the Landsat shortwave surface albedo can be calculated using the equation from Liang (2001). Eq. (4-5) can be applied on the band conversion for both TM on board Landsat-5 and ETM+ on board Landsat-7, since they have the same multispectral bands with similar spectral coverages (Liang 2001).

$$\alpha_{short} = 0.356\alpha_1 + 0.130\alpha_3 + 0.3736\alpha_4 + 0.085\alpha_5 + 0.072\alpha_7 - 0.0018 \quad (4-5)$$

4.3.3 MODIS albedo products

MODIS Level 3 500m albedo (MCD43A3) together with the quality flags (MCD43A2) are available every 8 days which is based on the observations in a period of 16 days. The actual pixel size for this nominal “500m” Sinusoidal grid is 463.3127m. Shortwave broadband albedo is included in this product for both bi-hemispherical (white-sky) and directional-hemispherical (black-sky) albedos. In this study, the MODIS tile h11v04 is chosen to match with the Landsat scenes.

4.3.4 MISR albedo products

MISR Level 2 albedo products with a spatial resolution of 1100m are used in this study. The albedo data is stored in the grid system called Space Oblique Mercator (SOM). MISR albedo products contain both bi-hemispherical and directional-hemispherical albedos for each of the spectral bands. MISR shortwave broadband albedo is converted from the spectral albedos using the following equation (Liang 2001):

$$\alpha_{short} = 0.126\alpha_2 + 0.343\alpha_3 + 0.415\alpha_4 + 0.0037 \quad (4-6)$$

4.3.5 Inter-comparison at AmeriFlux sites

Figure 4-3 shows the time-series of MODIS, MISR, TM, and ETM+ albedo values with comparison to the ground measurements at the eight AmeriFlux sites. MODIS data with the highest quality are shown as good and other data are shown as bad. In this comparison, we can see that MODIS data have the stable and smooth annual curves. Since MODIS algorithm tends to generate snow-free albedo and the estimations from the magnitude version are flagged as low quality (Lucht et al. 2000; Schaaf et al. 2002), the abrupt changes caused by events such as ephemeral snow cannot be seen from MODIS good quality data. Besides, the scale difference is significant between MODIS data and ground measurements. MISR data have similar values to MODIS data. However, the fluctuation of MISR data seems to be a little bit higher because MISR algorithm only relies on the observations within a very short time. Landsat data provide the best match with the ground measurements because of the finest spatial resolution with the instantaneous information. The 16-day's repeating cycle of Landsat data provides similar data availability to MODIS and MISR if combining the data from TM and ETM+. Failure

of cloud detection on Landsat data is the major reason for the data uncertainties shown here. Outliers are contaminated by either clouds or cloud shadows.

Statistics on the paired comparison of Landsat data and ground measurements are shown in Figure 4-4. No significant differences are found for the data uncertainties on TM and ETM+. The standard deviation of the relative error of Landsat data is 25.74%, which means that Landsat data have a relative error of about 25.74% in general.

Then, MODIS and MISR data are reprojected into UTM projection and Landsat data are aggregated to match MODIS and MISR to evaluate their albedo estimation accuracies respectively. From the comparisons with aggregated Landsat data, MODIS albedo has a bias of -0.0263 with an RMSE of 0.0353, while MISR albedo has a bias of 0.0282 with an RMSE of 0.031.

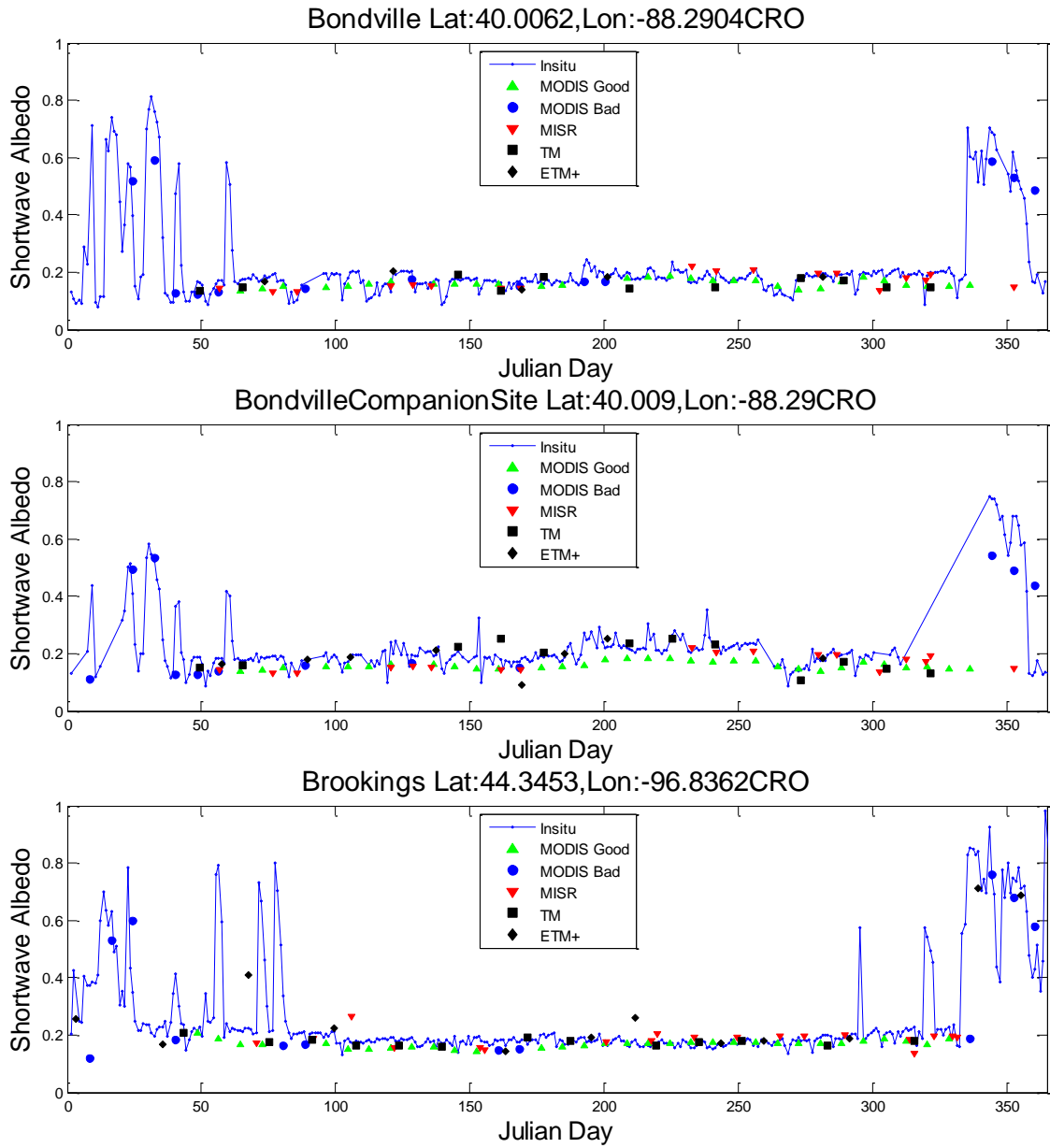


Figure 4-3 Time-series comparisons of different albedo datasets at the AmeriFlux sites

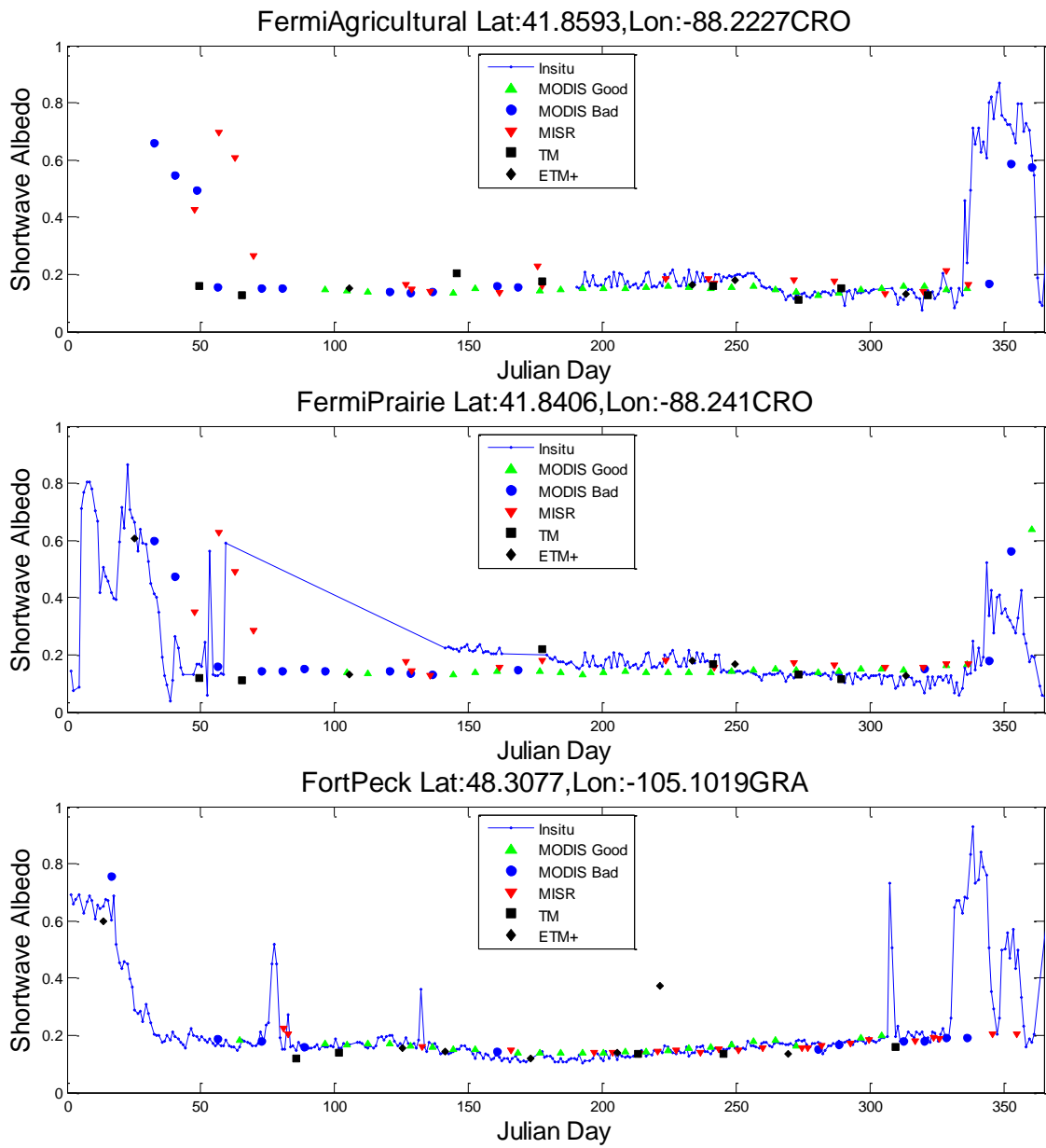


Figure 4-3 (continued)

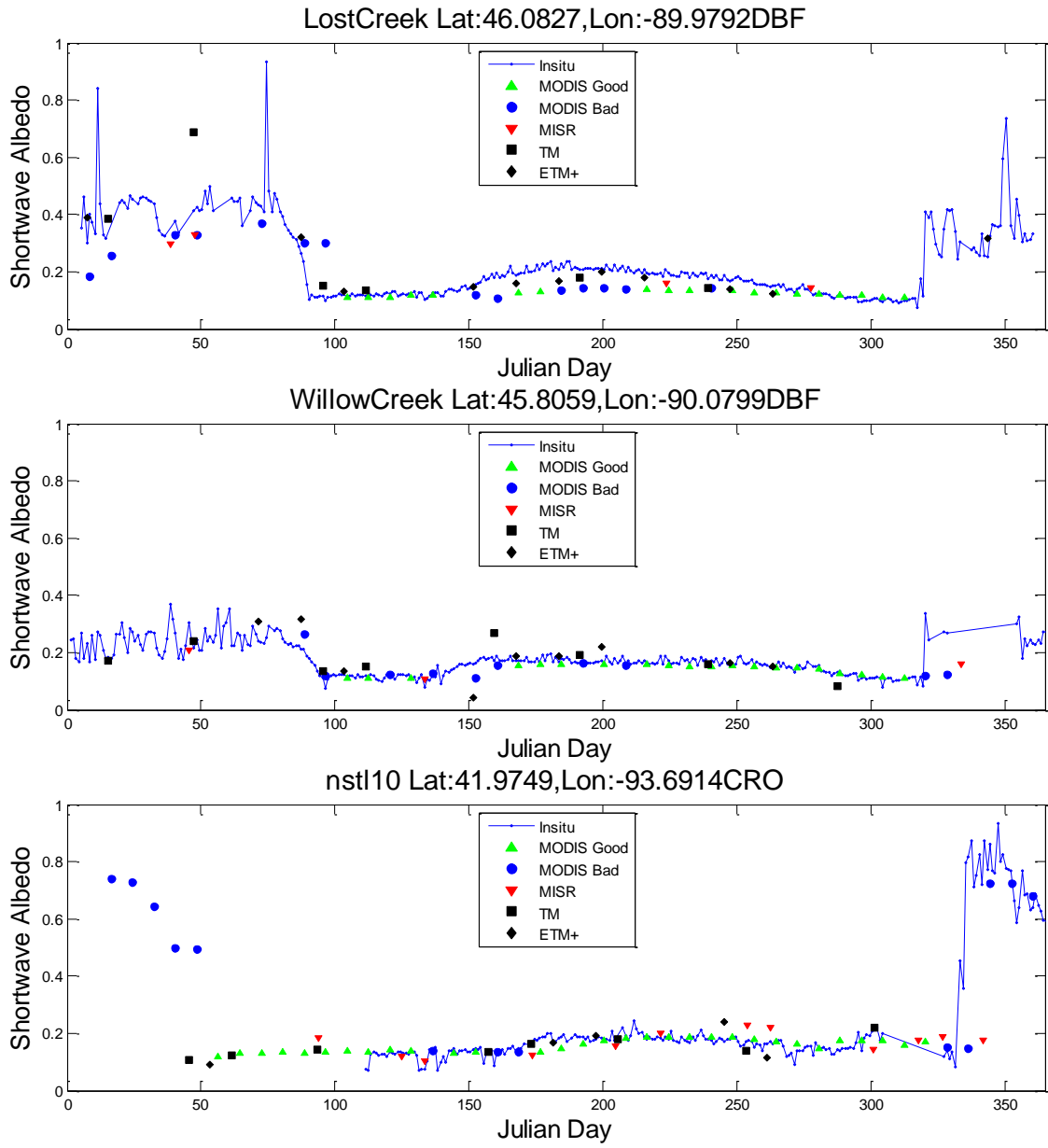


Figure 4-3 (continued)

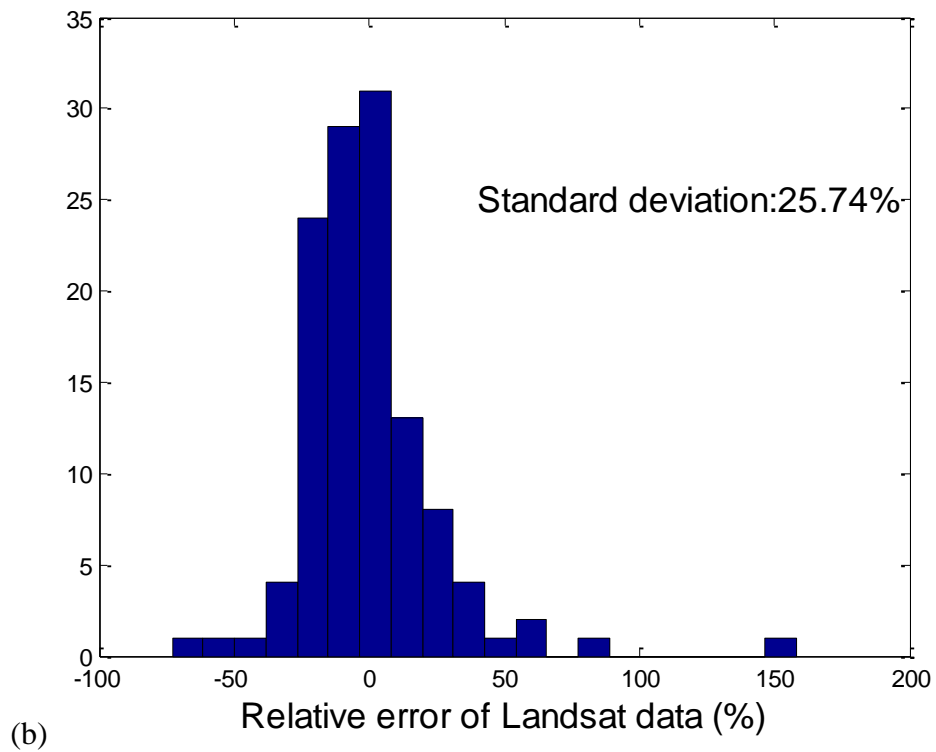
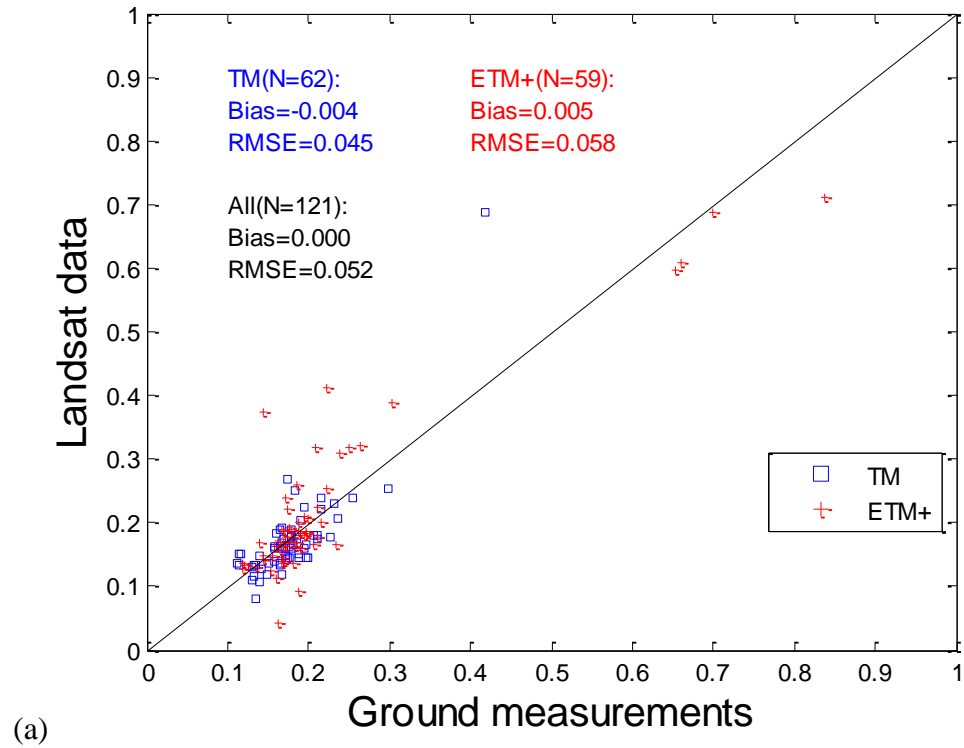


Figure 4-4 Evaluation of Landsat data using ground measurements: (a) paired comparison and (b) histogram

4.4 Results and discussion

4.4.1 Data selection and preprocess

To evaluate this method using three different satellite datasets, a subset of approximately $135 \text{ km} \times 135 \text{ km}$ area is extracted from all these products in the UTM projection. This area is located in the Landsat scene p025r028 and shares the same land cover types as that in the whole MODIS tile h11v04. The uncertainties of the albedo products are assumed to be the same as mentioned in the last section.

Criteria are made on the selection of data used in the experiment based on cloud coverage and timing of the data. Landsat surface reflectance is generated through the LEDAPS tool that gives both cloud flag and filling value for each of the cloud pixels detected. As shown in Figure 4-3, there are still some undetected cloud pixels with a lot of surrounding pixels covered by potential cloud shadow that the LEDAPS tool do not take into account. The high cloud covered scene may have high cloud shadow coverage. Besides, undetected thin clouds may deteriorate the quality of atmospheric correction. To reduce the risk of cloud contamination, Landsat scenes with less than 30% cloud coverage are used in this study. MODIS and MISR albedo products tend to generate cloud/cloud shadow free data relying on multiple observations that suffer less from cloud impacts.

The assumption that surface BRDF is invariant in 16 days is adopted in the MODIS albedo product. This assumption is followed in this study. In the following context, the DOY date refers to the 16-day time period around the specific date (e.g., DOY 184 means

the temporal window from DOY 177 to DOY 192). Due to the limited spatial coverage of each MISR swath and the cloud contamination, the MISR Level 2 albedo product often has many gaps for a single observation day. To reduce the impacts of missing data from MISR albedo, data from multiple days that are within the temporal window will be combined. The Landsat data close to the center of the temporal window is used.

4.4.2 Comparison on data before and after MRT

One of the basic assumptions in the MRT method is that the data on each scale shall have an expectation of zero mean in the spatial domain. However, the original albedo datasets cannot have a zero mean because of different land cover types, observation noises, and atmospheric correction accuracies. The spatial trend surface needs to be extracted and then removed from the original data. Research has been done finding the spatial trend surface using methods such as spline fitting and kriging. Using these methods are quite time consuming (Yue and Zhu 2006) and will limit the application in the operational practice. A simple method is used here by applying the median value of a moving window as the spatial mean. The window size is determined by the ratio of spatial resolutions from two satellite products with adjacent scales, e.g., MISR/MODIS and MODIS/Landsat. So, for Landsat data, the window size is set to be 15 and it is 3 for MODIS and MISR.

The observation errors for the satellite products are assumed to be proportional to the magnitude of albedo while the spatial random process of each satellite product is estimated by the variance within the window size from the detrended data.

The two-step MRT algorithm is implemented on the three products. All errors of the three albedo maps (Figure 4-5) have been significantly reduced after the implementation of MRT. From the comparisons of Landsat data before and after MRT, the spatial variation is well preserved, while most of the cloud effects have been removed based on the contributions from coarser resolution data that has less cloud masking difficulties. Also, the MODIS albedo product is retrieved from multiple days' observations, which should have the least cloud impacts.

The estimated detrended data are then added to the trend surface to generate the surface albedo. A time-series comparison of albedo is made from the results generated using data from DOY 151 to DOY 191 (Figure 4-6). Six cases in total are included in this time range. To be noted, the same Landsat data may be used in two adjacent cases. Some adjacent two cases can share part of the MISR data while MODIS albedo is always different. Results showed that the gaps, especially in MISR data and Landsat ETM+ data have been significantly filled, based on the supporting data from the other scale(s). Compared to the original satellite products, the datasets after MRT become consistent across scales.

According to the statistics comparison on the data before and after the data fusion (shown in Table 4-2), the bias between different products has been reduced and the values become consistent across the time. More significant improvements are: the relative RMSE has been reduced to almost half of its original value; and the outliers of the data have been removed in terms of the decrease in absolute values of maximum differences. These improvements indicate that the data fusion algorithm is capable of generating

consistent albedo products at different scales as well as reducing the risks of cloud contaminations and satellite system failure.

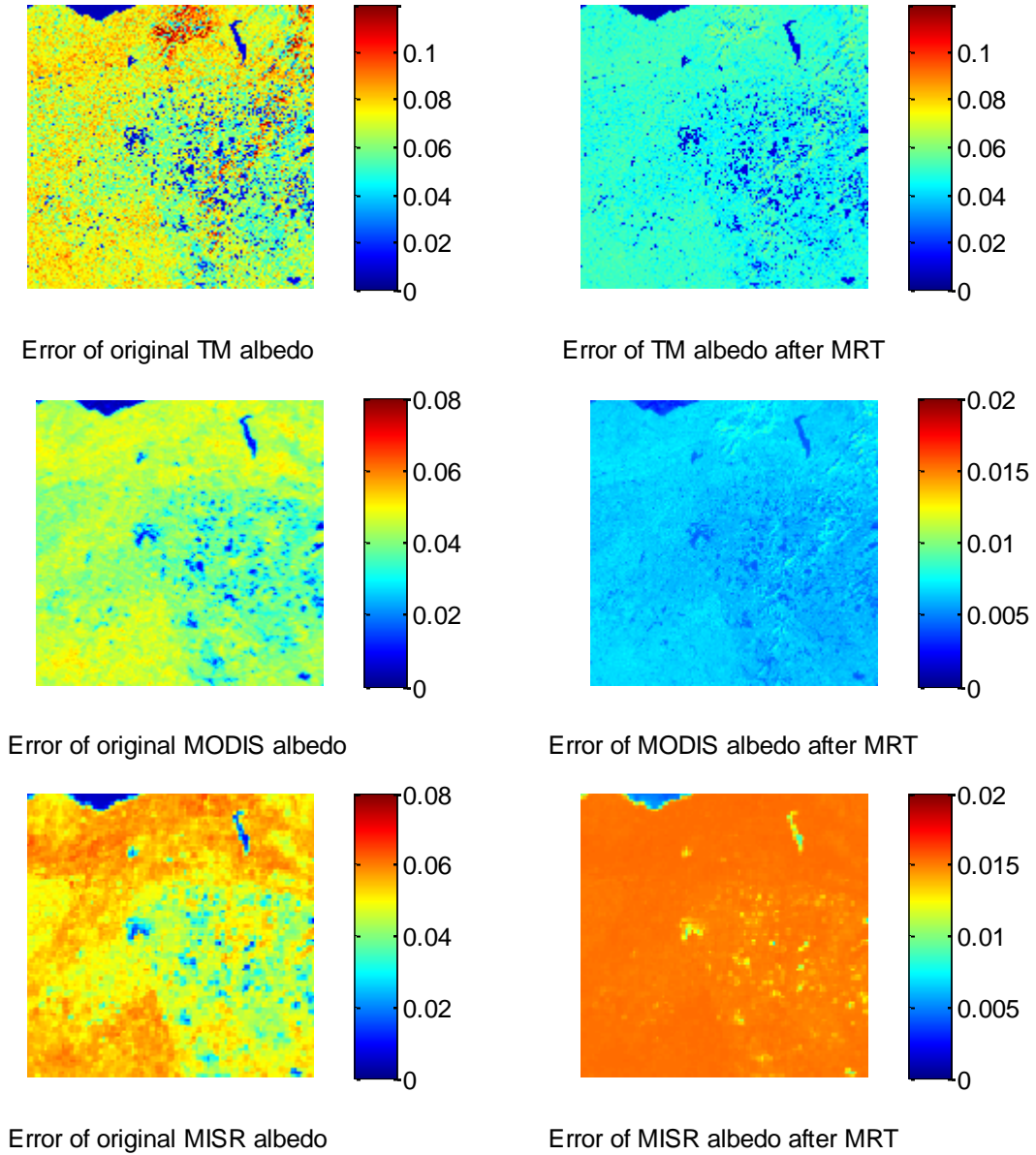


Figure 4-5 Error comparisons between albedo maps before and after MRT for the three products on DOY 184

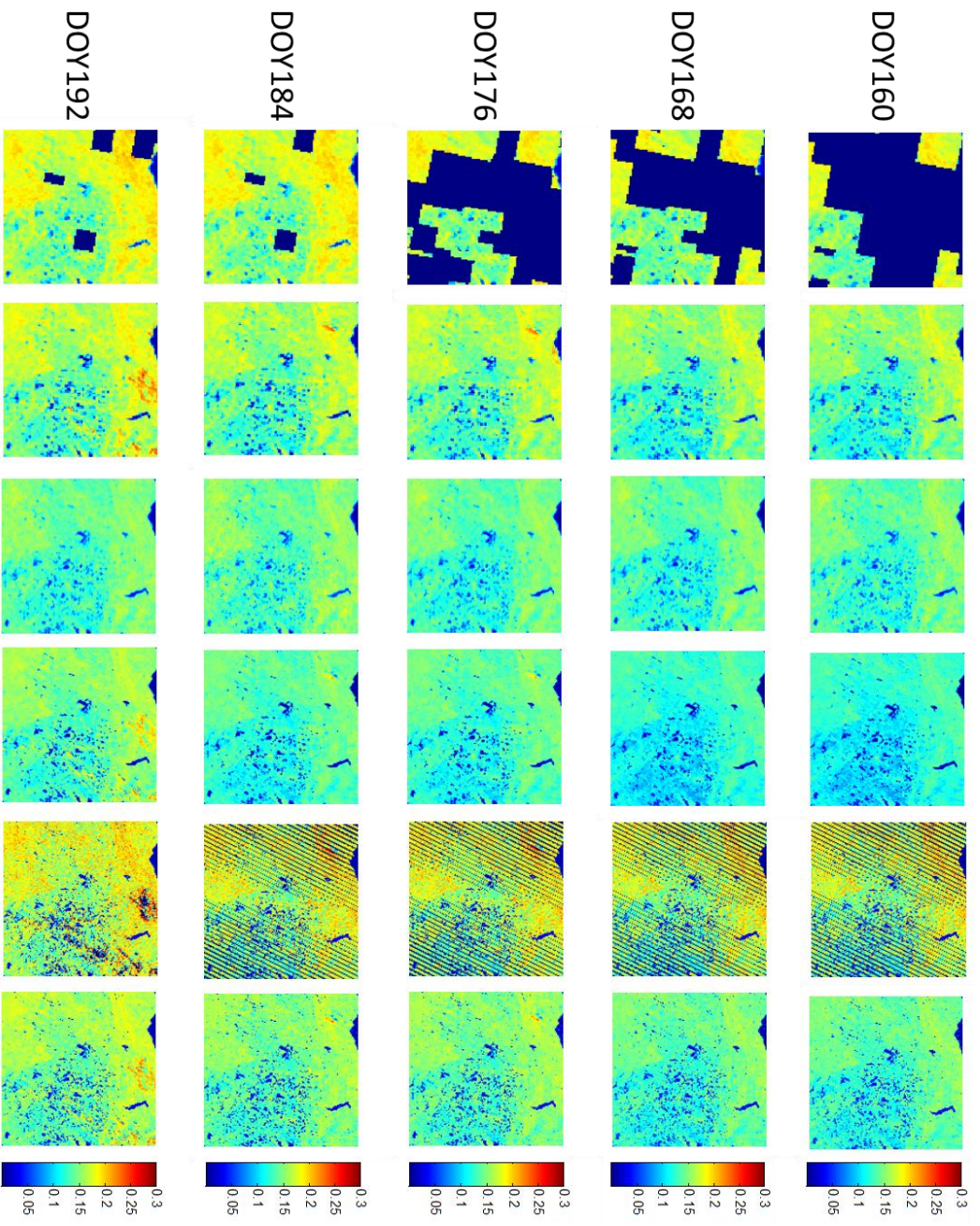


Figure 4-6 Time-series comparison of albedo maps before and after MRT (left-right order: original MISR albedo, MISR albedo after MRT, original MODIS albedo, MODIS albedo after MRT, original Landsat albedo, and Landsat albedo after MRT)

Table 4-2 Statistical comparison of different datasets before and after MRT

Date	MODIS vs Aggregated Landsat									
	Before MRT					After MRT				
	Bias	RMSE	RMSE(%)	Max	Min	Bias	RMSE	RMSE(%)	Max	Min
160	-0.022	0.030	20.467	0.102	-0.132	-0.016	0.018	14.270	0.094	-0.061
168	-0.024	0.031	20.399	0.095	-0.133	-0.015	0.017	13.814	0.095	-0.059
176	-0.027	0.033	22.170	0.105	-0.179	-0.011	0.014	11.260	0.100	-0.055
184	-0.020	0.030	21.572	0.116	-0.179	-0.011	0.014	11.254	0.100	-0.055
192	-0.027	0.036	23.023	0.111	-0.467	-0.007	0.011	10.310	0.110	-0.055
232	-0.005	0.023	19.720	0.112	-0.213	-0.007	0.011	11.953	0.095	-0.060
240	-0.007	0.023	18.985	0.110	-0.215	-0.007	0.011	11.950	0.095	-0.060
248	-0.010	0.025	18.957	0.111	-0.756	-0.008	0.011	10.762	0.093	-0.053
256	0.004	0.017	18.144	0.110	-0.108	-0.008	0.011	11.356	0.083	-0.057
264	0.003	0.016	17.442	0.106	-0.102	-0.008	0.011	11.193	0.083	-0.060
Date	MISR vs Aggregated MODIS									
	Before MRT					After MRT				
	Bias	RMSE	RMSE(%)	Max	Min	Bias	RMSE	RMSE(%)	Max	Min
160	0.023	0.027	20.886	0.094	-0.057	0.025	0.027	22.699	0.060	-0.004
168	0.029	0.032	27.494	0.110	-0.071	0.024	0.025	21.392	0.062	-0.012
176	0.032	0.035	29.152	0.111	-0.071	0.020	0.021	16.020	0.069	-0.013
184	0.026	0.029	21.887	0.100	-0.077	0.019	0.020	14.901	0.052	-0.013
192	0.028	0.031	23.978	0.110	-0.074	0.014	0.015	9.821	0.053	-0.015
232	0.014	0.034	33.842	0.068	-0.066	0.011	0.018	22.800	0.058	-0.001
240	0.029	0.035	29.281	0.126	-0.091	0.010	0.012	9.822	0.058	-0.011
248	0.027	0.032	27.509	0.133	-0.094	0.011	0.012	10.445	0.049	-0.011
256	0.021	0.024	20.462	0.114	-0.085	0.011	0.011	10.639	0.046	-0.010
264	0.020	0.024	20.899	0.123	-0.089	0.011	0.011	10.518	0.050	-0.010

RMSE(%): relative RMSE in percentage; Max: maximum value for the difference; Min: minimum value for the difference.

4.4.3 Summary and conclusions

Land surface albedo is an essential geophysical variable controlling the surface radiation budget. However, the current satellite albedo products cannot fully satisfy the accuracy requirements of the climate modeling studies. Errors of satellite albedo products may come from issues such as sensor calibration, temporal/angular composition, and cloud contamination. To reduce the uncertainty of the albedo products, it is important to

take advantage of different albedo datasets. This study proposes a novel approach to combine albedo datasets together.

A data fusion method using MRT is proposed to improve current satellite albedo products from multiple datasets. The purpose of using this data fusion method is to generate a set of temporally and spatially complete, continuous, and consistent albedo products across different scales. The MRT algorithm is proven to be capable of generating consistent albedo products across scales while reducing the uncertainties. This is the first time of data-fusing more than two albedo datasets at different spatial scales.

The proposed method works well to reduce the difference between albedo products at different spatial resolutions. Since the MRT method is very time efficient and the methodology presented here is applicable to other satellite albedo data and scalable to other areas, it can be used to generate some global albedo datasets at different spatial scales to better serve the albedo retrieving algorithms and the land surface modeling purposes.

The proposed approach requires the uncertainty estimations of existing satellite albedo products. Simplifications are made on the land surfaces by assuming that the land cover types are the same within the study area and the albedo uncertainty is proportional to the magnitude regardless of the surface type. In order to extend this approach to other areas with different land cover types (snow and urban areas, etc.), more efforts are needed to evaluate the products' accuracies.

CHAPTER 5 CONCLUSIONS

Land surface albedo products are of great importance in climate change and land surface modeling studies. Surface albedo varies spatially and evolves seasonally based on solar illumination changes, vegetation growth, and human activities such as cutting/planting forests and slash-and-burn agricultural practices. To detect the rapid surface changes, it requires accurate and consistent satellite albedo products with high spatial and temporal resolutions. However, most of current satellite albedo products suffer from several common problems, such as 1) the compositing time period is too long for monitoring abrupt changes on Earth surfaces; and 2) the “dark object” atmospheric correction algorithm is not suitable for non-vegetated surfaces. Moreover, data gaps and inconsistency are found among those products. As a result, current satellite albedo products cannot satisfy the needs of climate studies. This dissertation proposes two major methods to improve the current albedo products.

5.1 Major findings

In this dissertation, I designed a unified algorithm to estimate surface albedo by using the atmospheric radiative transfer with surface BRDF modeling. This unified algorithm is capable of simulating the interactions between atmosphere and non-Lambertian surfaces by accounting for the surface anisotropy. The proposed algorithm combines information of satellite observations and albedo prior knowledge. Thus, a much smaller temporal composition window is needed to estimate both surface albedo and instantaneous AOD. The reduced composition window size provides better capability of monitoring abrupt changes in surface albedo.

Following the same general retrieving procedure, surface albedo has been generated from different satellite datasets – MODIS and SEVIRI, respectively. Extensive validation over different land surfaces with various data sources are used to evaluate the performance of the proposed algorithm. Generally, the algorithm performs well on simultaneous estimations of surface albedo and AOD. For the retrievals from MODIS observations, validations of surface albedo are made over vegetated sites (SURFRAD) and snow-covered sites (GC-Net). The absolute bias is around 0.012 for snow-covered areas and around 0.002 for non-snow surfaces, while the RMSE is 0.0654 for snow-covered sites (less than 8% of the magnitude) and 0.0268 for non-snow sites. The directional surface reflectance by-product together with the AOD estimations have also been validated at AERONET sites to help verify the atmospheric correction accuracy in the proposed algorithm. The reflectance estimations for all the seven MODIS bands have a bias of less than 0.015 and the AOD retrievals have similar accuracy with MODIS products, which means the atmospheric correction is accurate in this algorithm.

With the success of application to MODIS data, this algorithm is revised and applied to SEVIRI data. Diurnal change and day-to-day change in surface albedo can be well captured from SEVIRI observations, whereas the 16-day MODIS products can only have an updated value every eight days. The evaluation of diurnal albedo estimation shows that the albedo retrievals have larger error with larger solar zenith angle, mainly because of failure of surface BRDF models. However, as the downward shortwave solar radiation decreases with solar zenith angle, the instantaneous estimation of surface shortwave energy budget turns out to have similar accuracy for both large and small solar zenith angles. The scene comparison between the retrieved values from this study and the

MODIS products shows that the proposed algorithm can generate albedo with good accuracy (bias: 0.0112; RMSE: 0.0318). The AOD retrievals at 550 nm from this study are compared to the MISR observations. The result shows a small bias of -0.012 with the RMSE of 0.083 for all the seven IMECC sites together.

The overall accuracy of albedo estimations from MODIS and SEVIRI can satisfy the accuracy requirements for the climate change studies and for the application of future GOES-R/ABI surface albedo algorithm (Liang et al. 2011).

A data fusion method MRT is used to improve current satellite albedo products from multiple datasets. The purpose of using this data fusion method is to generate a set of temporally and spatially complete, continuous, and consistent albedo products across different scales. The MRT algorithm is proven to be capable of generating consistent albedo products across scales. At the same time, it can reduce the uncertainties by using the information across different spatial resolutions.

5.2 Major contributions

This dissertation provides a new framework of estimating land surface albedo from satellite data. This framework provides a direction of how to generate accurate land surface albedo estimations at a finer temporal resolution for the future satellite applications. First, the approach was designed to estimate surface and atmospheric properties simultaneously using both satellite observations and prior knowledge of surface albedo. Second, the proposed approach was applied to both polar-orbiting and

geostationary satellite data. In the end, a method was proposed to improve the prior knowledge of surface albedo from multiple satellite products.

This is the first study of algorithm development for simultaneous estimations of surface albedo and instantaneous AOD by using the atmospheric radiative transfer with surface BRDF modeling for both polar-orbiting and geostationary satellite data. Existing methods usually follow a three-step procedure: atmospheric correction, surface BRDF model fitting, and broadband albedo conversion from spectral BRDF. To avoid error propagation at each step, the proposed algorithm in this dissertation estimates surface albedo and AOD directly from satellite observations. More importantly, the proposed approach provides the albedo estimations with much finer temporal resolution than the current satellite products, which benefits the climate change and terrestrial ecological monitoring communities with improved understanding of ephemeral snow events and vegetation growth, etc.

Extensive validations made from the comparison between the retrievals of albedo and AOD in this study and other data sources have shown that the accuracy of albedo estimations from MODIS and SEVIRI can satisfy the requirements for climate and meteorology studies and applications. Polar-orbiting satellites can provide good spatial resolution over high latitude regions while geostationary satellites can provide good temporal resolution for other regions. One of the main contributions is that this dissertation provides a unified algorithm to produce consistent albedo and AOD estimations from both kinds of satellites platforms (He et al. 2012a; He et al. 2012c). In addition, this algorithm has been slightly revised and applied as the prototype of future

GOES-R/ABI land surface albedo estimation algorithm (He et al. 2011; Liang et al. 2011). Given the very fine temporal resolution of geostationary satellites, the accurate diurnal albedo estimations from the proposed algorithm in this dissertation provides good understanding of diurnal energy budget estimations, which will contribute much to the climate change studies by demonstrating the surface albedo feedback to global warming.

Another major contribution of this dissertation is designing a framework using MRT to integrate multiple satellite albedo products at different spatial scales to build the spatially and temporally continuous albedo maps (He et al. 2012b). This is the first time of data fusing multiple albedo datasets to generate consistent albedo products across different spatial scales to generate. Uncertainties of albedo maps have been reduced significantly after the data fusion.

Current satellite albedo products have been evaluated extensively using various data sources. It has been found that those satellite albedo dataset cannot always meet the accuracy requirements for the applications on land surface modeling, weather forecasting, and terrestrial monitoring studies, etc. The innovative approaches proposed in this dissertation helps improve surface albedo estimations in terms of reducing data gaps and uncertainties, increasing temporal resolutions, and providing diurnal albedo changes. All these improvements can eventually help improve the predicting capabilities of global and regional models for climate change studies.

5.3 Suggestions for future study

This dissertation is a preliminary study in estimating surface albedo using information from both satellite observations and albedo climatology. Simplifications are made on the mathematical formula by assuming the unknown variables are independent to each other. However, there may be some correlation between different variables (e.g., autocorrelation in the aerosol information observed from geostationary satellites). Covariance of different variables in the retrieving algorithms needs to be exploited in the future to improve the accuracy of albedo and AOD estimations.

Some of the intrinsic aerosol properties (e.g., aerosol type and Angström exponent) are assumed to be invariant within the current retrieving procedure. Inclusion of global aerosol climatology and aerosol type selection methods is needed to improve the aerosol estimations.

Since the kernel models used in this dissertation are designed for vegetated land covers, snow BRDF models (e.g., Aoki et al. 2000; Hudson et al. 2006) and prior information (e.g., Wu et al. 2012) need to be incorporated into the proposed algorithm to account for the snow surface anisotropy signatures that intend to forward scatter the sunlight. Improvements on snow albedo estimation could be expected.

Multi-year MODIS albedo products are used as the prior information in current retrieving algorithm. Only relying on MODIS products to derive the albedo priori has two problems: first, the albedo priori has systematic bias; second, the prior information correlates with MODIS observations. Since the data fusion on albedo products provides

promising and unbiased albedo maps, the results from data fusion can be used as the prior information in the retrieving procedure.

In addition, since the MRT method is very time efficient and the methodology presented here is applicable to other satellite albedo data and scalable to other areas, it can be used to generate some global albedo datasets at different spatial scales to better serve the albedo retrieving algorithms and the land surface modeling purposes.

REFERENCES

- Aoki, T., Fukabori, M., Hachikubo, A., Tachibana, Y., & Nishio, F. (2000). Effects of snow physical parameters on spectral albedo and bidirectional reflectance of snow surface. *Journal of Geophysical Research-Atmospheres*, *105*, 10219-10236
- Augustine, J.A., Hodges, G.B., Dutton, E.G., Michalsky, J.J., & Cornwall, C.R. (2008). An aerosol optical depth climatology for NOAA's national surface radiation budget network (SURFRAD). *Journal of Geophysical Research-Atmospheres*, *113*
- Ba, M.B., Nicholson, S.E., & Frouin, R. (2001). Satellite-derived surface radiation budget over the African continent. Part II: Climatologies of the various components. *Journal of Climate*, *14*, 60-76
- Breon, F.M., Maignan, F., Leroy, M., & Grant, I. (2002). Analysis of hot spot directional signatures measured from space. *Journal of Geophysical Research-Atmospheres*, *107*, 15
- Chou, K.C., Willsky, A.S., & Nikoukhah, R. (1994). Multiscale systems, Kalman filters, and Riccati-equations. *Ieee Transactions on Automatic Control*, *39*, 479-492
- Clark, R.N., Swayze, G.A., Wise, R., Livo, E., Hoefen, T., Kokaly, R., & Sutley, S.J. (2007). USGS digital spectral library splib06a: U.S. Geological Survey, Digital Data Series 231. In
- Derrien, M., & Le Gleau, H. (2005). MSG/SEVIRI cloud mask and type from SAFNWC. *International Journal of Remote Sensing*, *26*, 4707-4732
- Derrien, M., & Le Gleau, H. (2010). Improvement of cloud detection near sunrise and sunset by temporal-differencing and region-growing techniques with real-time SEVIRI. *International Journal of Remote Sensing*, *31*, 1765-1780
- Dickinson, R.E. (1983). Land surface processes and climate surface albedos and energy balance. *Advances in Geophysics*, *25*, 305-353
- Diner, D.J., Martonchik, J.V., Borel, C., Gerstl, S.A.W., Gordon, H.R., Myneni, R.B., Pinty, B., Verstraete, M.M., & Knyazikhin, Y. (1999). Level 2 Surface Retrieval Algorithm Theoretical Basis Document. *NASA/JPL, JPL D-11401, Rev. D*.
- Diner, D.J., Martonchik, J.V., Kahn, R.A., Pinty, B., Gobron, N., Nelson, D.L., & Holben, B.N. (2005). Using angular and spectral shape similarity constraints to improve MISR aerosol and surface retrievals over land. *Remote Sensing of Environment*, *94*, 155-171
- Duan, Q.Y., Gupta, V.K., & Sorooshian, S. (1993). Shuffled complex evolution approach for effective and efficient global minimization. *Journal of Optimization Theory and Applications*, *76*, 501-521

- Duan, Q.Y., Sorooshian, S., & Gupta, V.K. (1994). Optimal use of the SCE-UA global optimization method for calibrating watershed models. *Journal of Hydrology*, 158, 265-284
- Fang, H.L., Liang, S.L., Kim, H.Y., Townshend, J.R., Schaaf, C.L., Strahler, A.H., & Dickinson, R.E. (2007). Developing a spatially continuous 1 km surface albedo data set over North America from Terra MODIS products. *Journal of Geophysical Research-Atmospheres*, 112
- Gastellu-Etchegorry, J.P., Martin, E., & Gascon, F. (2004). DART: A 3D model for simulating satellite images and studying surface radiation budget. *International Journal of Remote Sensing*, 25, 73-96
- Geiger, B., Carrer, D., Franchisteguy, L., Roujean, J.L., & Meurey, C. (2008). Land surface albedo derived on a daily basis from Meteosat Second Generation observations. *IEEE Transactions on Geoscience and Remote Sensing*, 46, 3841-3856
- Govaerts, Y.M., Wagner, S., Lattanzio, A., & Watts, P. (2010). Joint retrieval of surface reflectance and aerosol optical depth from MSG/SEVIRI observations with an optimal estimation approach: 1. Theory. *Journal of Geophysical Research-Atmospheres*, 115
- Grant, I.F., Prata, A.J., & Cechet, R.P. (2000). The impact of the diurnal variation of albedo on the remote sensing of the daily mean albedo of grassland. *Journal of Applied Meteorology*, 39, 231-244
- He, T., Liang, S., Wang, D., Wu, H., Yu, Y., & Wang, J. (2012a). Estimation of surface albedo and directional reflectance from Moderate Resolution Imaging Spectroradiometer (MODIS) observations. *Remote Sensing of Environment*, 119, 286-300
- He, T., Liang, S., Wang, D., Yu, Y., & Wang, J. (2012b). Generating complete and consistent surface albedo products across scales from different satellite sensors using a multi-resolution tree (MRT) method. *Internal review*
- He, T., Liang, S., Wu, H., & Wang, D. (2011). Prototyping GOES-R albedo algorithm based on MODIS data. In, *Geoscience and Remote Sensing Symposium (IGARSS), 2011 IEEE International* (pp. 4261-4264)
- He, T., Liang, S., Yu, Y., Wang, D., Wang, J., & Wu, H. (2012c). Daily-based estimation of surface albedo from Meteosat Second Generation (MSG) observations. *Submitted to Journal of Geophysical Research*
- He, T., Xiao, Z., & Wang, J. (2008). An improved algorithm to produce spatio-temporally continuous MODIS albedo product in China. In, *Geoscience and Remote Sensing Symposium, 2008. IGARSS 2008. IEEE International* (pp. III - 1095-III - 1098)

- Holben, B.N., Tanre, D., Smirnov, A., Eck, T.F., Slutsker, I., Abuhassan, N., Newcomb, W.W., Schafer, J.S., Chatenet, B., Lavenue, F., Kaufman, Y.J., Castle, J.V., Setzer, A., Markham, B., Clark, D., Frouin, R., Halthore, R., Karneli, A., O'Neill, N.T., Pietras, C., Pinker, R.T., Voss, K., & Zibordi, G. (2001). An emerging ground-based aerosol climatology: Aerosol optical depth from AERONET. *Journal of Geophysical Research-Atmospheres*, 106, 12067-12097
- Huang, H.C., Cressie, N., & Gabrosek, J. (2002). Fast, resolution-consistent spatial prediction of global processes from satellite data. *Journal of Computational and Graphical Statistics*, 11, 63-88
- Hudson, S.R., Warren, S.G., Brandt, R.E., Grenfell, T.C., & Six, D. (2006). Spectral bidirectional reflectance of Antarctic snow: Measurements and parameterization. *Journal of Geophysical Research-Atmospheres*, 111
- Jin, Y.F., Gao, F., Schaaf, C.B., Li, X.W., Strahler, A.H., Bruegge, C.J., & Martonchik, J.V. (2002). Improving MODIS surface BRDF/Albedo retrieval with MISR multiangle observations. *IEEE Transactions on Geoscience and Remote Sensing*, 40, 1593-1604
- Jin, Y.F., Schaaf, C.B., Woodcock, C.E., Gao, F., Li, X.W., Strahler, A.H., Lucht, W., & Liang, S.L. (2003). Consistency of MODIS surface bidirectional reflectance distribution function and albedo retrievals: 2. Validation. *Journal of Geophysical Research-Atmospheres*, 108
- Ju, J.C., Roy, D.P., Shuai, Y.M., & Schaaf, C. (2010). Development of an approach for generation of temporally complete daily nadir MODIS reflectance time series. *Remote Sensing of Environment*, 114, 1-20
- Kahn, R.A., Gaitley, B.J., Garay, M.J., Diner, D.J., Eck, T.F., Smirnov, A., & Holben, B.N. (2010). Multiangle Imaging Spectroradiometer global aerosol product assessment by comparison with the Aerosol Robotic Network. *Journal of Geophysical Research-Atmospheres*, 115, 28
- Kahn, R.A., Gaitley, B.J., Martonchik, J.V., Diner, D.J., Crean, K.A., & Holben, B. (2005). Multiangle Imaging Spectroradiometer (MISR) global aerosol optical depth validation based on 2 years of coincident Aerosol Robotic Network (AERONET) observations. *Journal of Geophysical Research-Atmospheres*, 110
- Kotchenova, S.Y., Vermote, E.F., Matarrese, R., & Klemm, F.J. (2006). Validation of a vector version of the 6S radiative transfer code for atmospheric correction of satellite data. Part I: Path radiance. *Applied Optics*, 45, 6762-6774
- Kuusk, A. (1995a). A Fast, invertible canopy reflectance model. *Remote Sensing of Environment*, 51, 342-350
- Kuusk, A. (1995b). A Markov-chain model of canopy reflectance. *Agricultural and Forest Meteorology*, 76, 221-236

- Leroy, M., Deuze, J.L., Breon, F.M., Hautecoeur, O., Herman, M., Buriez, J.C., Tanre, D., Bouffies, S., Chazette, P., & Roujean, J.L. (1997). Retrieval of atmospheric properties and surface bidirectional reflectances over land from POLDER/ADEOS. *Journal of Geophysical Research-Atmospheres*, *102*, 17023-17037
- Li, X.W., & Strahler, A.H. (1992). Geometric-optical bidirectional reflectance modeling of the DISCRETE crown vegetation canopy effect of crown shape and mutual shadowing. *IEEE Transactions on Geoscience and Remote Sensing*, *30*, 276-292
- Liang, S., Wang, D., He, T., & Yu, Y. (2011). GOES-R Advanced Baseline Imager (ABI) algorithm theoretical basis document for surface albedo. *NOAA/NESDIS, Version 2.0*
- Liang, S.L. (2001). Narrowband to broadband conversions of land surface albedo I Algorithms. *Remote Sensing of Environment*, *76*, 213-238
- Liang, S.L. (2007). Recent developments in estimating land surface biogeophysical variables from optical remote sensing. *Progress in Physical Geography*, *31*, 501-516
- Liang, S.L., & Strahler, A.H. (1994). 4-Stream solution for atmospheric radiative transfer over a non-Lambertian surface. *Applied Optics*, *33*, 5745-5753
- Liang, S.L., & Strahler, A.H. (1995). An analytic radiative transfer model for a coupled atmosphere and leaf canopy. *Journal of Geophysical Research-Atmospheres*, *100*, 5085-5094
- Liu, J.C., Schaaf, C., Strahler, A., Jiao, Z.T., Shuai, Y.M., Zhang, Q.L., Roman, M., Augustine, J.A., & Dutton, E.G. (2009). Validation of Moderate Resolution Imaging Spectroradiometer (MODIS) albedo retrieval algorithm: Dependence of albedo on solar zenith angle. *Journal of Geophysical Research-Atmospheres*, *114*
- Liu, Q., Wen, J., Qu, Y., He, T., Zhang, X., & Wang, L. (2012). Broadband albedo. In S. Liang, X. Li, & J. Wang (Eds.), *Advanced remote sensing*
- Liu, S.H., Liu, Q.A., Liu, Q.H., Wen, J.G., & Li, X.W. (2010). The angular and spectral kernel model for BRDF and albedo retrieval. *Ieee Journal of Selected Topics in Applied Earth Observations and Remote Sensing*, *3*, 241-256
- Lucht, W., Schaaf, C.B., & Strahler, A.H. (2000). An algorithm for the retrieval of albedo from space using semiempirical BRDF models. *IEEE Transactions on Geoscience and Remote Sensing*, *38*, 977-998
- Maignan, F., Breon, F.M., & Lacaze, R. (2004). Bidirectional reflectance of Earth targets: Evaluation of analytical models using a large set of spaceborne measurements with emphasis on the Hot Spot. *Remote Sensing of Environment*, *90*, 210-220

- Masek, J.G., Vermote, E.F., Saleous, N.E., Wolfe, R., Hall, F.G., Huemmrich, K.F., Gao, F., Kutler, J., & Lim, T.K. (2006). A Landsat surface reflectance dataset for North America, 1990-2000. *IEEE Geoscience and Remote Sensing Letters*, 3, 68-72
- Meador, W.E., & Weaver, W.R. (1980). 2-stream approximations to radiative transfer in planetary atmospheres: A unified description of existing methods and a new improvement. *Journal of the Atmospheric Sciences*, 37, 630-643
- Minnis, P., Mayor, S., Smith, W.L., & Young, D.F. (1997). Asymmetry in the diurnal variation of surface albedo. *IEEE Transactions on Geoscience and Remote Sensing*, 35, 879-891
- Moody, E.G., King, M.D., Platnick, S., Schaaf, C.B., & Gao, F. (2005). Spatially complete global spectral surface albedos: Value-added datasets derived from terra MODIS land products. *IEEE Transactions on Geoscience and Remote Sensing*, 43, 144-158
- Moody, E.G., King, M.D., Schaaf, C.B., Hall, D.K., & Platnick, S. (2007). Northern Hemisphere five-year average (2000-2004) spectral albedos of surfaces in the presence of snow: Statistics computed from Terra MODIS land products. *Remote Sensing of Environment*, 111, 337-345
- Moody, E.G., King, M.D., Schaaf, C.B., & Platnick, S. (2008). MODIS-derived spatially complete surface albedo products: Spatial and temporal pixel distribution and zonal averages. *Journal of Applied Meteorology and Climatology*, 47, 2879-2894
- Nobre, C.A., Sellers, P.J., & Shukla, J. (1991). Amazonian deforestation and regional climate change. *Journal of Climate*, 4, 957-988
- Pinty, B., Lavergne, T., Dickinson, R.E., Widlowski, J.L., Gobron, N., & Verstraete, M.M. (2006). Simplifying the interaction of land surfaces with radiation for relating remote sensing products to climate models. *Journal of Geophysical Research-Atmospheres*, 111
- Pinty, B., Roveda, F., Verstraete, M.M., Gobron, N., Govaerts, Y., Martonchik, J.V., Diner, D.J., & Kahn, R.A. (2000). Surface albedo retrieval from Meteosat - 1. Theory. *Journal of Geophysical Research-Atmospheres*, 105, 18099-18112
- Plumejeaud, C., Mathian, H., Gensel, J., & Grasland, C. (2011). Spatio-temporal analysis of territorial changes from a multi-scale perspective. *International Journal of Geographical Information Science*, 25, 1597-1612
- Pokrovsky, O., & Roujean, J.L. (2003). Land surface albedo retrieval via kernel-based BRDF modeling: I. Statistical inversion method and model comparison. *Remote Sensing of Environment*, 84, 100-119
- Qin, W.H., Herman, J.R., & Ahmad, Z. (2001). A fast, accurate algorithm to account for non-Lambertian surface effects on TOA radiance. *Journal of Geophysical Research-Atmospheres*, 106, 22671-22684

- Rahman, H., Pinty, B., & Verstraete, M.M. (1993). Coupled Surface-Atmosphere Reflectance (CSAR) model .2. Semi-empirical surface model usable with NOAA Advanced Very High-Resolution Radiometer data. *Journal of Geophysical Research-Atmospheres*, 98, 20791-20801
- Reda, I., & Andreas, A. (2004). Solar position algorithm for solar radiation applications. *Solar Energy*, 76, 577-589
- Roman, M.O., Schaaf, C.B., Woodcock, C.E., Strahler, A.H., Yang, X.Y., Braswell, R.H., Curtis, P.S., Davis, K.J., Dragoni, D., Goulden, M.L., Gu, L.H., Hollinger, D.Y., Kolb, T.E., Meyers, T.P., Munger, J.W., Privette, J.L., Richardson, A.D., Wilson, T.B., & Wofsy, S.C. (2009). The MODIS (Collection V005) BRDF/albedo product: Assessment of spatial representativeness over forested landscapes. *Remote Sensing of Environment*, 113, 2476-2498
- Roujean, J.L., Leroy, M., & Deschamps, P.Y. (1992). A bidirectional reflectance model of the Earth's surface for the correction of remote sensing data. *Journal of Geophysical Research-Atmospheres*, 97, 20455-20468
- Roy, D.P., Ju, J., Lewis, P., Schaaf, C., Gao, F., Hansen, M., & Lindquist, E. (2008). Multi-temporal MODIS-Landsat data fusion for relative radiometric normalization, gap filling, and prediction of Landsat data. *Remote Sensing of Environment*, 112, 3112-3130
- Roy, D.P., Lewis, P., Schaaf, C.B., Devadiga, S., & Boschetti, L. (2006). The global impact of clouds on the production of MODIS bidirectional reflectance model-based composites for terrestrial monitoring. *IEEE Geoscience and Remote Sensing Letters*, 3, 452-456
- Rutan, D., Rose, F., Roman, M., Manalo-Smith, N., Schaaf, C., & Charlock, T. (2009). Development and assessment of broadband surface albedo from Clouds and the Earth's Radiant Energy System Clouds and Radiation Swath data product. *Journal of Geophysical Research-Atmospheres*, 114
- Salomon, J.G., Schaaf, C.B., Strahler, A.H., Gao, F., & Jin, Y.F. (2006). Validation of the MODIS Bidirectional Reflectance Distribution Function and Albedo retrievals using combined observations from the Aqua and Terra platforms. *IEEE Transactions on Geoscience and Remote Sensing*, 44, 1555-1565
- Schaaf, C.B., Gao, F., Strahler, A.H., Lucht, W., Li, X.W., Tsang, T., Strugnell, N.C., Zhang, X.Y., Jin, Y.F., Muller, J.P., Lewis, P., Barnsley, M., Hobson, P., Disney, M., Roberts, G., Dunderdale, M., Doll, C., d'Entremont, R.P., Hu, B.X., Liang, S.L., Privette, J.L., & Roy, D. (2002). First operational BRDF, albedo nadir reflectance products from MODIS. *Remote Sensing of Environment*, 83, 135-148
- Sellers, P.J., Meeson, B.W., Hall, F.G., Asrar, G., Murphy, R.E., Schiffer, R.A., Bretherton, F.P., Dickinson, R.E., Ellingson, R.G., Field, C.B., Huemmrich, K.F., Justice, C.O., Melack, J.M., Roulet, N.T., Schimel, D.S., & Try, P.D. (1995).

- Remote sensing of the land surface for studies of global change - models, algorithms, experiments. *Remote Sensing of Environment*, 51, 3-26
- Shuai, Y.M., Masek, J.G., Gao, F., & Schaaf, C.B. (2011). An algorithm for the retrieval of 30-m snow-free albedo from Landsat surface reflectance and MODIS BRDF. *Remote Sensing of Environment*, 115, 2204-2216
- Song, J. (1998). Diurnal asymmetry in surface albedo. *Agricultural and Forest Meteorology*, 92, 181-189
- Stroeve, J., Box, J.E., Gao, F., Liang, S.L., Nolin, A., & Schaaf, C. (2005). Accuracy assessment of the MODIS 16-day albedo product for snow: comparisons with Greenland in situ measurements. *Remote Sensing of Environment*, 94, 46-60
- Strugnell, N.C., & Lucht, W. (2001). An algorithm to infer continental-scale albedo from AVHRR data, land cover class, and field observations of typical BRDFs. *Journal of Climate*, 14, 1360-1376
- Wagner, S.C., Govaerts, Y.M., & Lattanzio, A. (2010). Joint retrieval of surface reflectance and aerosol optical depth from MSG/SEVIRI observations with an optimal estimation approach: 2. Implementation and evaluation. *Journal of Geophysical Research-Atmospheres*, 115
- Wang, D., & Liang, S. (2010). Using multiresolution tree to integrate MODIS and MISR-L3 LAI products. In *Geoscience and Remote Sensing Symposium (IGARSS), 2010 IEEE International* (pp. 1027-1030)
- Wang, Y.J., Lyapustin, A.I., Privette, J.L., Cook, R.B., SanthanaVannan, S.K., Vermote, E.F., & Schaaf, C.L. (2010). Assessment of biases in MODIS surface reflectance due to Lambertian approximation. *Remote Sensing of Environment*, 114, 2791-2801
- Wang, Y.J., Lyapustin, A.I., Privette, J.L., Morisette, J.T., & Holben, B. (2009). Atmospheric correction at AERONET locations: A new science and validation data set. *IEEE Transactions on Geoscience and Remote Sensing*, 47, 2450-2466
- Widlowski, J.L., Taberner, M., Pinty, B., Bruniquel-Pinel, V., Disney, M., Fernandes, R., Gastellu-Etchegorry, J.P., Gobron, N., Kuusk, A., Lavergne, T., Leblanc, S., Lewis, P.E., Martin, E., Mottus, M., North, P.R.J., Qin, W., Robustelli, M., Rochdi, N., Ruiloba, R., Soler, C., Thompson, R., Verhoef, W., Verstraete, M.M., & Xie, D. (2007). Third Radiation Transfer Model Intercomparison (RAMI) exercise: Documenting progress in canopy reflectance models. *Journal of Geophysical Research-Atmospheres*, 112
- Wikle, C.K. (2003). Hierarchical models in environmental science. *International Statistical Review*, 71, 181-199

- Wu, H., Liang, L.S., Tong, L., He, T., & Yu, Y. (2012). Bidirectional reflectance for multiple snow-covered land types from MISR products. *IEEE Geoscience and Remote Sensing Letters*, *accepted*
- Yang, F.L., Mitchell, K., Hou, Y.T., Dai, Y.J., Zeng, X.B., Wang, Z., & Liang, X.Z. (2008). Dependence of land surface albedo on solar zenith angle: Observations and model parameterization. *Journal of Applied Meteorology and Climatology*, *47*, 2963-2982
- Yue, W., & Zhu, J. (2006). On estimation and prediction for multivariate multiresolution tree-structured spatial linear models. *Statistica Sinica*, *16*, 981-1020
- Zhang, X.T., Liang, S.L., Wang, K.C., Li, L., & Gui, S. (2010). Analysis of global land surface shortwave broadband albedo from multiple data sources. *Ieee Journal of Selected Topics in Applied Earth Observations and Remote Sensing*, *3*, 296-305
- Zhu, J., & Yue, W. (2005). A multiresolution tree-structured spatial linear model. *Journal of Computational and Graphical Statistics*, *14*, 168-184
- Zhu, X.L., Chen, J., Gao, F., Chen, X.H., & Masek, J.G. (2010). An enhanced spatial and temporal adaptive reflectance fusion model for complex heterogeneous regions. *Remote Sensing of Environment*, *114*, 2610-2623